THE UNIVERSITY OF CHICAGO

ENGINEERING TUMOR BINDING POLYMERIC GLYCO-ADJUVANTS FOR CANCER IMMUNOTHERAPY

A DISSERTATION SUBMITTED TO

THE FACULTY OF THE PRITZKER SCHOOL OF MOLECULAR ENGINEERING

IN CANDIDACY FOR THE DEGREE OF

DOCTOR OF PHILOSOPHY

BY

LEVI Y. BENNISH

CHICAGO, ILLINOIS

MARCH 2023

DEDICATION

To my dear wife Minna Bennish who has consistently supported me throughout the challenges and triumphs of my doctoral degree. The long nights in the lab, the academic stress of classes, and the setbacks of failed experiments. Your unwavering support, while nurturing and caring for our precious children Menachem, Yehuda, Devorah Leah, and Zalmi is forever appreciated.

TABLE OF CONTENTS

LIST OF FIGURES

ACKNOWLEDGMENTS

I owe enormous gratitude to those who have helped me along the way on this arduous journey in beginning, continuing, and ultimately completing my Ph.D. I am fortunate to have been with the Hubbell Lab for my Ph.D. – it has been a great lab for science, collaboration, life, and the occasional prank or two. I am fortunate to have had such great colleagues and friends.

First and foremost, I want to thank my advisor, Jeffrey Hubbell. You had the foresight and vision to enable a young graduate student with modest synthetic chemistry expertise to transform into an independent scientist and to move through small molecule chemistry, polymer chemistry, and a year of mouse experiments. I had hardly heard of a T cell when I joined the lab. I am forever grateful for your encouragement and consistent confidence in my abilities. I have learned so much from you as to how to formulate and frame a scientific question, plan and execute a scientific experiment, and report and contextualize the outcomes. I cannot thank you enough for your unwavering support over these years -- it is truly humbling.

Next, I also would like to thank the rest of my thesis committee, Prof. Melody Swartz and Prof. Aaron Esser-Kahn. Melody, you have always provided insightful guidance on my projects, and you were never shy to stop and ask how I was doing. Aaron, I appreciate your knowledge and guidance on all my research projects – especially in the area of small molecule adjuvants.

I would like to thank Dean Matt Tirrell for your leadership of the Pritzker School of Molecular Engineering. You had the foresight and strength to create a transformative graduate education in molecular engineering and the courage to push boundaries when needed. I am grateful to have received your full support and encouragement to complete my Ph.D.

Much of my doctoral research would not be possible without the mentorship and collaboration I had with many throughout my Ph.D. I owe tremendous gratitude to Prof. Scott Wilson, who as a postdoc in the Hubbell Lab developed much of the technology that several of my projects were based upon. You showed me the ropes of synthetic and polymer chemistry, followed by training me in appropriate cell culture techniques. You were always available to answer any questions that I had. Many thanks to Dr. L. Taylor Gray who has been a terrific collaborator on my earlier projects. I want to thank Anna Slezak who has been a wonderful collaborator on the pyridyl-disulfide polymer project, and I want to thank her for developing much of the technology that my final project was based. She has provided tremendous support in my learning of murine cancer models, and she always was happy to provide assistance in all areas of my project. I also want to thank Dr. Seounghun Kang for his help and support with my animal studies. Finally, I want to thank Dr. Aslan Mansurov who has greatly assisted in planning and analyzing experiments.

Thank you to all the past and present members of the Hubbell Lab that contributed to the welcoming, helpful, and friendly lab spirit. Thank you to Dr. Ruyi Wang for helping me get started with synthetic chemistry and for always being available to discuss chemistry. Thank you to our lab manager Suzana Gomes who takes care of so much in the lab and strives to ensure everyone has what they need in the lab. Thank you to Drs. Elyse Watkins, Andrew Tremain, Michael White, and Marcin Kwissa for your help and insight while beginning my research in the lab. Thank you to Joe Reda and Dr. Lucas Shores for your help and support in troubleshooting and assisting with projects.

I also would like to thank the many mentors who have guided me on my scientific journey while an undergraduate at Wayne State University. Firstly, thank you to my undergraduate advisor,

Prof. Zhongwu Guo, for his support and encouragement while I was a young undergraduate in his lab. He allowed me to be largely self-sufficient on my own research project – thus preparing me very well for graduate studies. Thank you to Prof. Peter Andreana, who always challenged me in chemistry and inspired me to do my best. Thank you to Prof. Charles Winter who urged me to pursue doctoral studies and insisted that I ought to apply to the University of Chicago.

Additionally, I would like to thank scientific mentors and friends from outside of the university for their support and guidance through the maze of graduate school. To Dr. Yitzchok (Ken) Chakiris, who has been a great friend and source of encouragement. To Prof. Tom Imbo, for your constant interest and encouragement of my graduate studies.

Finally, I want to thank my family for their constant encouragement and support. First and foremost, I am extremely thankful to my wife, Minna Bennish for her constant support and encouragement throughout graduate school. I would not have been able to do this journey with her support. To my parents, Dr. Aaron Bennish and Rivka Bennish, who have always supported my education and shown me the value of perseverance throughout the challenges of life. To my in-laws, Dr. Robert and Miriam Wolfe, for their interest in my research and encouragement of my studies. To my siblings, Dov, Mendel, Yisrael, Devorah, Yanky, and Bayla, who have been the best siblings I could have asked for. Lastly, I am deeply grateful to my wonderful children, Menachem, Yehuda, Devorah Leah, and Zalmi, who have been great supporters throughout this process and always welcomed me home regardless of the hour.

ABSTRACT

Cancer immunotherapy utilizing immune checkpoint inhibitors has been heralded as one of the most important scientific and medical breakthroughs in the early 21st century. It has revolutionized the standard of care in many challenging cancer types including colon cancer, melanoma, and Hodgkin lymphoma, leading to unprecedented clinical responses in these challenging tumors. Despite this, most patients fail to adequately respond to these treatments due to the lack of appropriate T cells within the tumor microenvironment. Further strategies are needed to enhance the T cell infiltrate and boost endogenous antitumor immunity. Many promising strategies have been developed; however, they are often associated with immune-related adverse events and require expensive patient-specific formulations. In this work, we aim to develop an in-situ cancer vaccine that relies on endogenous patient-specific tumor neoantigens. The benefit of this approach is that it can be tumor agnostic and is readily available without additional formulation. To achieve this, we engineered CpG-p(PDS-Man), a potent adjuvant-polymer conjugate able to bind unpaired cysteines on the tumor cell surface and on extracellular tumor debris in the tumor microenvironment. CpG is a potent adjuvant in clinical development and conjugating it to our cysteine binding polymer allows for sustained delivery in the tumor microenvironment, eliciting a strong antitumor immune response against endogenous tumor antigens. In this work, we found that our CpG-p(PDS-Man) conjugate could be readily constructed and purified. Upon intratumoral injection, CpG-p(PDS-Man) prolonged survival in multiple murine tumor models, including in tumors resistant to checkpoint inhibitors, such as the B16F10 melanoma. Furthermore, we found decreased systemic toxicity of our construct compared to free adjuvant. Our developed platform demonstrates a flexible, ready-to-use adjuvant-based immunotherapy that can trigger a widespread anti-tumor immune response with the appropriate

vigor for successful treatment. Our research illustrates the potential of using CpG-p(PDS-Man) as a treatment platform for various types of cancer.

CHAPTER 1:

INTRODUCTION

1.1 Motivation

Vaccines have been one of the greatest and most cost-effective public health achievements in history. They have played a critical role in eradicating or controlling the spread of many infectious diseases, such as smallpox, polio, measles, and tetanus. The development of vaccines and subsequent mass immunization efforts have saved millions of lives and prevented incalculable suffering and economic losses. Despite its celebrated history in the annals of public health, the field has numerous frontiers and challenges to overcome in developing new vaccines, specifically in vaccines against cancer. As opposed to infectious diseases, which are typically caused by a single pathogen, cancer is caused by a multitude of genetic and epigenetic changes. Consequently, the development of a vaccine that targets many of the appropriate cancer antigens is exponentially more challenging. Moreover, traditional vaccines thus far have mainly focused on the induction of neutralizing antibodies, while only a limited number have effectively produced potent cytotoxic T-lymphocyte (CTL) mediated immunity, a crucial component of an effective immune response against cancer cells.[1] The aim of the work in this thesis is therefore to design and develop a more potent in situ vaccine to treat cancer. This vaccine can be available as an off-the-shelf formulation and can be broadly applied to various cancers. By utilizing the patient's endogenous antigens within the tumor, our in-situ vaccine can achieve robust antitumor immunity. Our in-situ vaccine can achieve antitumor immunity in a matter that is both tumor and patient-agnostic; without any interrogation into the characteristics of the tumor itself.

1.2 The Immune System: Innate and Adaptive Immunity

The immune system represents a large network of organs, cells, proteins, chemicals and other processes that primarily function to protect the host from foreign antigens, such as pathogenic microbes (bacteria, fungi, and parasites) viruses, cancer cells, and toxins.[2,3] Environmental pathogens use a wide spectrum of complex pathological mechanisms to challenge and imperil the host. In an equivalent manner, the immune response to environmental pathogens relies on a complex set of protective mechanisms to either control or eliminate pathogens. The underlying principle behind the host's defensive mechanisms is to recognize the structural features of pathogens and subsequently identify them as non-host. With host-pathogen discrimination attained, the immune system can subsequently mount an effective immune response against the pathogen and limit damage to the host.

There are 2 general classes of mechanisms in which the host can effectively recognize and respond to pathogenic signatures. The first is a group of instinctive and innate responses encoded in the host's germline which recognizes molecular patterns expressed by many pathogens but not present in the mammalian host. This recognition and response mechanism is known as innate immunity. The second class of immune recognition to pathogenic threats arises not from gene elements found in the host's germline, rather, it arises via the recombination of somatic gene elements that rearrange to recognize individual antigen-specific molecules with unique specificity. the recognition and responses of the immune system in this fashion are known as the adaptive immune system.[2]

Innate immunity is typically viewed as the first line of defense against a pathogenic threat. It is not pathogen-specific and thus cannot recognize specific antigens. Because innate immunity recognizes a broad class of molecules, it can act swiftly after a pathogenic encounter. Responses

are mounted immediately or within hours after encountering a pathogen. Because the innate immune system does not recognize specific antigens it thus has no immune memory and cannot "memorize" and recognize the same pathogen should the host encounter the pathogen in the future. As opposed to innate immunity, adaptive immunity is both antigen-dependent and antigen-specific. To achieve this specificity toward a target antigen, antigen-specific receptors on T and B lymphocytes are assembled via somatic rearrangement of gene fragments to create an enormous diversity of different antigen receptors. When an antigen-specific T or B lymphocyte recognizes an antigen, there is a lag time before an effective immune response is mounted via the adaptive immune system to clear the pathogen. Additionally, being antigen-specific, the adaptive immune response can "memorize" pathogens and allows the host to mount a quicker and more effective immune response upon subsequent encounters.

Cells of the innate immune system include dendritic cells (DCs), macrophages, neutrophils, and natural killer (NK) cells. Collectively, these cells are excellent at detecting and responding effectively to either an invading pathogenic threat or physical injury via conserved molecular patterns.[4] Pathogen-associated molecular patterns (PAMPs) and damage-associated molecular patterns (DAMPs), are recognized as danger signals upon interacting with pattern recognition receptors (PRRs) of host immune cells. Several subclasses of PRRs have been identified, such as toll-like receptors (TLRs), nucleotide-binding oligomerization domain-like receptors (NLRs), C-type lectin receptors, retinoic acid-inducible (RIG) receptors, and absent in melanoma-2 (AIM2)-like receptors (ALRs). Different PRRs are expressed in essential cellular locations to detect a microbial threat, such as on the cell membrane as well as in intracellular compartments and the cytoplasm.

Collectively, they bind a wide array of motifs, such as nucleic acids, carbohydrates, lipoproteins, polysaccharides, as well as a few highly conserved microbial proteins. Many of these ligands are shared across a wide variety of pathogenic classes, thus allowing for broad recognition with a limited number of receptors.[5] Although pathogens tend to evolve and could avoid detection by the PRRs by simply altering their targeting molecules, innate immunity has evolved to recognize pathogenic components that are essential for pathogenic viability and thus less prone to modifications.

Upon PRR activation, a signaling cascade is activated leading the recruitment of professional antigen presenting cells (APCs), such as macrophages and DCs to the site of inflammation via chemokines. APCs begin to engulf and process extracellular debris and pathogens to yield small peptide fragments. These fragments are then loaded onto the major histocompatibility complex (MHC) class I or II molecules on the APC cell surface. MHC-I molecules are present on all cells except for red blood cells and typically present peptide fragments derived from proteins found inside the cell but can also present peptide fragments from proteins found outside the cell. MHC-II molecules on the other hand are found only on professional APCs. In contrast to MHC-I, peptide fragments loaded on MHC-II are derived from proteins found in the extracellular environment. Additionally, activated APCs also express important co-stimulatory ligands on their cell surface such as CD80 and CD86.

Activated dendritic cells migrate to the lymph node where antigen specific recognition of the MHC-peptide complex (on the APC) can interface with a corresponding T cell receptor (TCR) on a naïve T lymphocyte, either to a $CD8^+$ T cell (cytotoxic T lymphocyte) or to a or $CD4^+$ T cell (T helper lymphocyte). TCR stimulation by MHC-I or MHC-II molecules is known as signal-1 in the APC-T cell interaction. For an appropriate T cell activation to occur, co-stimulatory ligands on

APCs such as CD80 or CD86 must interact with their cognate receptor on the T-cell surface such as CD28, yielding signal-2. Co-stimulation is key to an effective immune response against pathogenic threat. If antigen specific T-cells interact with a corresponding MHC-complex on APCs without appropriate co-stimulation, the naïve T-cell may either undergo apoptosis or may become an immune suppressive regulatory T-cell. This an important mechanism in which the immune system prevents destruction of host tissues.

Upon appropriate T-cell activation, the T-cell undergoes clonal expansion, in which the activated T-cell with the unique specificity towards the antigen of interest is allowed to multiply, thus creating many more T-cells with the same unique specificity towards the antigen of interest. The ever-expanding T cell population drives the probability that $CD8^+$ T cells will engage the appropriate pathogen or cancer cell. CD4+ T cell expansion plays a key role in B cell immunity as well. B cells are active as APCs, in which they express peptide fragments on their cell surface MHC-II. Encounter of a CD4+ T cell with a B cell specific for such a peptide, the a CD4+ T cell helps activate the B cell for further proliferation and differentiation into plasma B cells (which secrete antibodies), or long lasting memory B cells[6].

In summary, antigen presentation via APCs is the critical link between innate and adaptive immunity, as it guides the antigen specific B or T cells to an appropriate immune response. Without appropriate co-stimulation (signal-2), immune tolerance will occur, an important mechanism of peripheral tolerance, so that aberrant immune attack towards self-antigens is avoided. With an appropriate co-stimulatory signal, the immune system can recognize antigen as foreign, and an appropriate immune response towards a pathogen can be mounted.

1.3 TLRs: Gatekeepers of the Immune System

TLRs are a family of transmembrane proteins that play a critical role is activating an appropriate innate immune response. They belong to the general family of PRRs, which as mentioned recognize various PAMPs. The TLRs are the most well understood and characterized receptors in this family. 13 specific TLRs have been identified, ten of which are found in humans. TLRs that are found on the cell surface include TLR 1, 2, 4, 5, 6, and 10. TLRs that can be found on the endosome include TLR 7, 8, and 9. Cell surface TLRs tend to recognize PAMPs located on the surface of a pathogen e.g., lipopolysaccharide (ligand for TLR4), while endosomal based TLRs recognize PAMPs internal to a pathogen, such as bacterial DNA (ligand for TLR9). Collectively, TLRs can recognize many different PAMPs, and many of the TLRs are not limited to recognizing only one ligand. For example, cell surface based TLR2 can recognize both lipoteichoic acid from gram positive bacteria, as well as zymosan, a key component of the cell wall in fungi.

TLRs are characterized as type-I integral membrane glycoproteins, comprised of an extracellular N-terminal ligand binding domain, composed of an extracellular horseshoe shaped motif composed of leucine-rich repeats (LRRs) which are responsible for pathogen recognition, followed by a transmembrane helix, and finally a C-terminal cytoplasmic Toll/interleukin 1 (IL-1) receptor (TIR) homology domain. Upon ligand binding, TLR dimerization is induced. TLR dimers can be formed between two of the same TLRs (homodimerization), or between two different TLRs (heterodimerization). Dimerized cytosolic TIR domains subsequently induce signaling via heterophilic interactions with cytosolic TIR-domain-dependent adapter proteins such as TIR domain-containing adapter protein (TIRAP), myeloid differentiation primary response protein 88 (MyD88), and TIRAP-inducing IFN-β (TRIF)-related adaptor molecule (TRAM)[7].

Based on the distinct complexes formed, TLR signaling pathways can be generally classified as either being a MyD88-dependant pathway, which induces inflammatory cytokines, or TRIF-dependent pathway, which induces type-1 interferons (IFN), in addition to inflammatory cytokines[8]

Additionally, signaling via TLRs induces DCs to undergo maturation. This process upregulates costimulatory ligands (signal-2) on DCs, which in addition to DCs displaying signal-1 (exogenous antigens), allows for an effective pathogen specific adaptive immune response. shape the specificity of the immune response.

DC activation via different microbial PAMPS yields different classes of immune responses. Information about the particular pathogenic threat is provided by specific TLR engagement, thus the effector response can be tailored to that particular pathogenic threat and dictates which cytokines the activated DCs produce, which will shape the differentiation of naïve $CD4^+$ T-cells[9]. Not all DCs are a functionally heterogenous population, and specific subsets have been identified that express subset specific PRRs. Resultingly, the cellular responses will differ, leading to distinct signaling pathways. For example, plasmacytoid DCs (pDCs), express endosomal TLRs that recognize viral components, but do not express TLRs to detect bacterial cell components. Thus, pDCs may be a unique subset to detect viral infection[9].

Questions remain as to how activating different TLRs induces different immune responses and how they cooperate with each other[10]. Many pathways are coupled. TLRs allow DCs to recognize a plethora of pathogenic compounds. As mentioned, DCs provide IL-12, a key cytokine in innate responses and upon challenge to host, immature DCs mature, allowing them to migrate to the lymph node for antigen presentation. Consequently, DC activation via TLRs allows DCs to

integrate signals from specific pathogens, and ultimately plays a key role in linking an innate immune response to an appropriate long lasting adaptive immune response of a suitable class[7].

1.4 Vaccines: Engineering Adaptive Immunity

Leveraging adaptive immunity to benefit human health has a long and rich history. As early as 430 BC it was observed that individuals who survived smallpox were subsequently immune to further smallpox infections. Survivors were therefore called upon assist the ill. Inoculation, derived from the Latin *inoculare*, meaning "to graft," referring to the transfer of smallpox matter from the pustule of an afflicted individual to a non-immune individual. The inoculator would introduce this material subcutaneously into the arms or legs of the non-immune individual. Inoculation was likely practiced in Africa, China, and India, long before being introduced to Europe in the beginning of the 18th century[11]. In 1715, Lady Montague defied convention and ordered that her 5-year-old son be inoculated[12]. Early inoculation took place in Boston during 1721[13]. General George Washington ordered his soldiers at Valley Forge Word spread to others. Yet, all the above was by taking postulate matter of smallpox itself – fatality rate was 2% as opposed to 20% for smallpox[14].

Vaccination, in which the immune system achieves immunity towards a specific disease by means of a vaccine, took a major turn with Jenner. The earliest vaccines have traditionally contained either an attenuated or an inactivated form of the pathogenic microbe or virus (known as a live attenuated vaccine or an inactivated vaccine respectively). Indeed, Jenner's original vaccine against smallpox was derived from cowpox (hence the term vaccine, derived from the latin *vacca* for "cow"). In 1796, Jenner observed that milkmaids who had cowpox were immune against smallpox infection. He exposed an 8 year old boy to the milkmaids' lesions and subsequently observed that the boy was immune to smallpox.

Subsequent discoveries by Louis Pasteur provided insight into live attenuated vaccines, in which the serial passage of the virus or bacteria often reduce the virulence of the pathogen. The attenuated virus can be used as an effective vaccine in inducing a strong immune response in the host. In 1885, Pasteur produced his rabies vaccine by attenuating the virus in a rabbit host, and subsequently harvesting it from the infected rabbit spinal cord. More powerful attenuation techniques developed by Albert Calmette and Camille Guérin, yielded Bacillus Calmette–Guérin (BCG) vaccine against tuberculosis. Bovine tuberculosis bacteria was passaged 230 times in a glycerol/potato media to yield an appropriate attenuated strain[15]. Albert Sabin's oral polio vaccine (OPV) was obtained by serial passage of the three major poliovirus strains in cultured primate cells until appropriate non-virulent strains were produced[16]. Sabin's OPV was inexpensive to produce, and its ease of administration proved a key factor in mass vaccination rollouts worldwide[17]. Additional attenuated vaccines include the measles and varicella vaccines.

Inactivated vaccines provided an alternative strategy to an attenuated live vaccine. Pathogens can be rendered inactivated by heat or chemical treatment, which allows for the formerly infectious pathogen to be safely used as a vaccine. Much of the original immunogenicity of the pathogen can be retained if the inactivation is done carefully, often with formaldehyde fixation. In 1896 an inactivated vaccine against typhoid was developed independently by Almroth Wright in England and Richard Pfeiffer in Germany[15]. Whole-cell pertussis vaccines composed of whole killed bordetella pertussis, were first licensed in the US in 1914[18]. In developing the inactivated polio vaccine (IPV), Jonas Salk used formaldehyde to inactive the poliovirus without destroying its immunogenic properties. Additional inactivated vaccines include the hepatitis A vaccine and the current rabies vaccine.

While both inactivated and attenuated vaccines have had a tremendous impact on human health, there are distinct disadvantages to both vaccine types. Many inactivated vaccine candidates may contain incompletely inactivated viral particles, such as the case for foot-and-mouth disease virus. Nucleocapsid proteins can be crosslinked with RNA, which can consequently prevent RNA degradation, and some viral particles can escape formaldehyde inactivation. Additionally, some inactivated vaccine candidates based on formaldehyde inactivation simply do not induce potent virus neutralizing antibodies and are ineffective upon viral challenge. Formaldehyde can also modify the viral antigenic sites, such as in the case of poliovirus, leading to a poorer immune response. Even with approved inactivated vaccines, several booster immunizations are required to achieve long lasting immunity[19].

While on the one hand live attenuated vaccines can elicit a robust immune response being that the vaccine is indeed a live virus itself (albeit attenuated), this itself is its disadvantage. Attenuated viruses are intact viruses, and capable of mutating. Secondary mutations of the attenuated virus can cause the virus to return to a virulent form. Such is the case of the attenuated Sabin OPV. While it has been used for more than 50 years and billions of doses distributed worldwide, the risk of vaccine-associated paralytic poliomyelitis for OPV is present, with an occurrence rate for first dose recipients of OPV of about 1 case per 750,000 children immunized. Additionally, vaccine-derived polioviruses can cause polio outbreaks within under immunized communities[20]. An additional major drawback of attenuated viruses is that they can't safely be administered to immunocompromised individuals. Attenuated vaccines have led to serious infections in immunodeficient patients, and occasionally death has been reported. The previous decades have seen an increase in patients using immunosuppressive medications due to organ or

bone marrow transplants, leading to an increased number of patients that the live vaccine may pose a danger to[21].

To ameliorate the above-described safety concerns, and as well as to enable vaccine candidates where traditional approaches have failed, modern rationally designed vaccines increasingly rely on subunit vaccine technology. As opposed to the traditional approach of the entire pathogen being used (in either live attenuated vaccines or inactivated vaccines), only a subset of the antigenic proteins or carbohydrates are used. Subunit vaccines demonstrate several advantages over traditional vaccines: (1) The antigens used in subunit vaccines tend to be significantly better defined; antigen may be produced recombinantly with enhanced purity and reproducibility. (2) There is no possibility for the vaccine to have any infectious properties as it exclusively contains a subunit of the pathogen. (3) They often have an increased safety profile, which allows them to be administered to the immunocompromised. (4) Recombinant production of antigen can often be better mass produced. (5) They often have a better stability profile and can be transported and stored at room temperature, thus maintaining efficacy in a wide range of environmental settings.

While subunit vaccine technology has indeed been quite successful at providing clinically approved vaccines, including more modern vaccines such as the hepatitis B vaccine and the human papillomavirus (HPV), the subunit alone fails to elicit an appropriate immune response to achieve long lasting vaccine immunity. Being a subunit of the pathogen, these subunits alone are not immunogenic enough to trigger an antigen-specific immune response. To achieve long lasting vaccine immunity using a subunit vaccine, vaccine adjuvants are added to the vaccine formulation. Vaccine adjuvants stimulate the immune system and enhance the overall immunogenicity of the vaccine, thus leading to long lasting vaccine induced immunity.

1.5 Vaccines: The Role of Adjuvants

As mentioned, many modern vaccines require adjuvants to enhance the overall immunogenicity of the vaccine to achieve durable immunity. Adjuvants often contain PAMPS that can be either pathogen derived or produced synthetically. Adjuvants can be used to enhance both the magnitude and durability of the immune response[22].

Adjuvants can enhance the immune response to a vaccine according to three general mechanisms: (1) They improve antigen uptake, transport, and ultimately presentation by APCs to T cells in the lymph node draining from the vaccine injection site. (2) They allow for prolonged antigen delivery, thus exposing the immune system to the antigen for a longer duration. This mimics natural infection, where the pathogen is trapped at the site of infection. A more complete immune response can be elicited with a slower antigen release. This continual immune stimulation is known as the depot effect. (3) PRRs are activated at the site of injection, triggering innate immune cells to release cytokines essential for enhanced expression of costimulatory ligands[23].

Few vaccine adjuvants are currently approved for human use. The oldest and most widely used adjuvant class are aluminum-based salts. Potassium aluminum sulfate (alum) has been widely used as a vaccine adjuvant since 1926[24]. However, this has been largely replaced by aluminum hydroxide and aluminum phosphate[25]. More recently approved adjuvants include oil in water emulsions containing squalene such as MF59 and AS03. Many vaccine adjuvant candidates were largely based on empirical observation. Despite their widespread use, the molecular mechanisms behind how these adjuvants work in humans remains not well understood[26].

However, recent advances in immunology and vaccinology have allowed for a more rational approach to vaccine and adjuvant design. Development of new and rationally designed

adjuvants are necessary because the small number of approved adjuvants are not optimal in achieving effective immunity towards different target pathogens such as HIV and malaria[27]. With the discovery of PRRs and elucidation of the TLR structures, modern adjuvant candidates are often rationally designed to mimic the endogenous adjuvants present in live attenuated vaccines which elicit robust immune responses, often by activating specific PRRs. For example, the BCG vaccine against tuberculosis, has been shown to activate multiple TLRs such as TLR2, TLR4 and TLR9. Live attenuated yellow fever vaccine activates multiple TLRs as well[26].

Considering the above findings, TLR agonists have become important components in rational adjuvant design. Furthermore, by understanding their molecular mechanisms, appropriate direction can be given to bias a specific immunological response. Much attention has been given to direct T helper (Th) responses, in which Th1 cells are more appropriate for cell-mediated immunity which is necessary to protect against intracellular pathogens such as virus infected cells. On the other hand, a Th2 response is more appropriate for humoral immunity, which is necessary to protect against extracellular pathogens such as extracellular microbes. Synthetic TLR agonists as have been demonstrated as appropriate vaccine adjuvants in non-human primate (NHP) studies. When vaccinated with recombinant protein antigens, these synthetic TLR ligands promoted enhanced antibody responses[26]. Furthermore, recent success in rational adjuvant design based on TLR agonists, has led to the approval of two new adjuvants. ASO4, an adjuvant system containing Monophosphoryl Lipid A (MPLA) and aluminum hydroxide, is an important component of the HPV vaccine. MPLA is a potent TLR4 agonist, and is derivative of lipid A. Additionally, CpG 1018, a potent TLR9 agonist, has been formulated as an adjuvant in Heplisav-B, a potent hepatitis B vaccine.

1.5 Cancer and The Immune System

As mentioned above, our immune system can recognize potentially harmful pathogens by recognizing foreign antigens. Through mechanisms to prevent an immune response against otherwise healthy self, T cells capable of recognizing self-antigens are purged either through thymic development or via peripheral tolerance, a mechanism that is constantly ongoing in secondary lymphoid tissues and the immune periphery.

1.5.1 Cancer and the Immune System: Tumor Antigens

Cancer is characterized by a large number of variable genetic alterations and the eventual loss of typical cellular regulatory processes[28]. Generally, these tumor antigens can be divided into two classes: (1) Tumor associated antigens (TAAs) which result from over or abnormal expression of non-mutated proteins. And (2) Tumor-specific antigens (TSAs), also known as neoantigens that arise via inherent mutational nature of the cancer.

Tumor associated antigens[29] are often overexpressed proteins that can be subdivided into four general categories: (1) Cancer testis antigens, normally found on spermatocytes or spermatogonia such as Melanoma-associated antigen (MAGE), or New York esophageal squamous cell carcinoma-1 (NY-ESO-1). Generally, these antigens are thought to be concealed from the immune system to prevent destruction of germ cells by host immune system. (2) Differentiation antigens, which are cell surface markers to distinguish one cell type from another. These can be found on cells that are of the same lineage as the tumor (e.g., gp100 and TRP-1) (3) Oncofetal antigens, such as Alpha-fetoprotein (AFP) and Carcinoembryonic antigen (CEA) proteins that are normally expressed during fetal development but generally not found in healthy adults. (4) Overexpressed tumor associated antigens, which are normal proteins that are found in

healthy individuals but are up regulated in cancer cells. These include Tumor protein P53 (TP53) and epidermal growth factor receptor (EGFR).

Because TAAs are found in healthy tissue, the immune system is unlikely to mount an immune response against them. Additionally, these TAAs are likely to have induced an tolerogenic response towards them[30]. Furthermore, if somehow a vaccine is engineered towards TAAs, serious or fatal autoimmune damage could occur[31].

On the other hand, TSAs or neoantigens are uniquely expressed by cancer cells. These arise from the multitude of somatic mutations in the development of cancer and are therefore tumor specific. Occasionally, these TSAs are shared amongst a subset of individuals with a particular cancer[32], however most TSAs are patient specific. TSAs are highly tumor and patient dependent and vary widely between tumor types. Being that they are tumor specific, they have significantly increased likelihood of being immunogenic as compared to TAAs. Given their specificity, they theoretically make excellent candidates for targeted immunotherapeutics, however they are often highly individualized in each patient, making them quite challenging to identify.

1.5.2 Cancer and the Immune System: A Complex Interplay

As mentioned, when healthy cells turn into cancer cells, this is often accommodated by a diverse set of genetic modifications, which is accompanied by the expression of mutated proteins, thus allowing for detection by the immune system. A patient's immune system can often demonstrate a wide variety of antitumor effects[33]. For example, NK cells can perceive cancer cells upon ligand encounter on tumor cells, which can directly lead to the destruction of some cancer cells[34]. Alternatively, this can lead to further uptake and processing of the cancer cell fragments by macrophages and DCs, which lead to inflammatory cytokine secretion and TAAs presentation T and B cells. T and B cells activation can lead to further production of inflammatory cytokines

that can further activate the innate immune system leading to tumor-specific T cell expansion and production.

Tumor immunosuppression can be achieved by a variety of tumor infiltrating immune cells. Regulatory T (Treg) cells, interleukin (IL)-10 producing B cells, as well as B regulatory cells are all suppressive lymphocytes associated with cancer. Myeloid-derived suppressor cells (MDSC)s as well as tumor associated macrophages (TAM)s have been heavily associated with cancer. Furthermore, cells of the tumor stroma can also promote the recruitment and activation of immunosuppressive cells. Changes in protein expression levels can also accomplish immunosuppression. MHC class I can be downregulated by tumor cells to evade detection by APCs or alternatively to restrict other components of antigen processing to avoid T cell recognition. Furthermore, inhibitory surface receptors can be upregulated in a ploy to evade immune response.

1.6 Clinical Landscape of Cancer Immunotherapeutics

As discussed above, the immune system plays a critical role in cancer development. Therefore, many clinical strategies have been put forth to overcome the immunosuppressive mechanisms developed by the tumor. Immunotherapies have been developed to both subdue these immunosuppressive mechanisms as well as train the immune system to eliminate cancer cells as a standalone therapy. Much clinical progress has been made in the area of immune checkpoint inhibitors, with several approved by the Food and Drug Administration (FDA). Cancer immunotherapeutics is very active field of research. In 2022 alone there have been 5,683 clinical trials evaluating anti-PD1/PDL combination regimens.[35] Additionally, a large number of clinical trials are focusing on other immunotherapies, such as adjuvant based therapies[36], cytokine therapeutics[37], adoptive T cell transfer[38], antitumor antibodies[39], and oncolytic viruses[40]. A full

discussion of and review of immunotherapeutic strategies is beyond the scope of this work, rather we will focus on strategies that are more relevant to this work, namely immune checkpoint inhibitors and adjuvant-based therapies that are either clinically approved or in clinical trials.

1.6.1 Immune Checkpoint Inhibitors (ICIs)

Immune checkpoint inhibitors (ICIs) represent the most extensively used form of cancer immunotherapeutics. Immune checkpoints are intrinsic protective mechanisms employed by the immune system to prevent destruction against self. Cancers take advantage of this mechanism by expressing ligands to bind these inhibitory receptors, thus diminishing immune activation within the tumor. By administering antibodies against either immune checkpoint ligands or receptors, the immune checkpoint is "blockaded," thus yielding the term "checkpoint blockade," and the tolerogenic immune response to cancer can be reversed to promote antitumor immunity[41].

Ipilimumab (Yervoy), a monoclonal antibody against CTLA-4 (cytotoxic T-lymphocyte–associated antigen 4) was approved in 2011 by the FDA for patients with metastatic melanoma[42]. However, anti-CTLA-4 therapy did include a number of severe adverse immune-related events (irAEs) in patient[43]. Alternative clinical strategies to CTLA-4 have since emerged, with an aim towards a more favorable toxicity profile. Such strategies have focused on PD-L1/PD-L2 (programmed death-ligand 1 or 2) or PD1 (programmed cell death protein-1). PD1 is an additional inhibitory receptor expressed on antigen-stimulated T cells, and its activation inhibits T-cell cytoxicity[41]. Anti-PD-1 antibodies pembrolizumab (Keytruda), and nivolumab (Opdivo) were approved in 2014. Anti-PD-L1 antibodies atezolizumab (Tecentriq) and Avelumab (Bavencio) were subsequently approved in 2016 and 2017 respectively. Currently, 7 ICIs have received FDA approval[44].

While ICIs have made huge clinical strides, most patients fail to benefit from ICIs[44]. Many mechanisms of resistance have been postulated such low mutational burden or the tumor[45], or inhibitory cytokines within the tumor microenvironment[46]. Further research is ongoing into blockading other immune checkpoint molecules such as lymphocyte activation gene 3 (LAG3) protein and T-cell immunoglobulin and mucin domain 3 (Tim-3)[47].

1.6.2 Adjuvant Based Immunotherapy

In a prophylactic setting, adjuvant-based immunotherapy has had a considerable amount of success with cancers that are of viral origin, such as human papillomavirus[48] and hepatitis B virus[49]. These are vaccines against the viruses that can cause cancer and are formulated as a subunit vaccine[50], containing adjuvants such as MPLA[51] or CpG (ODN 1018)[52].

However, adjuvant-based immunotherapies have struggled to make inroads in a therapeutic vaccine setting. Much focus has been dedicated to the development of peptide or recombinant protein-based vaccines which target either tumor associated antigens or tumor specific antigens. These vaccines often consist of the entire amino acid sequence (protein) or a short amino acid derived sequence (peptide) from these antigens, along with an appropriate adjuvant. However, for these peptide-based vaccines to be effective, attention must be given to the specific amino-acid sequence that is incorporated. Specific CD8+ epitopes must be included for antigen cross-presentation leading to antitumor immunity, and specific CD4+ epitopes must be included to activate T-helper cells[53]. Furthermore, the choice of tumor antigen is of critical importance; ideally the antigen should specific to cancer cells and highly immunogenic[54]. Many clinical studies have been undertaken with peptide or protein based therapeutic vaccines against TAAs or TSAs, such as utilizing a MAGE-A3 recombinant protient based vaccine in patients with MAGE-A3-positive

non-small-cell lung cancer[55] or utilizing a gp100 peptide based vaccine in patients with advanced melanoma[56].

While many of these candidates have shown promise in pre-clinical settings, clinically they have had limited efficacy, with not a single one attaining FDA approval[53]. Several possible explanations are given for the poor response in clinical trials, such as the lack of a suitable and robust adjuvant for an appropriate T-cell response[57], the inherent limited antigenicity of TAAs as they mostly resemble self-antigens and are inherently tolerogenic,[58] as well as the inherent heterogeneity of many tumors[59]. Other strategies have sought to utilize patient specific neoantigens utilizing next-generation sequencing and advanced computational methods to identify the specific genetic alterations in cancer cells of individual patients[60]. While such methods can yield a high level of specificity towards neoantigens, its associated high cost and high level of patient specificity preclude its widespread use.

As an alternative strategy to identifying and developing a vaccine towards specific TSAs and TAAs, a more generalizable approach may be put in place. Renewed interest has been generated towards localized adjuvant delivery to the tumor. By doing so, one can envision that APCs within the tumor increase inflammatory cytokines secretion, enhance antigen presentation, allowing for eventual T-cell priming against cancer antigens in the tumor. Indeed TLR2/TLR4 activating BCG vaccine is approved for superficial transitional cell carcinoma of the bladder, and TLR7 activating imiquimod (Aldara) is approved for basal cell carcinoma[61]. Both are locally delivered to the affected site (bladder and topically to the skin, respectively). This highlights the potential of utilizing PRR agonists, and specifically, TLR agonists, to reverse the tumor immunosuppressive mechanisms, and allow for the immune system to mount an effective

antitumor immune response against endogenous tumor antigens, with the aim of complete remission.

1.7 Biomaterial Design

Recent work in our lab has focused on a novel tumor targeting delivery platform that binds unpaired cysteines on tumor cell surfaces and tumor debris[62]. Given the dysregulated metabolism and increased hypoxia in solid tumors, this would result in an excess of unpaired cysteines on the surface of cancer cells and tumor debris. Previous studies demonstrated the ability of leveraging exofacial protein thiols for MRI contrast agent labeling in murine melanoma B16F10 utilizing pyridyl-disulfide cysteine binding chemistry[63]. Our lab further developed this technology and developed a multivalent polymer exploited these unpaired cysteines in the tumor microenvironment as a target for cysteine reactive drug delivery. Furthermore, by copolymerizing a pyridyl disulfide methacrylamide monomer with a TLR7 agonist monomer, our lab found enhanced antitumor efficacy utilizing this cysteine binding technology[62]. Earlier work in our lab focused on copolymerizing a small molecule TLR7 agonist as an effective strategy for to induce immunity against SARS-CoV-2[64] and as overall strategy to induce immunity against model antigen ovalbumin as well as against Plasmodium falciparum circumsporozoite protein (PfCSP)[65]. The focus of this work is to further develop the cysteine binding platform as an appropriate technology to deliver larger molecules to the tumor microenvironment for cancer immunotherapy by utilizing the polymer chain end. In this work, we used strain promoted alkyne- azide cycloaddition to conjugate CpG to an azide on the chain end.

Additionally, our adjuvating polymers contain multiple mannose monomers to increase phagocytosis of our polymer, as well as enhance localization of our polymer to the endosome, the location of TLR9. Mannose receptor (CD206) is expressed on the surface many APCs, and is a C-

type lectin, which can bind to different carbohydrates found on the surface of many microorganisms. When pathogen or pathogenic fragment bind to the mannose receptor, it is phagocytosed to the early endosome and loaded onto MHC-I for antigen cross presentation. Here, we take advantage of this pathway to enhance uptake and appropriate localization of our polymer-adjuvant conjugate to engage the endosomal TLR9.

In this work, our adjuvant of choice is CpG. As mentioned, CpG are synthetic oligodeoxynucleotides containing one or several motifs of cytosine triphosphate deoxynucleotide (C) linked via a phosphodiester bond (p) to guanine triphosphate deoxynucleotide (G). In some classes of CpG, some or all the phosphodiester bonds are replaced with a phosphorothioate bond instead. When these sequences are unmethylated they are recognized as a PAMP and are highly immunostimulatory. While CpG is synthetic, it mimics unmethylated CG dinucleotides which are present at a high incidence in bacterial DNA but are uncommon in eukaryotic DNA.

To date, four general classes of CpG have been described[66], each having specific structural motifs and eliciting a particular immune response. Class A (type D) induces high IFN-α secretion in plasmacytoid dendritic cells (pDCs). Class B (type K) induce strong B-cell activation, enhances pDC maturation, and boosts NF-κB signaling. Class C has features from both class A & B, and it can induce IFN-α secretion from pDCs as well as activate B cells. Class P has a similar immunological profile to class but contains two palindromic sequences.

CpG ODN1826, a mouse TLR9 agonist, has shown much promise in preclinical mouse models as an effective adjuvant for cancer immunotherapy. In one study, it showed a strong effect in combination with radiotherapy in slowing tumor growth in Lewis lung cancer model[67]. In another study, it showed a profound effect in promoting antitumor immunity in B16 melanoma cells expressing mucin 1[68]. Additionally, earlier work by the Esser-Kahn group demonstrated the

amenability of CPG1826 to further conjugation. In their work, the 3′ end was labeled with a fluorescein tag for quantification, while the 5′ end was conjugated to other PRR agonists.

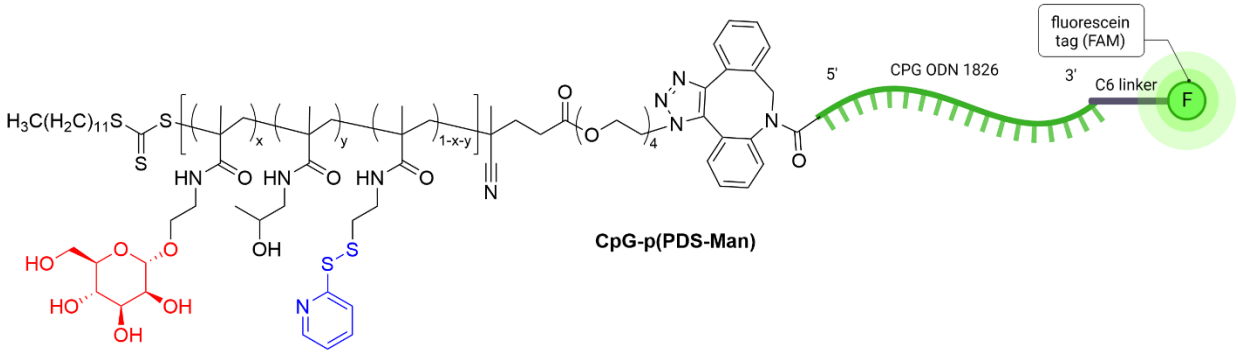

Figure 1: Fully envisioned CpG-p(PDS-Man) polymer-adjuvant conjugate

p(PDS-Man) is a random copolymer containing pendant mannose (red) and pyridyl-disulfide (blue) monomers. HPMA is added as a diluent. Polymer is synthesized via RAFT polymerization and subsequently conjugated to DBCO-CpG-Fam via strain-promoted alkyne- azide cycloaddition to yield the final CpG-p(PDS-Man) conjugate.

Based on the above, our full polymer is envisioned (Figure 1), demonstrating the multifaceted (but modular), approach of the polymer. Multiple copies of mannose (Man), pyridyl-disulfide (PDS) as well as HPMA (diluent), are present within the polymer. This polymer, hereby referred to as p(PDS-Man), can be synthesized via reversible addition-fragmentation chain transfer (RAFT) polymerization. RAFT mediated polymerization allows for precise control over molecular weight and can afford polymers with narrow molecular weight distributions[69]. Furthermore, RAFT polymerization has been extensively studied and utilized for biomedical applications[70]. Additionally, the polymer chain end contains an azide functional group which can undergo strain promoted alkyne- azide cycloaddition with a DBCO moiety on the 5′ end of CPG1826. As noted, the 3′ end is labeled with a fluorescein tag for CpG quantification.

CHAPTER 2:

MATERIALS AND METHODS

2.1 Mice

C57BL/6 female mice and BALB/c female mice aged between 8-10 weeks were purchased from Charles River Laboratory. Mice were housed in specific pathogen free environment at the University of Chicago. All animal studies were done in accordance with procedures approved by Institutional Animal Care and Use Committee at the University of Chicago.

2.2 Cell Culture

B16F10 murine melanoma, MC38 colon carcinoma, and CT26 colon carcinoma cell lines were purchased from ATCC. B16F10, MC38 cells, and CT26 cells were cultured in Dulbecco's Modified Eagle Medium (DMEM) supplemented with 10% heat inactivated fetal bovine serum (FBS), 1% Penicillin/Streptomycin, and 0.05mM Beta-mercaptoethanol. Cells were maintained at a density of approximately 10^6 cells/mL. Cells were routinely checked for mycoplasma contamination. For tumor inoculation, cell media was aspirated, 2mL of trypsin (Gibco TrypLE Select) were then added to detach adherent cells. Cells were incubated for 2 minutes at 37° C, and then 10 mL of DMEM medium was added to flask. Cells were spun down at 300 relative centrifugal force (RCF) for 5 minutes. Cells were then washed twice with phosphate buffered saline (PBS), counted using trypan blue, and resuspended in PBS.

Bone marrow derived dendritic cell (BMDC) activation studies used the following procedure: BMDCs were prepared from isolated monocytes of 6 week old C57BL/6 mice as

previously described[71]. BMDCs were used on day 8-9, in which 1 x 10^5 cells per well were plated in 96 well plates in Roswell Park Memorial Institute (RPMI) 1640 HEPES containing medium (Gibco), supplemented with 10% heat inactivated fetal bovine serum (FBS), 1% Penicillin/Streptomycin, and 0.05mM Beta-mercaptoethanol. Cells were incubated with varying concentrations of CpG-polymer or free CpG ODN 1826 (Invivogen) at 37° C for 24 hours. Cell supernatant was then harvested, and cytokine concentration was measured and analyzed either via enzyme-linked immunosorbent assay ELISA (Invitrogen) or via LEGENDplex mouse inflammation panel (BioLegend) according to the manufacturer's instructions.

RAW-Blue™ mouse macrophage reporter cell activation studies were conducted as follows: 1×10^5 cells RAW-Blue™ mouse macrophage reporter cells (Invivogen) were plated in 96 well plates in 180 μL DMEM supplemented with 10% heat inactivated fetal bovine serum (FBS) and 1% Penicillin/Streptomycin. 20 μL of either CpG-polymer or free CpG ODN 1826 (Invivogen) were added at varying concentrations. Cells were then incubated at 37° C for 18 hours. Subsequently, 20 μL of the cell supernatant was added to 180 μL of freshly prepared QuantiBlue (Invivogen) solution in a 96 well flat bottom plate. Plate was subsequently incubated for 30 minutes at 37° C for 30 minutes. Plate absorbance was then measured using an Epoch Microplate Spectrophotometer (Biotek) at 620 nanometers.

2.3 Murine Inoculation and Treatment

For murine studies involving tumor growth and survival, as well all cytokine and toxicity studies, mice were inoculated with 5×10^5 cancer cells suspended in 30 μL sterile PBS. B16F10 cells were inoculated intradermally into the left flank of each C57BL/6 mouse. MC38 cells were inoculated subcutaneously into the left flank of each C57BL/6 mouse. Similarly, CT26 cells were

inoculated subcutaneously into the left flank of each BALB/c mouse. For the rechallenge mouse model, 2×10^5 B16F10 cells suspended in 30 μL sterile PBS were inoculated intradermally into the right flank of each rechallenged C57BL/6 mouse.

Tumor measurements began at 5-9 days after inoculation, with measurements occurring every 2-3 days. Tumors were measured using digital calipers, and measurements were recorded as the largest measurements in each perpendicular direction (with respect to depth, length, and width). Tumor volumes were calculated as depth × length × width × (π/6). In all tumor models, mice were euthanized when tumor volume had reached 500 mm^3. Mouse tumor volumes were measured blindly. Mice were treated on days indicated in figures and in figure legends. Treatment groups were randomized across cages to mitigate cage effects. CpG ODN 1826 VacciGrade™ (Invivogen) was used in free CpG treatments. CpG-polymer treatments were prepared as described below. Treatments or saline controls were injected intratumorally, except for anti-PD-1 (Rat anti-mouse PD-1, Clone 29F.1A12, Bio X Cell) which was injected intraperitoneally. Intratumoral injections for all studies had a total volume of 30 μL consisting of either treatment or saline (PBS). Anti-PD-1 treatment consisted of 100 μg of anti-PD-1 in 100 μL PBS.

2.4 Serum Cytokine Kinetics

Mice with established B16F10 tumors were intratumorally injected on day 9 post B16F10 inoculation with either 50 μg of CpG equivalent CpG-p(PDS-Man) polymer, 50 μg free CpG ODN 1826, or sterile PBS. 50 μL of blood were collected via submandibular bleed into heparin coated tubes. Blood was collected at 2 hours, 6 hours, 24 hours, and 48 hours after injection. Blood was centrifuged at 10,000 RCF for 10 minutes, and serum harvested. Serum was stored at -80°C.

Subsequent cytokine analysis of serum was performed using LEGENDplex Mouse Cytokine Release Syndrome Panel (BioLegend) following manufacturer's instructions.

2.5 Intratumoral Cytokine Analysis

Mice with established B16F10 tumors were intratumorally injected on days 9 and 12 post B16F10 inoculation with either 10 μg of CpG equivalent CpG-p(PDS-Man) polymer, 10 μg free CpG ODN 1826, or sterile PBS. Mice were sacrificed on day 14, tumors were collected and snap frozen in liquid nitrogen. Tumors were stored at -80°C. Subsequently, they were homogenized in Tissue Protein Extraction buffer (T-PER, Thermo Fisher) with protease inhibitor tablets (Roche) added to the T-PER buffer. Homogenization of tumors was performed using FastPrep tissue homogenizer (MP Bio), using Lysing Matrix D tubes (MP Bio). Cytokine analysis was performed using LEGENDplex Mouse Cytokine Release Syndrome Panel (BioLegend) following manufacturer's instructions. Cytokine levels were normalized to total protein concentration. Protein concentration was measured using Pierce BCA Protein Assay (Thermo Fisher) according to the manufacturer's instructions.

2.6 Blood Chemistry Analysis

Mice with established B16F10 tumors were intratumorally injected on day 13 post B16F10 inoculation with either 10 μg or 50 μg of CpG equivalent CpG-p(PDS-Man) polymer, 10 μg or 50 μg free CpG ODN 1826, or sterile PBS. 200 μL of blood was collected 48 hours after injection (day 15) via submandibular bleed into heparin coated tubes. Blood was centrifuged at 10,000 RCF for 10 minutes and serum harvested. Serum was then diluted 2x, and blood chemistry markers were determined using Vet Axcel blood chemistry analyzer (Alfa Wasserman) using manufacturer's instructions.

2.7 Statistical Analysis

Statistical analysis was performed using GraphPad Prism V9. For survival analyses pairwise log-rank (Mantel-Cox) tests were used and survival curves were directly compared to each other without further correction. For multiple comparisons, one way ANOVA was used followed by a Tukey post hoc test. For direct comparisons between two groups an unpaired t-test was used.

2.8 Polymer and Conjugate Synthesis:

All chemicals and solvents were reagent grade and purchased from either Sigma-Aldrich or Fisher Scientific unless otherwise noted. Chemicals were used without any further purification unless otherwise noted. Reactions were carried out at room temperature and under inert nitrogen gas unless otherwise indicated. All NMR spectra were collected using a Bruker Avance III HD Nanobay 400 MHz NMR. NMR spectra were processed using MNova Software (MestreLab). High pressure liquid chromatography (HPLC) – mass spectrometry (MS) analysis was conducted on a 1260 Infinity HPLC (Agilent) coupled to an Agilent 6130 single quadrupole MS using a HYPERSIL GOLD C8 3UM 100 mm X 4.6 mm LC column (Thermo Scientific) using a gradient of mobile phases consisting of 0.1 M Triethylammonium Acetate Buffer in Water (Phase A) to 100% acetonitrile (Phase B). Mass analysis was conducted using negative mode electrospray ionization. Agilent OpenLab CDS software was then used to deconvolute the charge-state ladder into the target mass.

Gel electrophoresis was conducted using Mini-PROTEAN TGX Stain-Free Gel (Bio-Rad) and imaged using a BioRad ChemiDoc MP Molecular Imager. Biorad Precision Plus Protein™ Unstained Protein Standards were used a MW standards for gel electrophoresis. Gel permeation chromatography (GPC) was conducted using a Tosoh EcoSEC GPC system with Tosoh SuperAW3000 + Tosoh SuperAW4000 columns. Mobile phase consisted of N,N-dimethylformamide (DMF) with 0.01 M LiBr at 50° C. Characterization analysis was conducted using EcoSec software (Tosoh) with InfinityLab EasiVial polymethyl methacrylate (PMMA) calibration standards. Preparatory size exclusion chromatography (SEC) was conducted using an ÄKTA-Avant 25 protein purification system (Cytiva) using a HiLoad 16/600 Superdex 75 pg

(Cytiva) size exclusion column with PBS as the mobile phase. UltraViolet-Visible Spectroscopy (UV/Vis) was conducted using a Nanodrop 2000 Spectrophotometer (Thermo Scientific).

Chemical abbreviations used: methanol (MeOH), methylene chloride (DCM), N,N-dimethylformamide (DMF), triethylamine (TEA), hexanes (Hex), Ethyl acetate (EtOAc), 2-Hydroxy-Propyl Methacrylate (HPMA), pyridyl disulfide (PDS), diethyl ether (Et_2O), dimethyl sulfoxide (DMSO), Polytetrafluoroethylene (PTFE), Fluorescein (FAM), ODN Oligodeoxynucleotide.

2.8.1 Synthesis of 1-(2-chloroethyl)-α-D-mannose (1)

1-(2-chloroethyl)-α-D-mannose (1). To a suspension of D-mannose (20.0 g, 111.1 mmol) in chloroethanol (80 mL, 827.4 mmol), acetyl chloride (8.7 mL, 122 mmol) was added dropwise at 0° C. Reaction was subsequently heated to 70° C for 4 hours. Reaction was cooled to room temperature and decanted into a 800 mL solution of ethyl acetate and DCM (3:1, v/v). The mixture was cooled at -20 ° C overnight, upon which a black gummy precipitate was formed. The supernatant was discarded, and the precipitate was redissolved in 800 mL ethanol, upon which 10 grams of activated charcoal was added. The suspension was mixed at room temperature for 2 hours

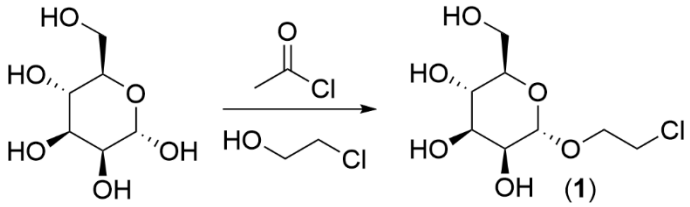

Scheme 1: Synthesis of 1-(2-chloroethyl)-α-D-mannose (1)

and filtered through celite. Ethanol was evaporated via rotary evaporator to yield a sticky brown

syrup (15.0 g, 55%): ^{1}H NMR (400 MHz, D_2O) δ 4.85 (d, J = 1.9 Hz, 1H), 3.91 (dt, J = 4.1, 2.0 Hz, 2H), 3.80 – 3.56 (m, 8H).

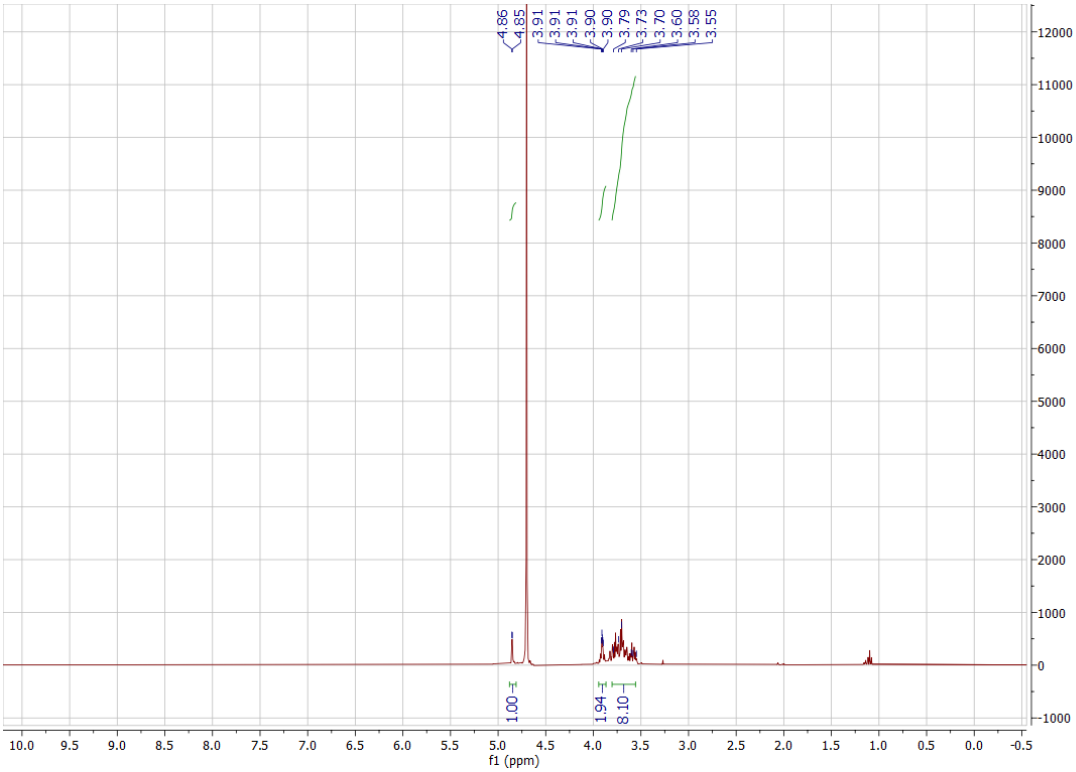

Figure 2: ^{1}H NMR (400 MHz, D_2O) of 1-(2-chloroethyl)-α-D-mannose (1)

2.8.2 Synthesis of 1-(2-azidoethyl)-α-D-mannose (2)

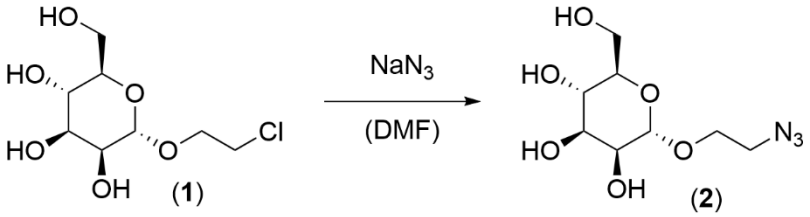

Scheme 2: Synthesis of 1-(2-azidoethyl)-α-D-mannose (2)

1-(2-azidoethyl)-α-D-mannose (2). Compound **1** (9.2 g, 38 mmol) was dissolved in 20 mL of DMF. Sodium azide (7.3 g, 112 mmol) was added to the solution. Suspension was heated to 90° C for 16 hours. Reaction was then cooled, filtered through celite, and solvent was removed via rotary evaporator. The residual substance was then absorbed onto silica gel and purified via flash chromatography (DCM : MeOH 9:1, v/v), to yield a brown syrup (4.55 g, 48%): ^{1}H NMR (400 MHz, D_2O) δ 4.84 (d, J = 1.8 Hz, 1H), 3.90 (dd, J = 3.5, 1.8 Hz, 1H), 3.87 – 3.36 (m, 9H).

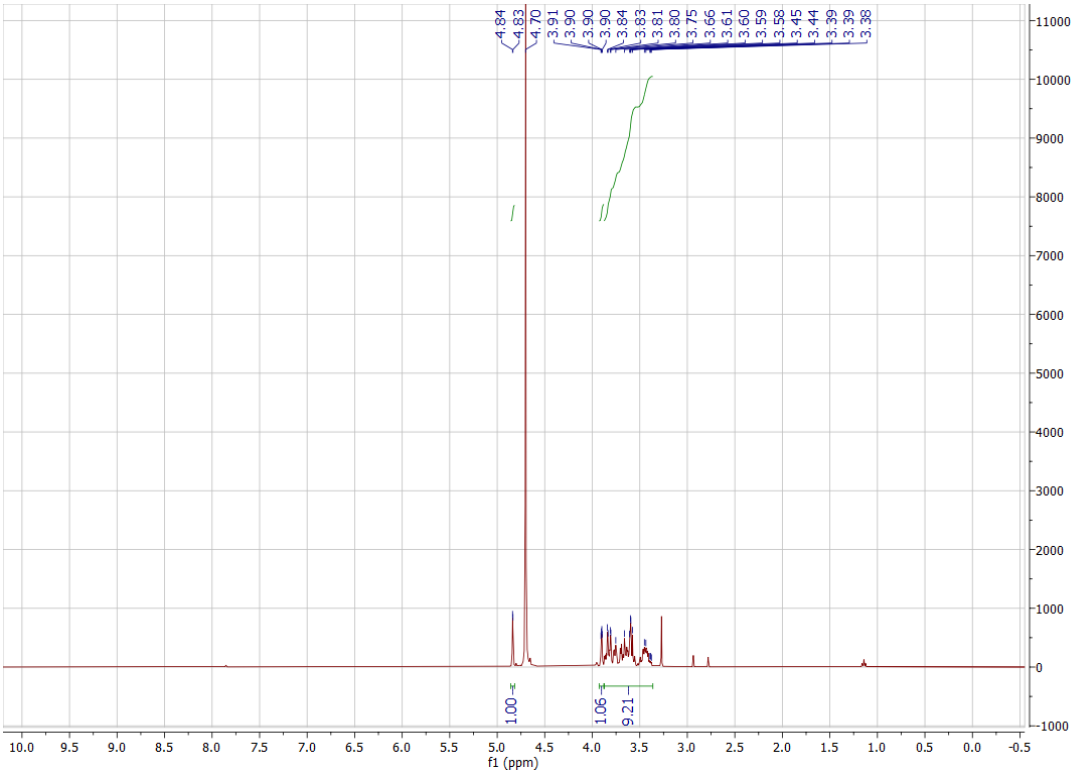

Figure 3: ^{1}H NMR (400 MHz, D_2O) of 1-(2-azidoethyl)-α-D-mannose (2)

2.8.3 Synthesis of 1-(2-aminoethyl)-α-D-mannose (3)

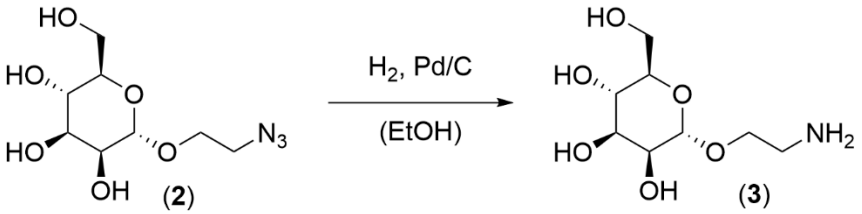

Scheme 3: Synthesis of 1-(2-aminoethyl)-α-D-mannose (3)

1-(2-aminoethyl)-α-D-mannose (3). Compound **2** (2.0 g, 8.0 mmol) was dissolved in 20 mL of ethanol, to which 10% palladium on carbon (200 mg) was added. 3 large hydrogen filled balloons provided positive hydrogen pressure to reaction vessel. Reaction was stirred overnight at room temperature and subsequently filtered through celite. Solvent was removed via rotary evaporator to yield a sticky syrup (1.7 g, 95%): ^{1}H NMR (400 MHz, D_2O) δ 4.78 (d, J = 1.8 Hz, 1H), 3.92 – 3.85 (m, 1H), 3.84 – 3.63 (m, 6H), 3.50 – 3.39 (m, 1H), 2.86 – 2.69 (m, 2H).

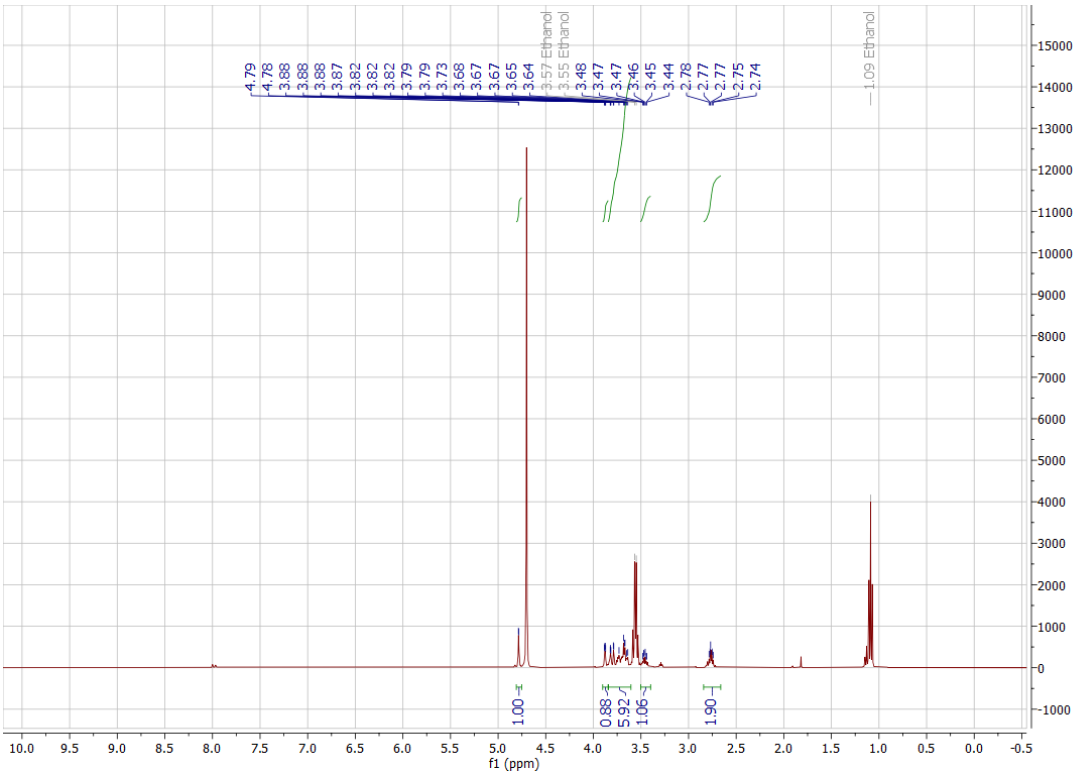

Figure 4: ^{1}H NMR (400 MHz, D_2O) of 1-(2-aminoethyl)-α-D-mannose (3)

2.8.4 Synthesis of N-[2-(α-D-mannose)ethyl] methacrylamide (4)

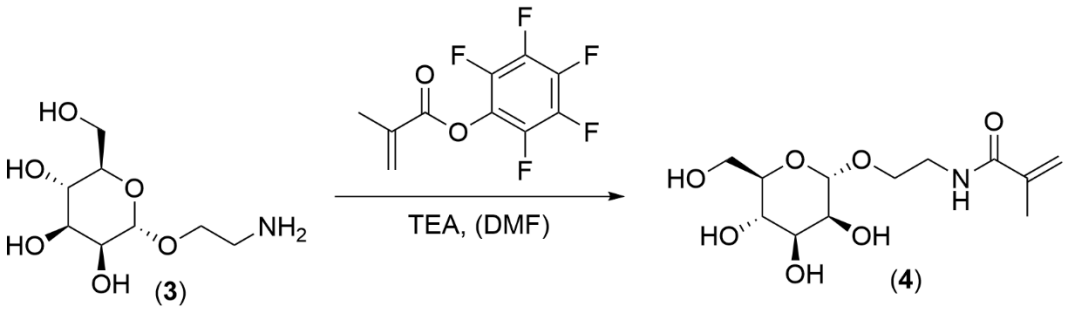

Scheme 4: N-[2-(α-D-mannose)ethyl] methacrylamide (4)

N-[2-(α-D-mannose)ethyl] methacrylamide (4). Compound **3** (2.0 g, 8.96 mmol) was dissolved in DMF (15 mL). To this, triethylamine (TEA), (1.4 mL, 9.86 mmol) was added. Mixture was cooled to 0° C, and pentafluoro-phenyl methacrylate was added dropwise to the reaction. Reaction was stirred at 0° C for 30 minutes and subsequently stirred at room temperature for 2 hours. The solvent was removed via rotary evaporator and the residual adsorbed onto silica gel. Flash chromatography (DCM : MeOH 9:1, v/v), yielded a pale yellow syrup (1.87 g, 72%) which was immediately dissolved in DMF to prevent polymerization: ^{1}H NMR (400 MHz, D_2O) δ 5.61 (t, J = 1.0 Hz, 1H), 5.38 (t, J = 1.3 Hz, 1H), 4.79 (d, J = 1.7 Hz, 1H), 3.85 (dd, J = 3.4, 1.8 Hz, 1H), 3.76 – 3.32 (m, 9H), 1.85 (t, J = 1.3 Hz, 3H).

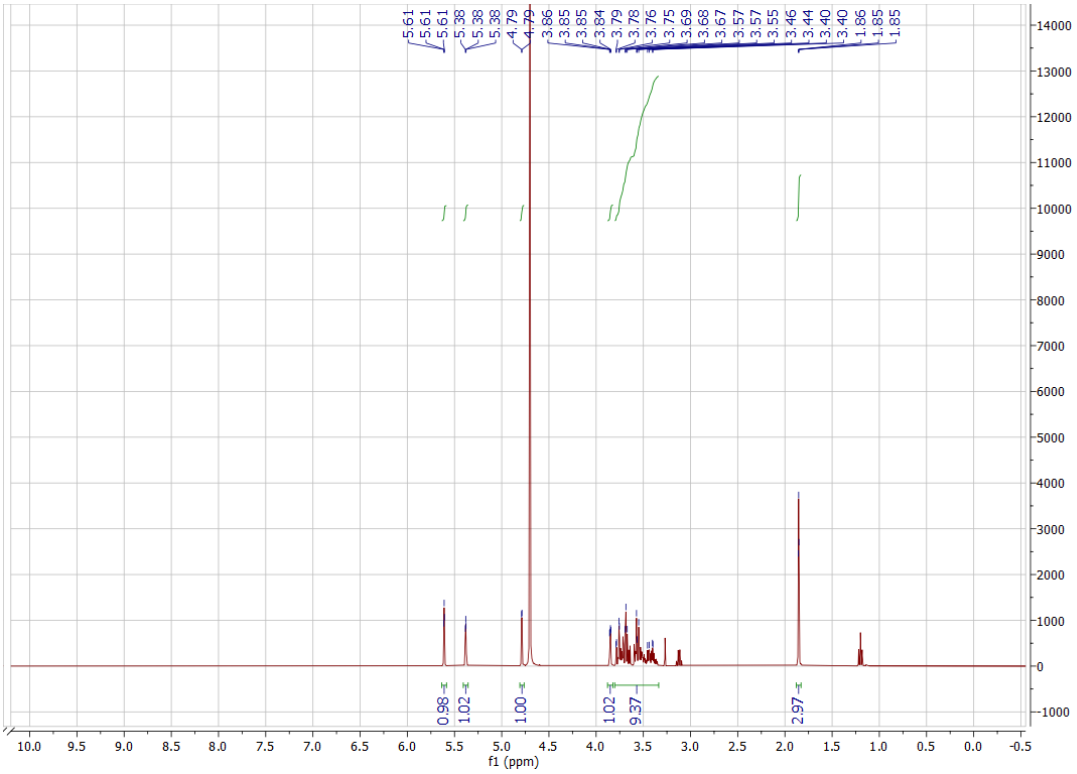

Figure 5: ^{1}H NMR (400 MHz, D_2O) of N-[2-(α-D-mannose)ethyl] methacrylamide (4)

2.8.5 Synthesis of N-(2-(pyridin-2-yldisulfaneyl)thyl)methacrylamide (5)

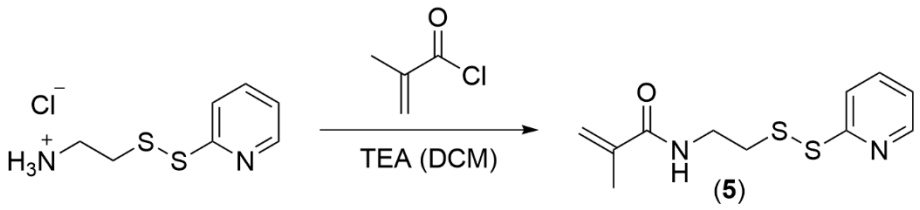

Scheme 5: Synthesis of N-(2-(pyridin-2-yldisulfaneyl)thyl)methacrylamide (5)

N-(2-(pyridin-2-yldisulfaneyl)ethyl)methacrylamide (5). S-(2-Pyridylthio)cysteamine hydrochloride (AmBeed) (300 mg, 1.35 mmol) was dissolved in 10 mL of DCM. Triethylamine (585 µL, 4.05 mmol) was then added, and the reaction was cooled to 0° C. Subsequently, methacryloyl chloride (160 µL, 1.6 mmol) was added dropwise. Reaction was stirred at 0° C for 1 hour. Reaction was then filtered to remove salt precipitates, following which solvent removed via rotary evaporator. Residual was adsorbed onto silica gel. Flash chromatography (Hex : EtOAc 2:1,

v/v) provided light brown oil (226 mg, 66%): ^{1}H NMR (400 MHz, $CDCl_3$) δ 8.44 (d, J = 4.0 Hz, 1H), 7.63 – 7.53 (m, 3H), 7.11 (ddd, J = 7.3, 4.9, 1.1 Hz, 1H), 5.78 (s, 1H), 5.34 (s, 1H), 3.57 (q, J = 6.0 Hz, 2H), 2.95 – 2.87 (m, 2H), 2.03 – 1.96 (m, 3H).

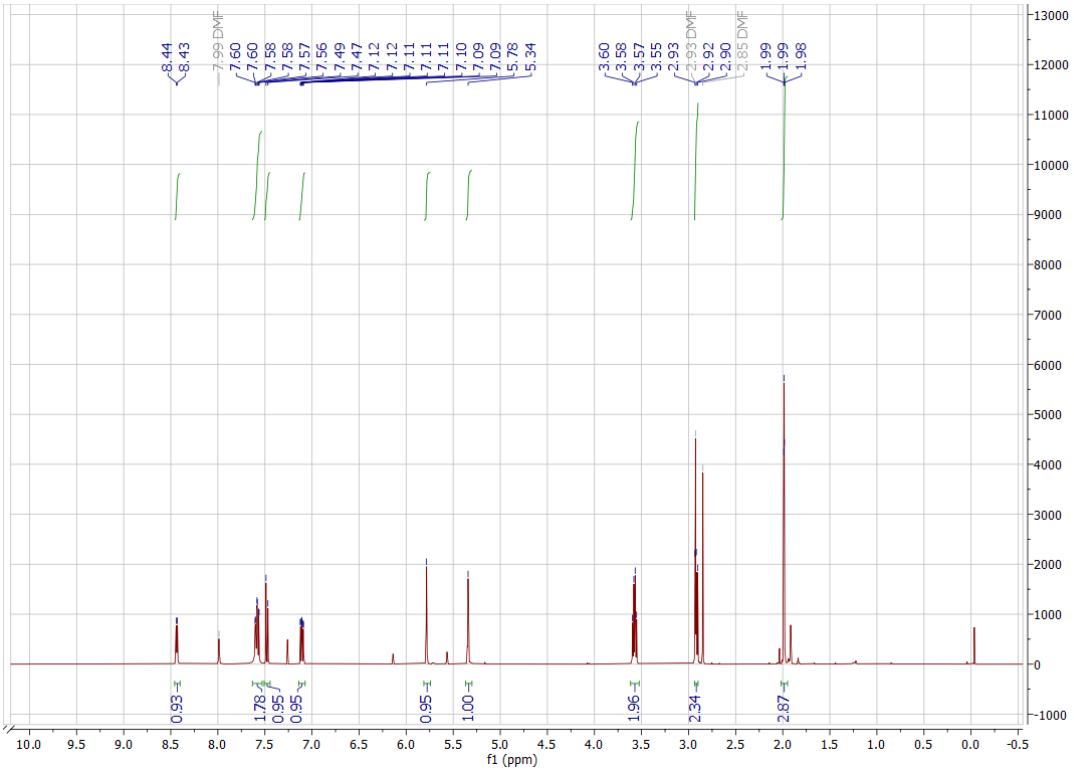

Figure 6: ^{1}H NMR (400 MHz, $CDCl_3$) of N-(2-(pyridin-2-yldisulfaneyl)ethyl)methacrylamide (5)

2.8.6 Synthesis of 2-(2-(2-(2-azidoethoxy)ethoxy)ethoxy)ethyl 4-cyano-4-(((dodecylthio)carbonothioyl)thio)pentanoate (6)

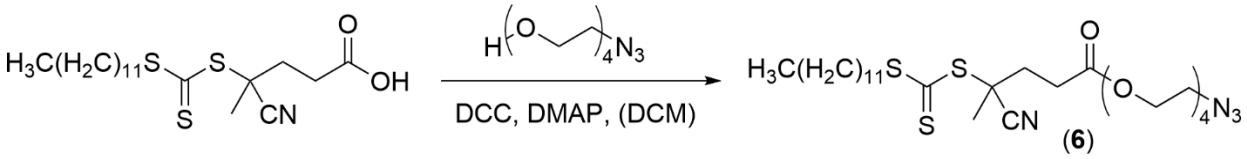

Scheme 6: Synthesis of 2-(2-(2-(2-azidoethoxy)ethoxy)ethoxy)ethyl 4-cyano-4-(((dodecylthio)carbonothioyl)thio)pentanoate (6)

2-(2-(2-(2-azidoethoxy)ethoxy)ethoxy)ethyl-4-cyano-4-(((dodecylthio)carbonothioyl)thio)pentanoate (6). A solution was made with 4-4-cyano-4-(((dodecylthio)carbonothioyl)thio)pentanoic acid (460 mg, 1.14 mmol), 2-(2-(2-(2-azidoethoxy)ethoxy)ethoxy)ethan-1-ol (Broadpharm) (500 mg, 2.28 mmol), 4-Dimethylaminopyridine (7 mg, 0.056 mmol) in DCM. Solution was cooled to 0° C. Subsequently, a solution of N,N'-Dicyclohexylcarbodiimide (258 mg, 1.25 mmol) in 5 mL DCM was added dropwise to the solution containing acid and alcohol. Reaction was subsequently warmed to room temperature and stirred overnight. Reaction was filtered to remove precipitates, and crude reaction was adsorbed onto silica gel. Flash chromatography (Hex : EtOAc 2:1, v/v) yielded a yellow oil (551 mg, 80%). ^{1}H NMR (400 MHz, $CDCl_3$) δ 4.29 – 4.22 (m, 2H), 3.76 – 3.59 (m, 12H), 3.39 (t, J = 5.1 Hz, 2H), 3.36 – 3.28 (m, 2H), 2.70 – 2.62 (m, 2H), 2.57 – 2.47 (m, 1H), 2.38 (ddd, J =

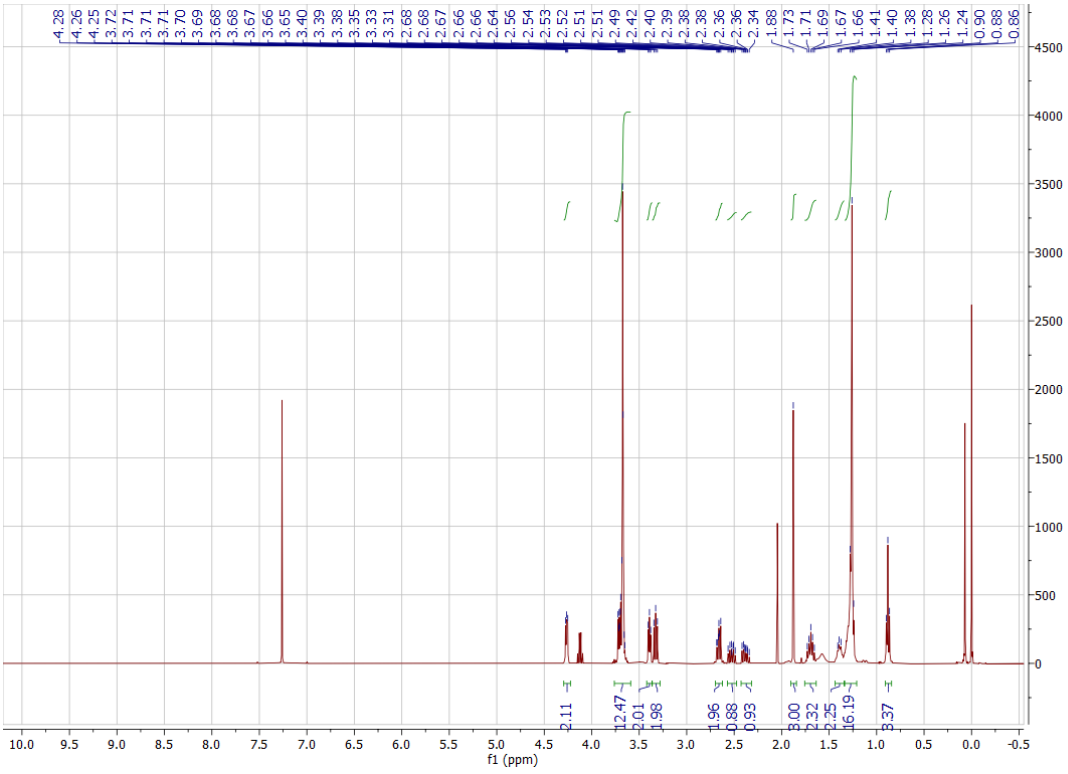

Figure 7: ^{1}H NMR (400 MHz, $CDCl_3$) of 2-(2-(2-(2-azidoethoxy)ethoxy)ethoxy)ethyl-4-cyano-4-(((dodecylthio)carbonothioyl)thio)pentanoate (6)

14.3, 9.3, 7.0 Hz, 1H), 1.88 (s, 3H), 1.69 (p, J = 7.4 Hz, 2H), 1.44 – 1.34 (m, 2H), 1.26 (s, 16H), 0.91 – 0.84 (m, 3H).

2.8.7 Synthesis of p(PDS-Man) (7)

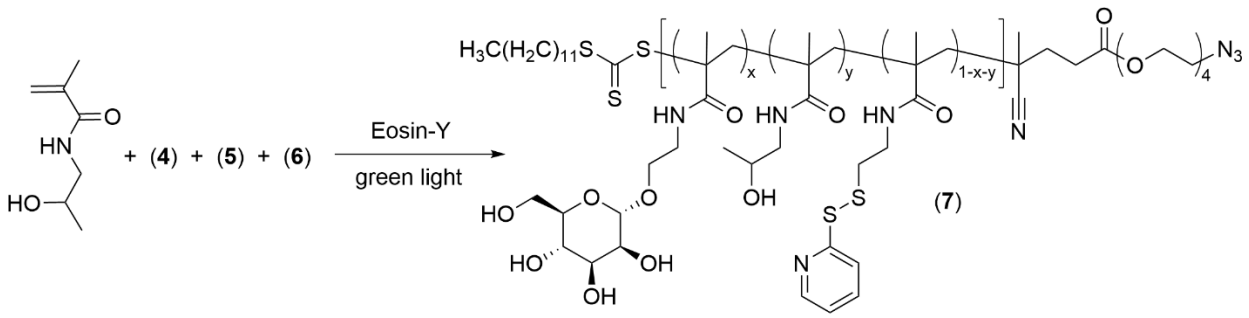

Scheme 7: Synthesis of p(PDS-Man) (7)

p(PDS-Man) (7). A solution was made of mannose monomer (**4**) (123 mg, 0.42 mmol), PDS monomer (**5**) (56 mg, 0.21 mmol), chain transfer agent (**6**) (12.0 mg, 0.02 mmol), and HPMA (freshly recrystallized from acetone) (150 mg, 1.05 mmol) in 2.0 mL DMSO. To this solution, 28 μL of a DMSO solution containing photoinitiator Eosin-Y (10 mg/mL) was added (0.28 mg, 0.4 μmol total Eosin-Y). Solution containing reactant and photoinitiator was filtered through a PTFE 0.2 μm membrane syringe filter and placed in a Schlenk tube. The tube was degassed using 3 freeze-pump-thaw cycles. The tube was subsequently placed inside green LED strip lights and wrapped with foil. Reaction was stirred with green lighting at room temperature for 16 hours. Polymer was then precipitated into 50 mL of cold mixture containing Et_2O : MeOH 20:1, (v/v). The polymer precipitate was centrifuged at 2,500 RCF for 3 minutes and then redissolved in 4 mL MeOH. This process was repeated 3 times. Residual solvents were removed under reduced pressure to yield 180 mg of polymer. GPC characterization (PMMA standards): number average molecular weight of 8,387 Dalton, and a weight average molecular weight of 10,642 Dalton. Number of PDS units per polymer was determined to be 7.2 by UV/Vis measurements at 343 nm

of reduced polymer (measuring pyridine-2-thione with an extinction coefficient of 8080 $M^{-1}cm^{-1}$). Representative ^{1}H NMR spectrum is shown (Figure 8).

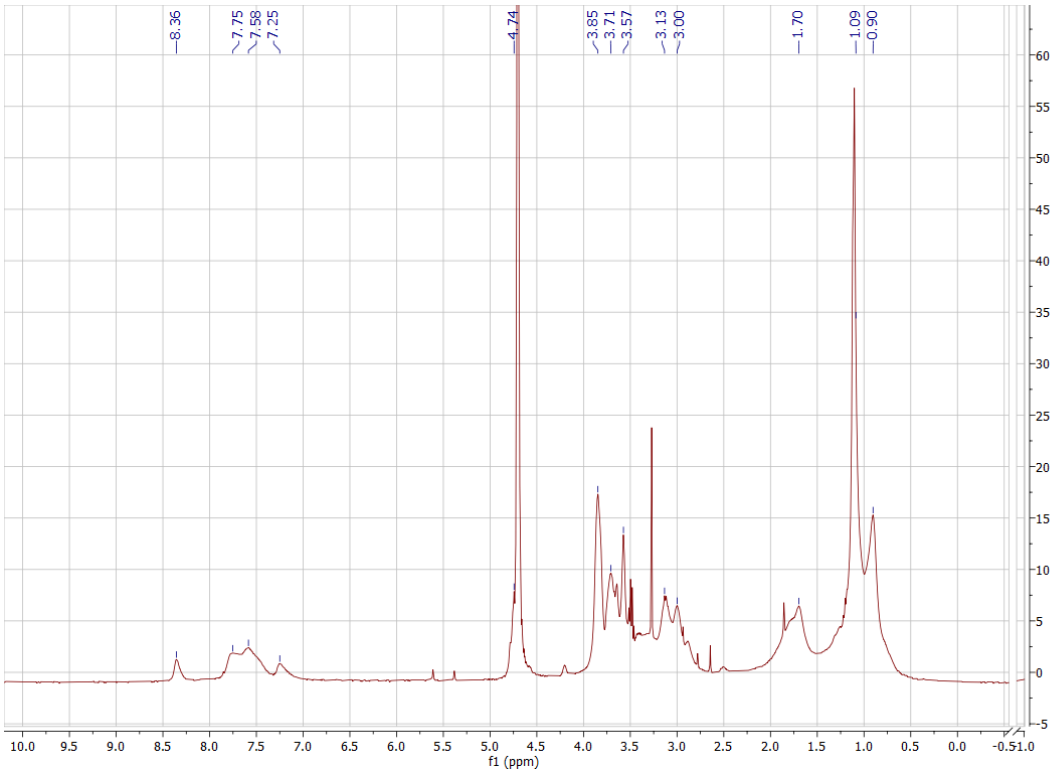

Figure 8: ^{1}H NMR (400 MHz, D_2O) of p(PDS-Man) (7)

2.8.8 Synthesis of p(PDS) (8)

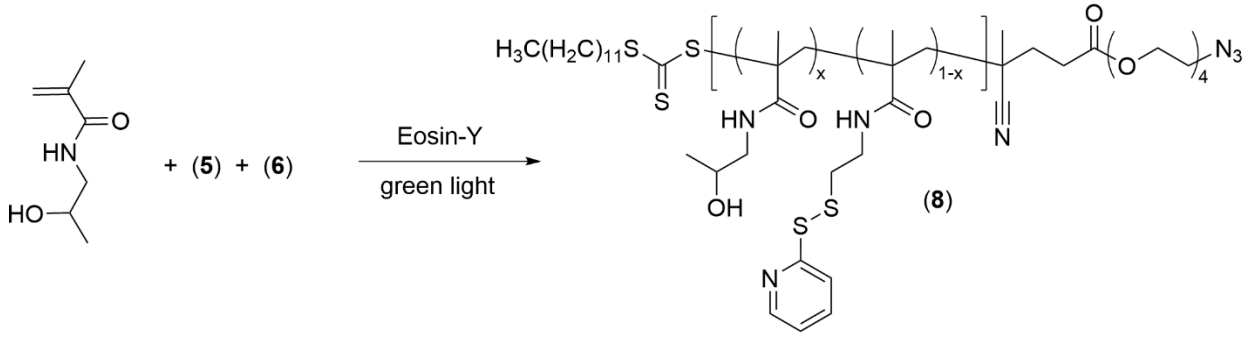

Scheme 8: Synthesis of p(PDS) (8)

p(PDS) (8). A solution was made of PDS monomer (**5**) (36 mg, 0.14 mmol), chain transfer agent (**6**) (8.5 mg, 0.014 mmol), and HPMA (freshly recrystallized from acetone) (100 mg, 70

mmol) in 2.0 mL DMSO. To this solution, 20 µL of a DMSO solution containing photoinitiator Eosin-Y (10 mg/mL) was added (0.20 mg, 0.4 µmol total Eosin-Y). Solution containing reactant and photoinitiator was filtered through a PTFE 0.2 µm membrane syringe filter and placed in a Schlenk tube. The tube was degassed using 3 freeze-pump-thaw cycles. The tube was subsequently placed inside green LED strip lights and wrapped with foil. Reaction was stirred with green lighting at room temperature for 15 hours. Polymer was then precipitated into 50 mL of cold mixture containing Et_2O : MeOH 20:1, (v/v). The polymer precipitate was centrifuged at 2,500 RCF for 3 minutes and then redissolved in 4 mL MeOH. This process was repeated 3 times. Residual solvents were removed under reduced pressure to yield 100 mg of polymer. GPC characterization (PMMA standards): number average molecular weight of 5,844 Dalton, and a weight average molecular weight of 7,895 Dalton. Number of PDS units per polymer was determined to be 6.8 by UV/Vis measurements at 343 nm of reduced polymer (measuring pyridine-

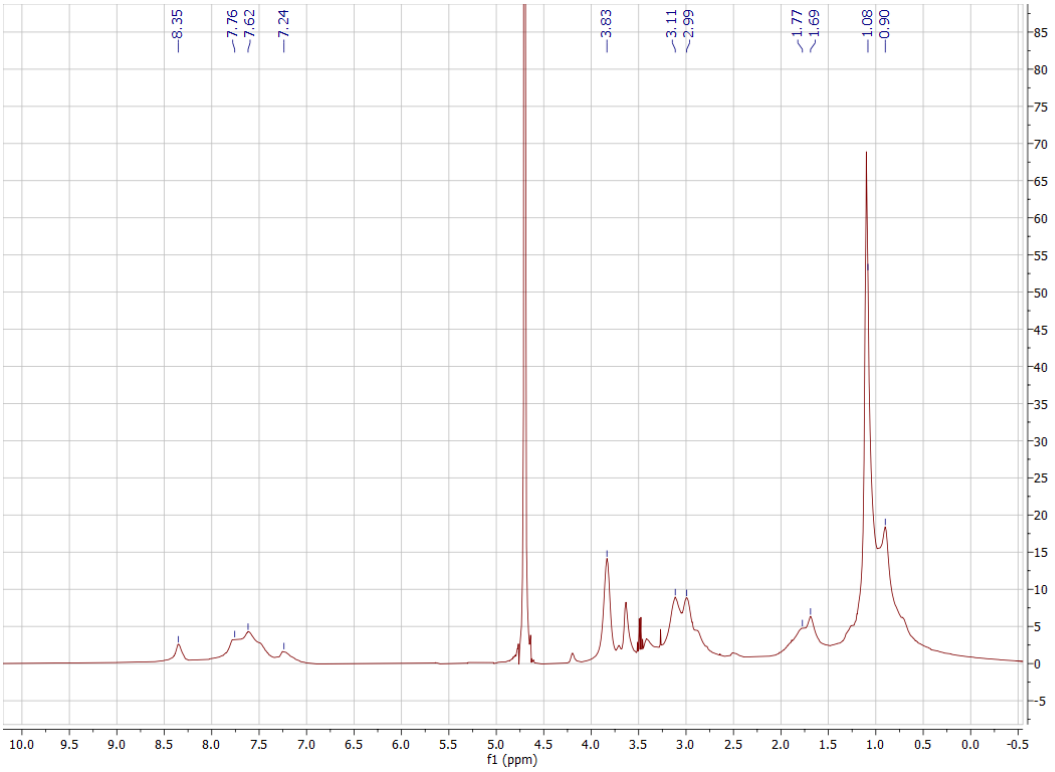

Figure 9: ^1H NMR (400 MHz, D_2O) of p(PDS) (8)

2-thione with an extinction coefficient of 8080 $M^{-1}cm^{-1}$). Representative ^{1}H NMR spectrum is shown (Figure 9).

2.8.9 Synthesis of p(Man) (9)

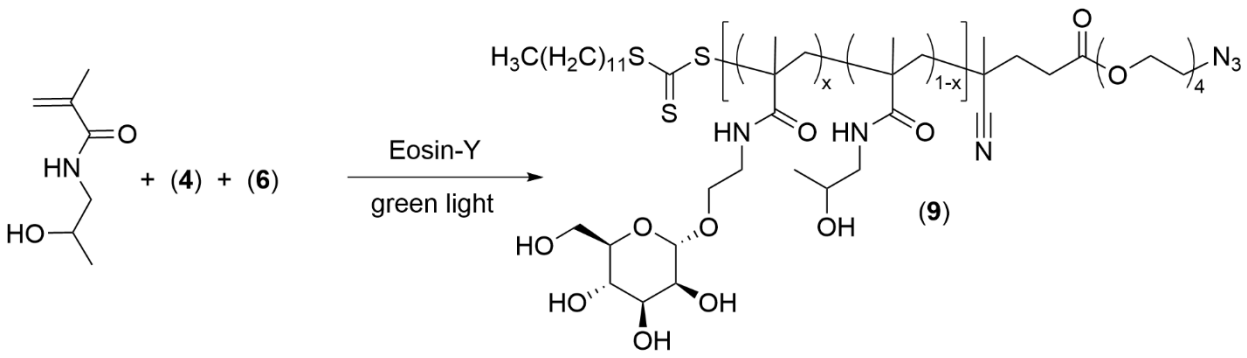

Scheme 9: Synthesis of p(Man) (9)

p(Man) (9). A solution was made of mannose monomer (**4**) (82 mg, 0.28 mmol), chain transfer agent (**6**) (8.5 mg, 0.014 mmol), and HPMA (freshly recrystallized from acetone) (100 mg, 70 mmol) in 2.0 mL DMSO. To this solution, 20 μL of a DMSO solution containing photoinitiator Eosin-Y (10 mg/mL) was added (0.20 mg, 0.4 μmol total Eosin-Y). Solution containing reactant and photoinitiator was filtered through a PTFE 0.2 μm membrane syringe filter and placed in a Schlenk tube. The tube was degassed using 3 freeze-pump-thaw cycles. The tube was subsequently placed inside green LED strip lights and wrapped with foil. Reaction was stirred with green lighting at room temperature for 16 hours. Polymer was then precipitated into 50 mL of cold mixture containing Et_2O : MeOH 20:1, (v/v). The polymer precipitate was centrifuged at 2,500 RCF for 3 minutes and then redissolved in 4 mL MeOH. This process was repeated 3 times. Residual solvents were removed under reduced pressure to yield 120 mg of polymer. GPC characterization (PMMA standards): number average molecular weight of 7,116 Dalton, and a

weight average molecular weight of 9,888 Dalton. Representative ^{1}H NMR spectrum is shown (Figure 10).

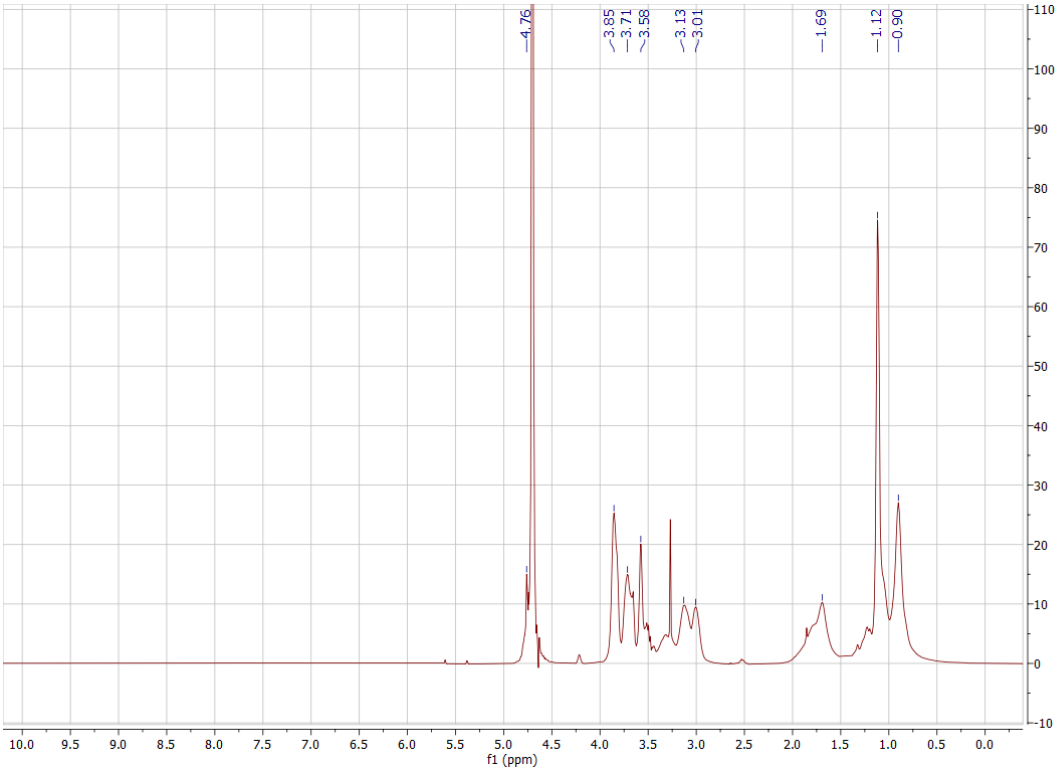

Figure 10: ^{1}H NMR (400 MHz, D_2O) of p(Man) (9)

2.8.10 Synthesis of p(HPMA) (10)

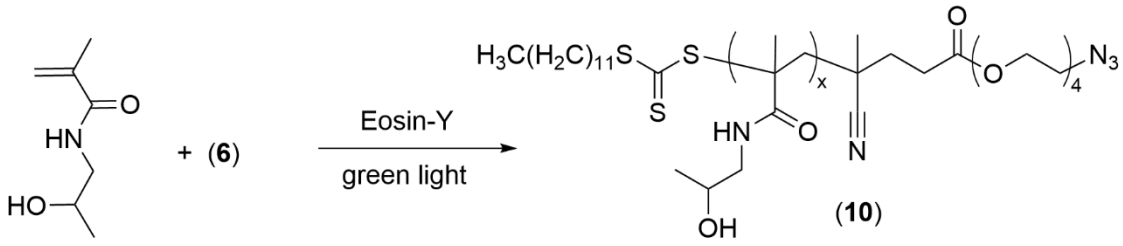

Scheme 10: Synthesis of p(HPMA) (10)

p(HPMA) (10). To A solution was made chain transfer agent (**6**) (8.5 mg, 0.014 mmol), and HPMA (freshly recrystallized from acetone) (100 mg, 70 mmol) in 2.0 mL DMSO. To this solution, 20 µL of a DMSO solution containing photoinitiator Eosin-Y (10 mg/mL) was added

(0.20 mg, 0.4 μmol total Eosin-Y). Solution containing reactant and photoinitiator was filtered through a PTFE 0.2 μm membrane syringe filter and placed in a Schlenk tube. The tube was degassed using 3 freeze-pump-thaw cycles. The tube was subsequently placed inside green LED strip lights and wrapped with foil. Reaction was stirred with green lighting at room temperature for 16 hours. Polymer was then precipitated into 50 mL of cold mixture containing Et_2O : MeOH 20:1, (v/v). The polymer precipitate was centrifuged at 2,500 RCF for 3 minutes and then redissolved in 4 mL MeOH. This process was repeated 3 times. Residual solvents were removed under reduced pressure to yield 1 mg of polymer. GPC characterization (PMMA standards): number average molecular weight of 5,776 Dalton, and a weight average molecular weight of 6,944 Dalton. Representative ^{1}H NMR spectrum is shown (Figure 11).

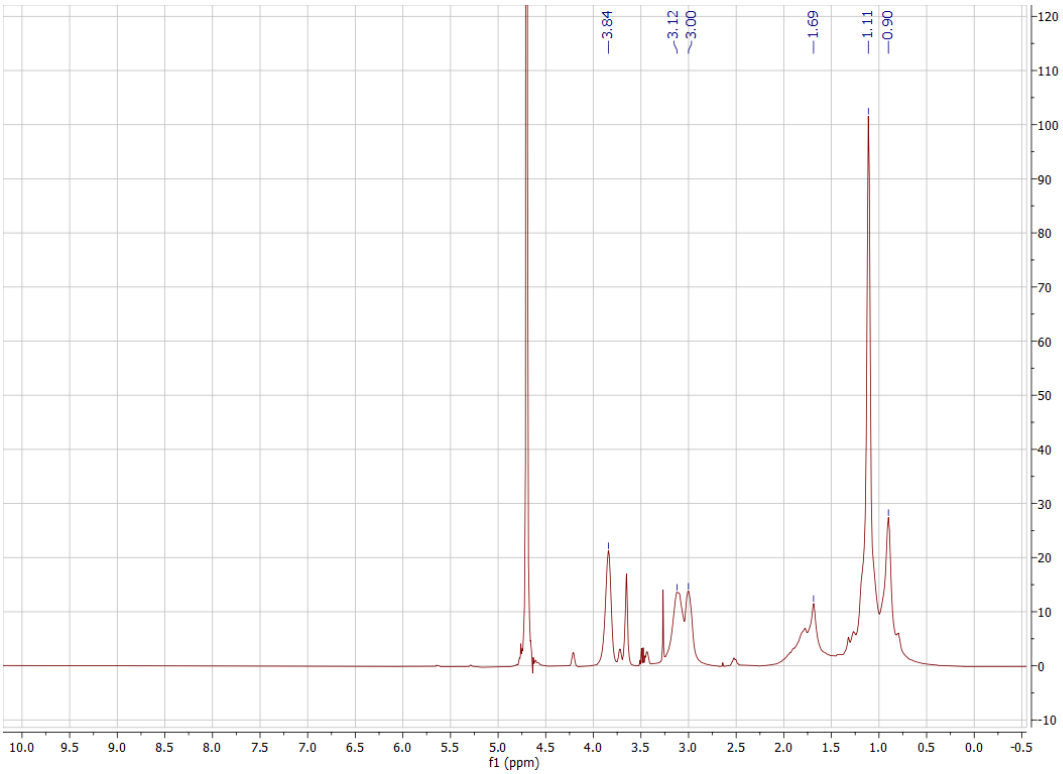

Figure 11: ^{1}H NMR (400 MHz, D_2O) of p(HPMA) (10)

2.8.11 Synthesis of DBCO-CpG-Fam (11)

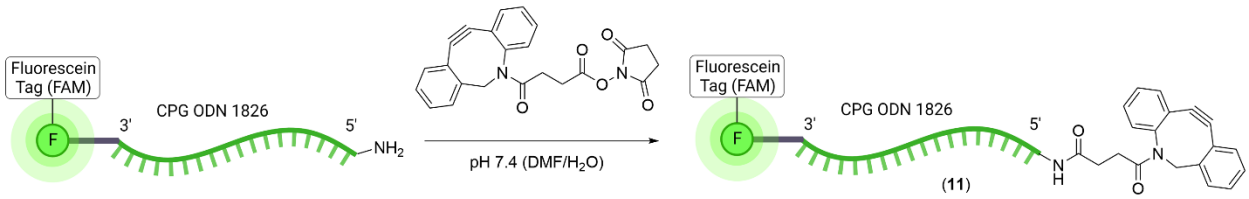

Scheme 11: Synthesis of DBCO-CpG-Fam (11)

Modified single stranded CpG-ODN1826, amine-C6-5′-TCCATGACGTTCCTGACGTT-3′-6-FAM (amine-CPG-FAM), with a phosphorothioated backbone was purchased from Integrated DNA Technologies and dissolved at 10 mg/mL in PBS. (2,5-dioxopyrrolidin-1-yl) 4-(2-azatricyclo[10.4.0.04,9]hexadeca-1(16),4,6,8,12,14-hexaen-10-yn-2-yl)-4-oxobutanoate (DBCO-NHS) was dissolved in DMF at 100 mg/mL. 1 mL of amine-CPG-FAM solution (10 mg) was added to 1 mL of DMF, followed by 100 µL of potassium phosphate buffer (pH 8.0). 20 molar equivalents of DBCO-NHS in DMF was then added to amine-CPG-FAM mixture. Solution was then stirred in the dark at room temperature for 2 hours. Reaction was monitored for completion using HPLC-MS (Figure 12; A and B), with target mass found to

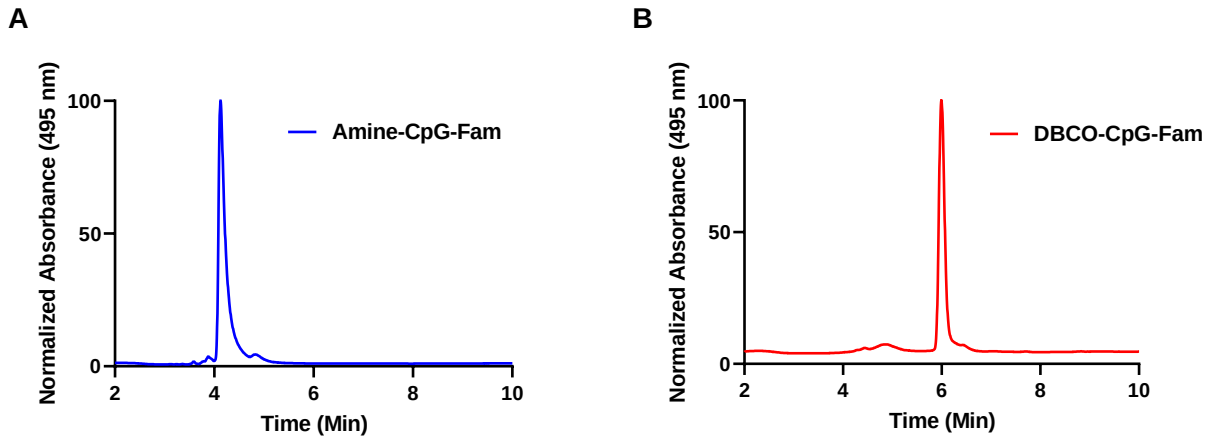

Figure 12: HPLC analysis of DBCO-CpG-Fam reaction

(A) HPLC trace of unconjugated amine-CpG-Fam demonstrates a sharp peak at 4 minutes. (B) HPLC trace of conjugated DBCO-CpG-Fam yields a sharp peak at 6 minutes.

7,400.2 Dalton using charge deconvolution. Reaction was then diluted to 8 mL using PBS, and excess DBCO-NHS was removed using Zeba desalting columns with a 7K molecular weight cutoff (MWCO) (Thermo Scientific). Solution was then filtered again using Zeba filtration (7K MWCO) for a total of two rounds of Zeba filtration. Subsequently, solution was concentrated via Amicon centrifugal concentrator with a MWCO of 3 kDa (MilliporeSigma™) to a final volume of 1 mL. DBCO-CpG-Fam (**11**) was then immediately used for conjugation with polymer.

2.8.12 Synthesis and Characterization of CpG-Polymer Conjugates

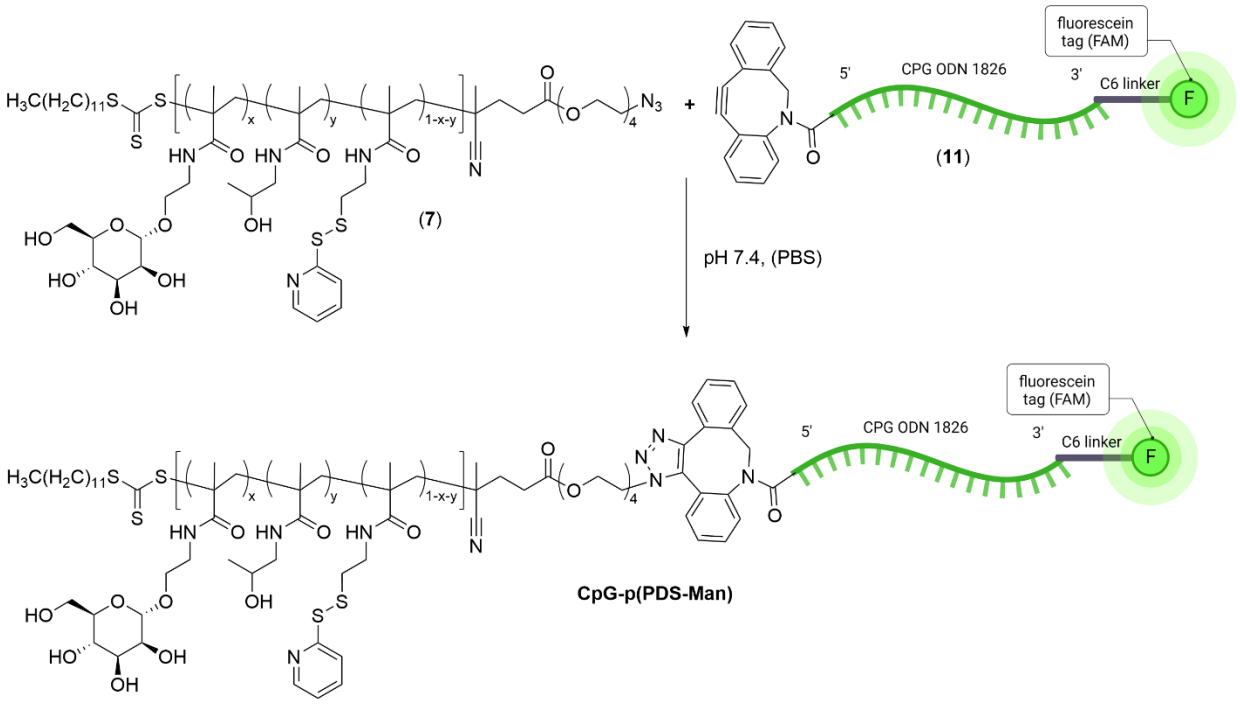

Scheme 12: Synthesis of CpG-Polymer Conjugates (CpG-p(PDS-Man shown)

General procedure for preparation of CpG-polymer conjugates: To a 1 mL solution of containing 7 mg DBCO-CpG-Fam (**11**) 3 molar equivalents of polymer in 1 mL PBS was added. The reaction mixture was stirred overnight in the dark at room temperature. Conjugation to polymer was confirmed as an increase in molecular weight via gel electrophoresis as (Figure 13),

CpG-polymer conjugate was purified via SEC. Fractions corresponding to CpG-polymer conjugate were pooled and concentrated via Amicon centrifugal concentrator with a MWCO of 10,000 Dalton (MilliporeSigma™) to yield purified CpG-polymer construct, with an average yield of 3 mg CpG (30%) after the two steps of DBCO conjugation to yield (**11**) including subsequent polymer conjugation and purification. Concentration of CpG in CpG-polymer conjugate was determined via UV/Vis measurements at 495 nm using an extinction coefficient of 75,000 $M^{-1}cm^{-1}$.

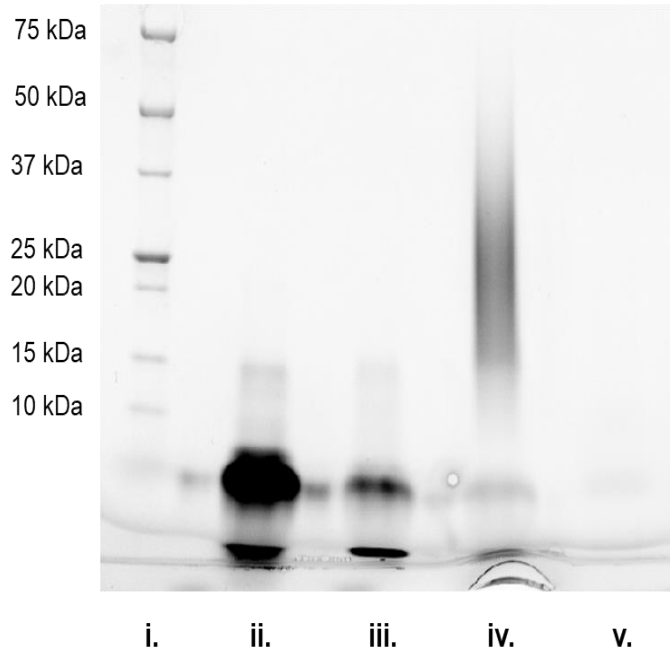

Figure 13: Gel electrophoresis analysis of conjugation reaction between CpG and polymer

(i) Precision protein standards (Biorad). (ii) amine-CpG-Fam. (iii) DBCO-CpG-Fam (11). (iv) CpG-p(PDS-Man) conjugation reaction (unpurified). (v) p(PDS-Man) alone was not visible with U/V imaging.
Similar results were obtained when conjugating DBCO-CpG-Fam to either p(PDS), p(Man), or p(HPMA).

CHAPTER 3:

RESULTS

3.1 Synthesis and Characterization of Cysteine-Reactive CpG-Polymer Conjugates

Based on earlier work with pyridyl disulfide, we hypothesized that we could apply this as well. We hypothesized that using PET-RAFT (photoinduced electron/energy transfer-reversible addition−fragmentation chain transfer, we were able synthesize four polymers. Our primary

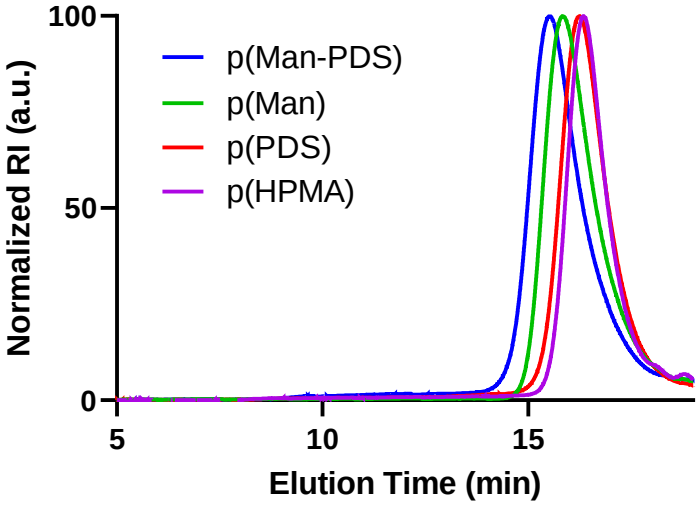

Figure 14: GpC elution profiles of polymers

p(Man-PDS), p(Man), p(PDS), and p(HPMA) have similar GPC elution profiles. As expected, p(Man-PDS) demonstrates the highest molecular weight while p(HPMA) demonstrates the lowest.

binding polymer, containing both PDS and mannose [p(PDS-Man)], can be synthesized utilizing PET-RAFT, with appropriate molecular weight and relatively low dispersity (Figure 14). Additionally, we synthesized a library of other control polymers lacking some or all of the side chains utilizing PET-RAFT. As illustrated (Figure 14) all four polymers displayed low dispersity

and appropriate number average and weight average molecular weight, commensurate with their feed ratios. Additionally, we found that all polymers were at least moderately water soluble.

Next, we sought to conjugate CpG. For this, we choose an orthogonal chemistry strategy, using a free end amine. To do this, we choose a copper free DBCO. Using NHS chemistry, we conjugated a DBCO moiety to the 5′ end of the CpG Oligodeoxynucleotide, which was readily detected via HPLC-MS analysis (Figure 12). Excess DBCO-NHS was readily removed using

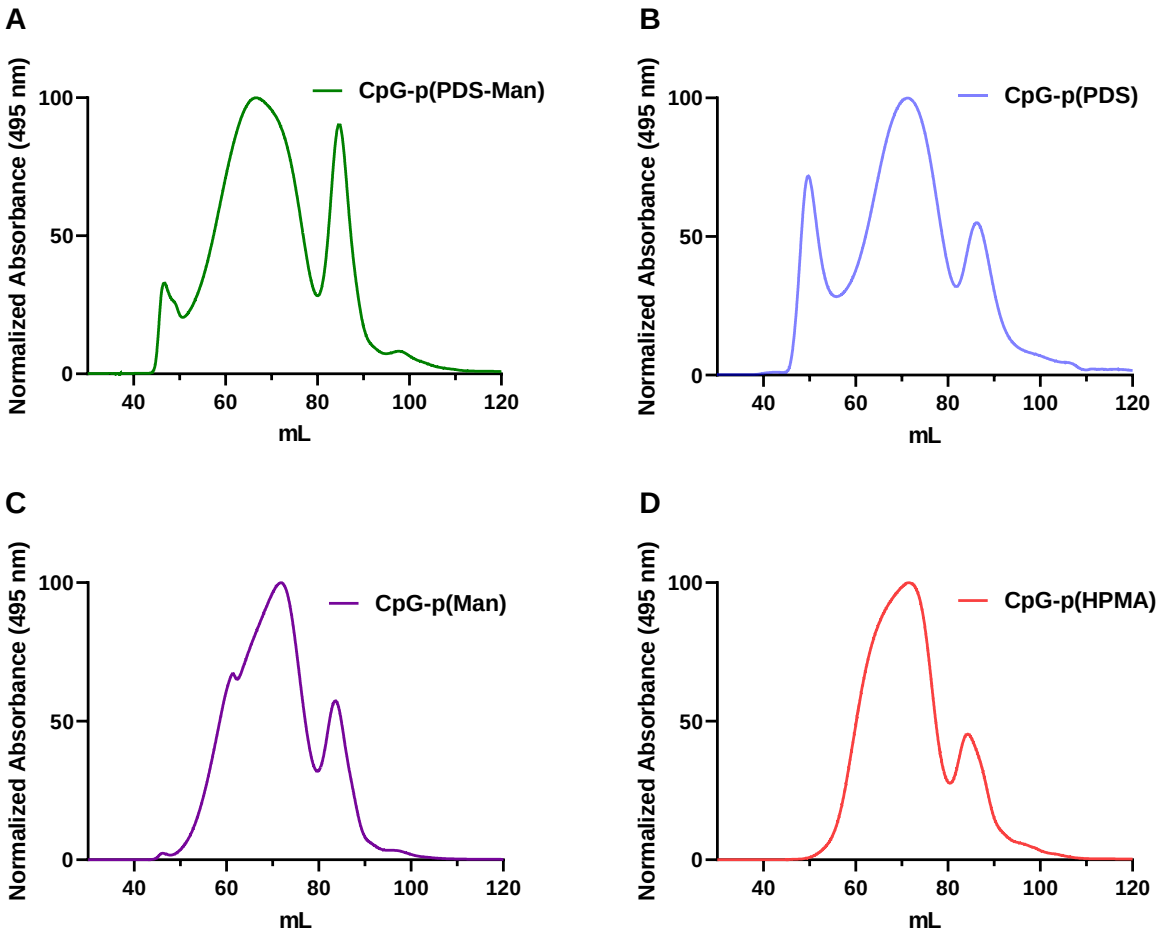

Figure 15: AKTA SEC traces of all CpG-polymer conjugates

(A) AKTA SEC of CpG-p(PDS-Man) conjugate. (B) AKTA SEC of CpG-p(PDS) conjugate. (C) AKTA SEC of CpG-p(Man) conjugate. (D) AKTA SEC of CpG-p(HPMA) conjugate. CpG-polymer conjugates containing PDS display a high molecular weight peak at ~ 45 mL corresponding to polymer cross-linking. Low molecular weight peak at ~ 85 mL corresponds to unreacted DBCO-CPG-FAM.

ZEBA spin columns. Conjugation of DBCO-CpG-Fam to our polymer of interest occurred readily using strain-promoted azide-alkyne cycloaddition. This allowed us to avoid using copper as a traditional catalyst to achieve azide-alkyne click chemistry cycloaddition. Consistent molecular shifts were observed using gel electrophoresis. By using fluorescence imaging looking for fluorescein in the polyacrylamide gel, we were able to observe molecular weight differences of the labeled CpG to monitor the conjugation reaction (figure 12). After the reaction was complete, CpG-polymer construct was purified using SEC to remove excess unconjugated DBCO-CpG-FAM or any remaining amine-CpG-FAM. As illustrated in Figure 15, SEC traces yielded purified construct between approximately 60-80 mL. As expected, the CpG-p(PDS-Man) conjugate (Figure 15A) demonstrated the largest molecular weight increase due to its largest polymer size (incorporating both PDS and mannose). Interestingly that there seemed to be sharp peaks in both PDS and PDS-Man which would correspond to crosslinking due to disulfide exchange. Both CpG-

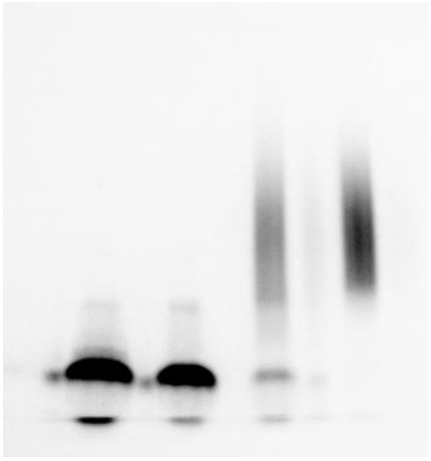

Figure 16: Gel electrophoresis analysis of purified construct

Polyacrylamide gel was fluorescently imaged to detect fluorescein. (i) amine-CpG-Fam. (ii) DBCO-CpG-Fam (11). (iii) CpG-p(PDS-Man) conjugation reaction (unpurified). (iv) purified p(PDS-Man) construct. Protein size standards as well as free polymer was not detectable with flourescant imaging. Similar results were obtained when conjugating DBCO-CpG-Fam to either p(PDS), p(Man), or p(HPMA).

p(Man) and CpG-p(HPMA) exhibited nice single peaks corresponding to CpG-polymer conjugate. Fractions were analyzed for purity using gel electrophoresis, and pure fractions were pooled and concentrated to yield a final product (as illustrated in Figure 16). Further disulfide reduction of CpG-polymers utilizing Dithiothreitol (DTT) and measuring absorbance at 343 nm demonstrated intact PDS functionality in CpG-p(PDS-Man) and CpG-p(PDS).

3.2 *In Vitro* Characterization of Cysteine-Reactive CpG-Polymer Conjugates

As a first pass to evaluate the biological activity of the CpG-polymer construct, we choose

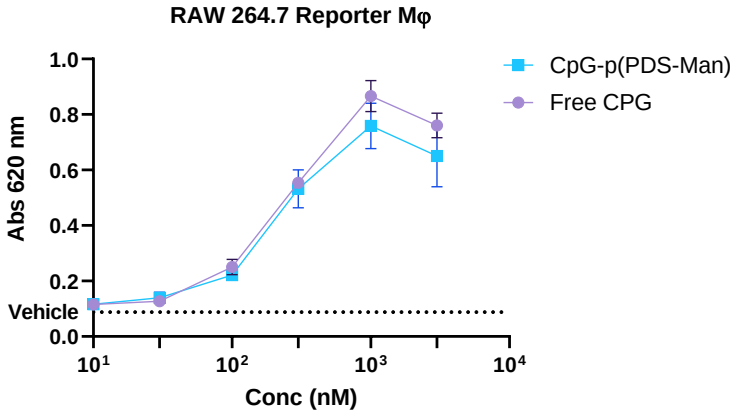

Figure 17: CpG-p(PDS-Man) activates macrophages in-vitro

Reporter RAW 264.7 macrophages were treated with different concentrations of either CpG-p(PDS-Man) or free CpG. CpG-p(PDS-Man) demonstrates a dose-response curve in an equimolar fashion to free CpG.

to validate our CpG-polymer construct on a mouse macrophage reporter cell line (RAW-Blue™ cells), which are derived from murine RAW 264.7 macrophages. The reporter cell line integrates a secreted embryonic alkaline phosphatase (SEAP) reporter which is inducible via NF-κB and AP-1. This cell line expresses many PRRs, including many TLRs, thus a useful tool for in-vitro characterization of TLRs. Levels of SEAP expressed upon activation can be measured using QUANTI-Blue™.

As illustrated in Figure 17, we found our CpG-p(PDS-Man) to be an effective immunostimulant, and that it retained its immunostimulatory properties after being conjugated to p(PDS-Man). We observed a dose dependent increase in activation from our CpG conjugate, and the activation range was almost identical to free (unbound) CpG.

Next, we wanted to demonstrate and characterize the immune-stimulatory activity of our CpG-polymer conjugates in a more representative model of APCs, and specifically of DCs. For

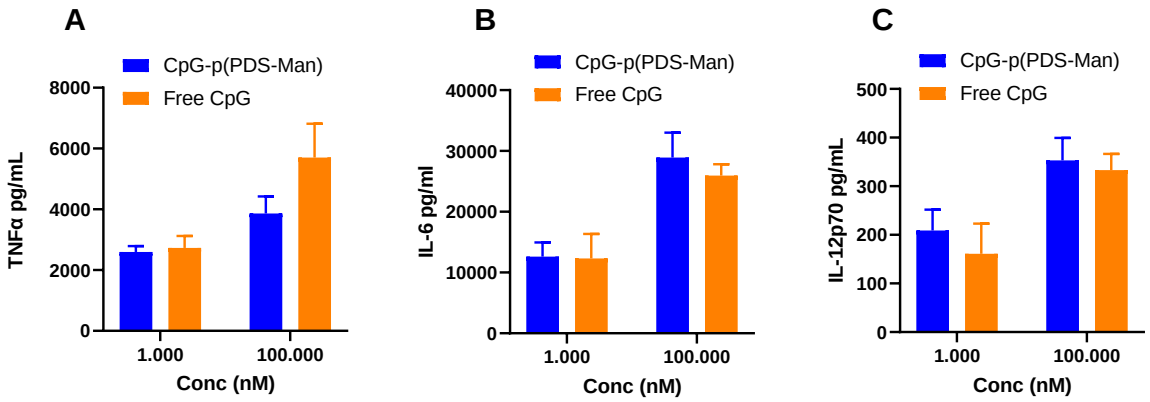

Figure 18: CpG-p(PDS-Man) actives BMDCs

CpG-p(PDS-Man) activates BMDCs in an equimolar fashion to free CpG at both 1 nM and 100 nM concentrations of agonist (CpG based). BMDCs were stimulated for 18 hours, and the supernatant was analyzed via ELISA for TNFα (A), IL-6 (B), and IL-12p70 (C). Columns and error bars indicate mean ± SEM; $n = 3$.

this we used BMDCs and characterized their proinflammatory cytokines with ELISA. As illustrated in Figure 18, we found the cytokine profile of our CpG-p(PDS-Man) conjugate to be as effective as unbound (free) CpG upon BMDC stimulation in an equimolar fashion.

Additionally, being that BMDCs express C-type lectins such as CD206 and C209, we wanted to see if there was an enhanced cytokine profile from our mannose containing CPG-p(Man) vs free CpG. As illustrated in figure 18 we were able to observe a significant increase with mannose when measured at 1 nM.

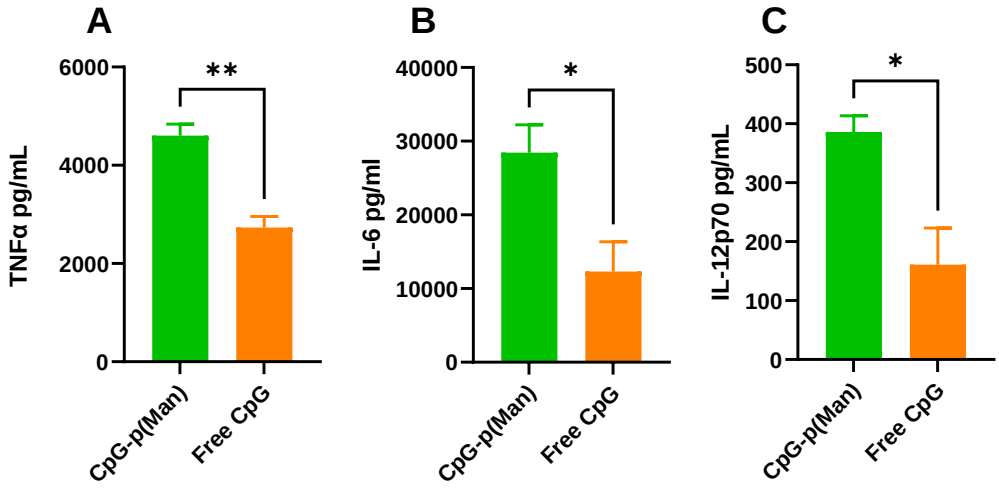

Figure 19: Mannose enhances BMDC activation at 1 nM

CpG-p(Man) enhances inflammatory cytokine secretion at 1 nM compared to free CpG. BMDCs were stimulated for 18 hours, and the supernatant was analyzed via ELISA for TNFα (A), IL-6 (B), and IL-12p70 (C). Columns and error bars indicate mean ± SEM; $n = 3$. Statistical tests utilized unpaired *t*-tests. *p < 0.05; **p < 0.01.

3.3 *In Vivo* Evaluation of CpG-p(PDS-Man) in MC38 Colon Carcinoma

Next, we sought to evaluate our CpG-p(PDS-Man) conjugate in a translationally relevant murine tumor model. For this, we choose the MC38 tumor model, a widely used preclinical model for colon cancer. The MC38 tumor model is useful preclinical model as it exhibits many similar characteristics of human colon cancer, including a high degree of genetic instability[72] and is seen an immune responsive model.

As illustrated in Figure 20 we found our CpG-p(PDS-Man) conjugate to eradicate established MC38 colon carcinoma. This was seen is a dose dependent manner, with our lower

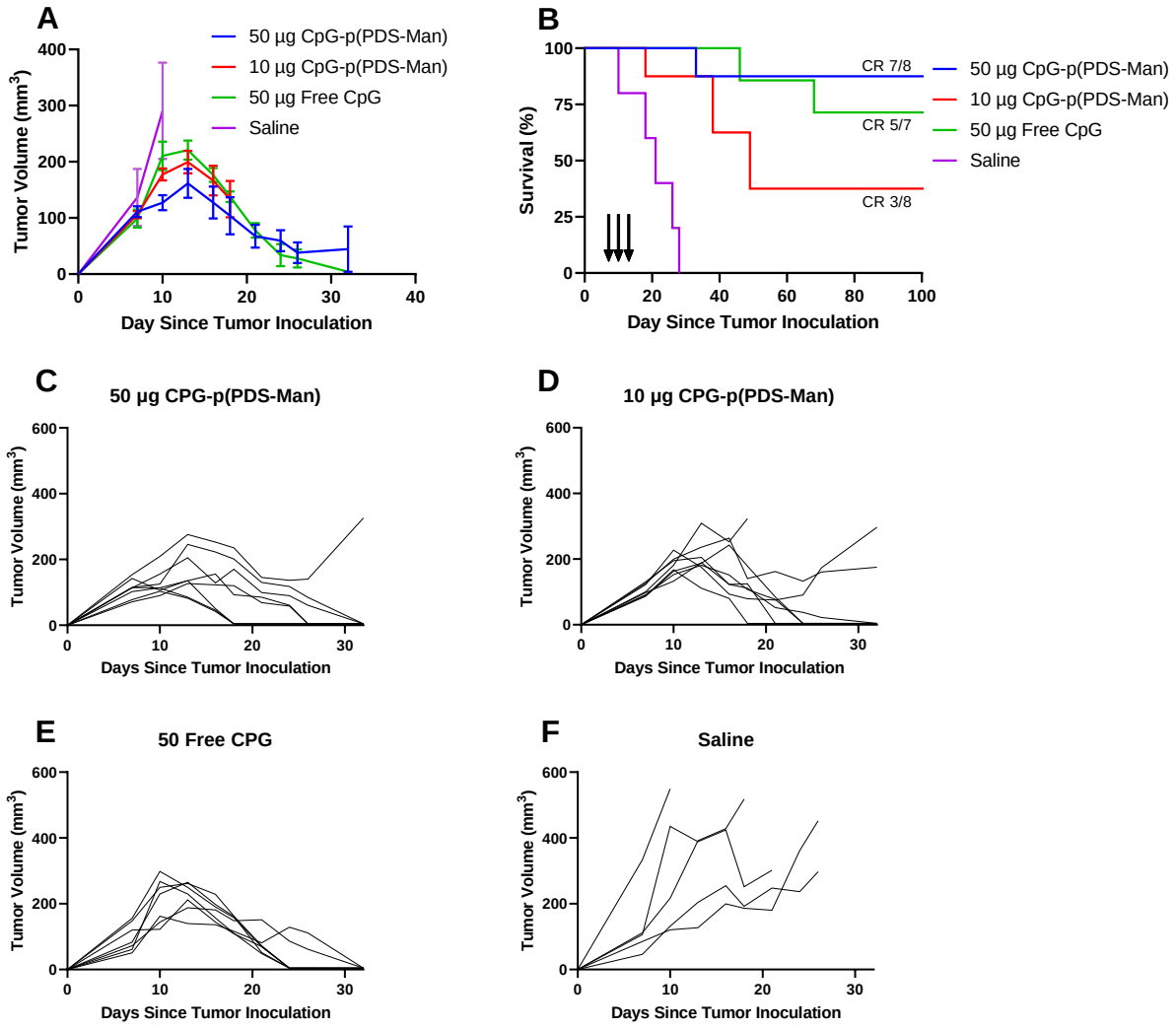

Figure 20: Tumor and survival curves in MC38 colon carcinoma

Mice (*n* = 5-7) were inoculated on day 0 with MC38 cells as described. Mice were treated on days 7, 10 and 13 with 10 or 50 µg of CpG-P(PDS-Man) (CpG based) or 50 µg free CpG. (A) Tumor growth curves (volume ± SEM). (B) Survival plots until endpoint. (C-F) Tumor growth curves for all individual mice.

dose treatment (10 µg CpG equivalent) responding to therapy, however complete remission was observed in only 3 out of 8 mice. In our high dose treatment (50 µg CpG equivalent), we observed complete remission in 7 out of 8 mice. In comparison to free CpG, we observed complete remission in 5 out of 7 mice.

Additionally, we wanted a non-invasive early readout of severe toxicity (if any) with our CpG-p(PDS-Man) treatment. For this, we tracked the bodyweight of the MC38 carcinoma bearing mice through the course of treatment with either low dose CpG-p(PDS-Man) (10 µg CpG equivalent), high dose CpG-p(PDS-Man) (50 µg CpG equivalent), free CpG (50 µg) or saline. Over the course of treatment with repeated doses no substantiative weight loss was observed in any of the mice (Figure 21).

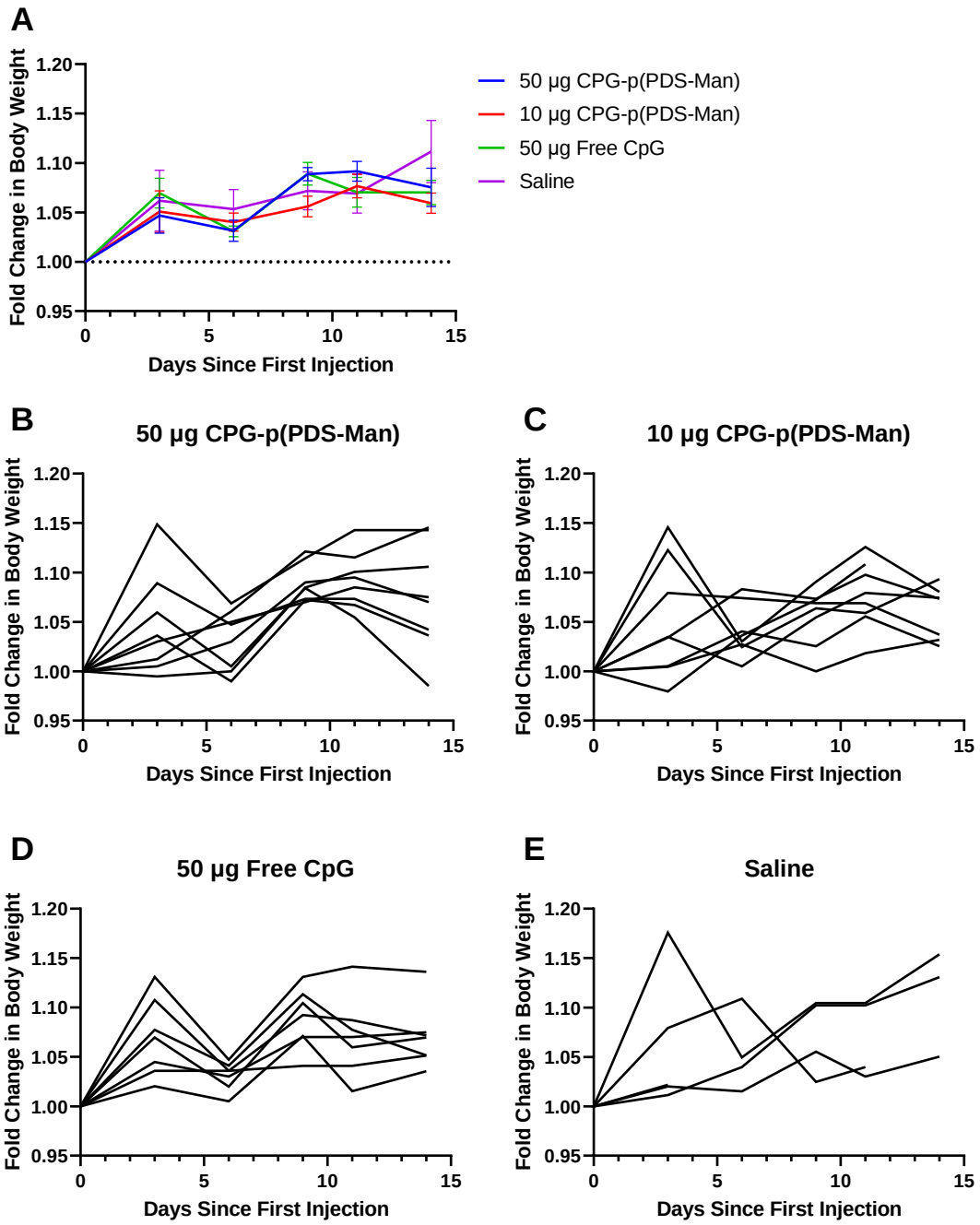

Figure 21: Repeated CpG treatment does not cause weight loss in tumor-bearing C57BL/6 mice

C57BL/6 mice were inoculated with MC38 tumors as described. Mouse body weight was monitored as fold change with respect to initial body weight at the beginning of treatment (day 7 to tumor inoculation). Mice were weighed on the first day of injection (day 0) and subsequently intratumorally injected with either 10 or 50 µg of CpG-P(PDS-Man) (CpG based) or 50 µg free CpG on days 0, 3, and 6. (A) Averaged body weight plotted by treatment (n = 5-7), mean ± SEM. (B-E) Fold change in body weight for all individual mice.

3.4 CpG-p(PDS-Man) Dose Response Study in Established B16F10 Melanoma

Being that we saw good efficacy of our CpG-p(PDS-Man) in a more immunologically "hot" tumor which is responsive to checkpoint therapy (MC38), we shifted our attention to a more immunologically "cold" tumor, the B16F10 melanoma model. This is seen as a more relevant preclinical model of melanoma as it exhibits many of the characteristics as human melanoma, such as a high degree of genetic instability[73], overall resistant to chemotherapy, and a demonstrated ability to metastasize. It is a non-immunogenic model, and generally does not respond to checkpoint therapy alone. It is quite aggressive with tumors doubling in volume every 2 days.

Here, we sought to establish a dose response to our CpG-p(PDS-Man) construct in the B16F10 model. Mice were treated on days 6 and 11 after tumor inoculation (tumor volume being ~45mm^3 on day 6). Mice were treated intratumorally with escalating doses of CpG-p(PDS-Man), with the lowest dose being 10 µg, an intermediate dose of 50 µg, and the highest dose being 100 µg. As illustrated in Figure 22, we saw slowed tumor growth in all treatments compared to saline. Furthermore, survival was prolonged in all treatment groups compared to saline (Figure 22). However, there were minimal differences between any of the treatment groups, with the efficacy of the lowest dose (20 µg) being almost the same as the highest dose (100 µg), thus in subsequent studies, something closer to the lower dose (20 µg) would seem preferable in the B16F10 melanoma model.

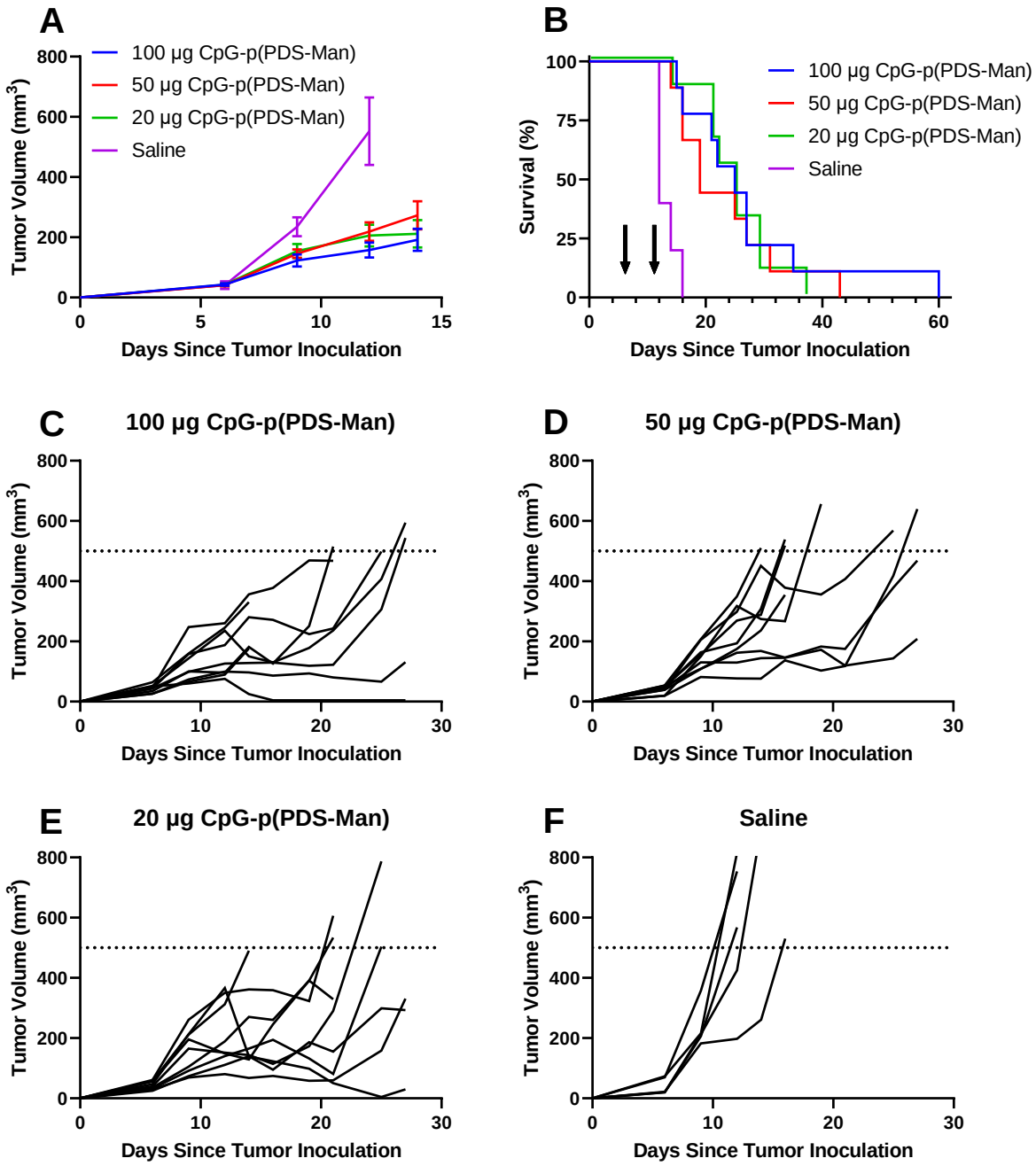

Figure 22: Tumor and survival curves in a B16F10 Melanoma dosing study

Mice (*n* = 5-9) were inoculated on day 0 with B16F10 cells as described. Mice were treated on days 6 and 11 with either 20 µg, 50 µg, or 100 µg of CpG-P(PDS-Man) (CpG based). (A) Tumor growth curves (volume ± SEM). (B) Survival plots until endpoint. (C-F) Tumor growth curves for all individual mice.

3.5 CpG-p(PDS-Man) Significantly Improves Survival in Established B16F10 Melanoma

3.5.1 CpG-p(PDS-Man) Significantly Outperforms Free CpG; Trends Towards Enhanced Efficacy Over Mannosylated CpG-p(Man)

Based on our observations of slower tumor growth and prolonged survival of our CpG-p(PDS-Man) construct in B16F10 melanoma when compared to saline, we sought to do a head-to-head equimolar comparison of CpG-p(PDS-Man) vs either CpG-p(Man) or free CpG, all at 10 μg CpG equivalent. By doing so, we can evaluate the advantageous effect of the cysteine binding pyridyl disulfide component of CpG-p(PDS-Man) over the non-cysteine binding CpG-p(Man), as well as against free CpG.

In this study, we were able to observe significant slowing of tumor growth in mice treated with CpG-p(PDS-Man) when compared to free CpG (Figure 23A). Additionally, we saw a trend towards slower tumor growth when comparing the cysteine binding CpG-p(PDS-Man) and the non-cysteine binding CpG-p(Man).

Furthermore, significant differences were observed in survival between our CpG-p(PDS-Man) and free CpG (Figure 23B). Moreover, our CpG-p(PDS-Man) treatment induced complete remission (CR) in 2 out of 9 B16F10 tumor bearing mice. Of note, there was a trend towards enhanced survival with CpG-p(PDS-Man) when compared to CpG-p(Man). This supports the hypothesis that it is the cysteine binding component of the polymer (pyridyl disulfide) that enhances the retention of CpG in the tumor, leading to enhanced antitumor efficacy. Finally, when comparing CpG-p(Man) to free CpG, we see a trend towards enhanced efficacy with CpG-p(Man).

This supports the hypothesis that mannose enhances CpG uptake in the tumor environment via mannose binding to C-type lectins on the surface of immune cells.

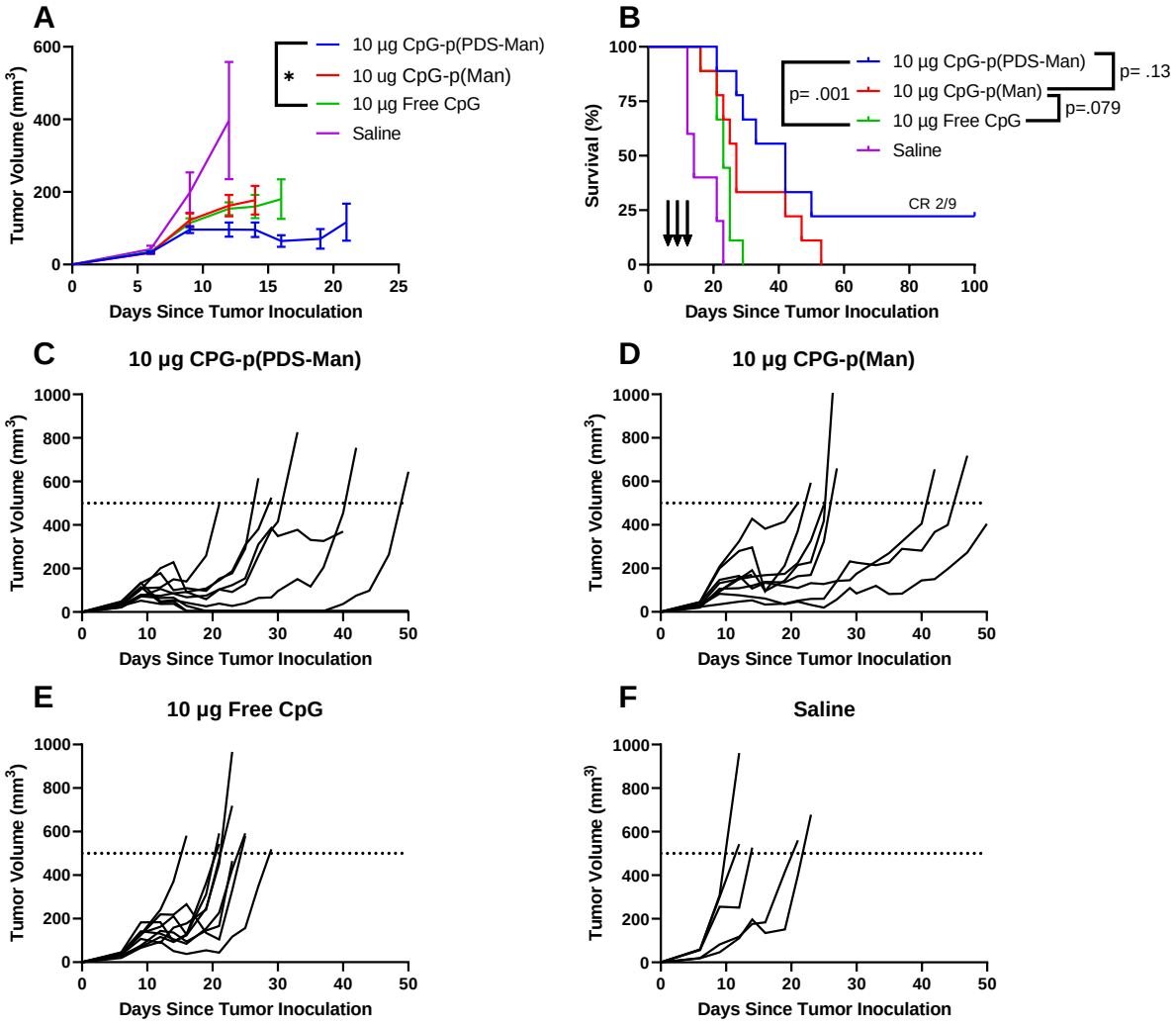

Figure 23: CpG-p(PDS-Man) significantly enhances survival in B16F10 melanoma compared to free CpG

Mice (n = 5-9) were inoculated on day 0 with B16F10 cells as described. Mice were treated on days 6, 9 and 12 with 10 µg of CpG either as CpG-P(PDS-Man), or as CpG-P(Man), or as free CpG. (A) Tumor growth curves (volume ± SEM). (B) Survival plots until endpoint. (C-F) Tumor growth curves for all individual mice. Statistical analysis of tumor growth curves was performed using unpaired t-tests on day 16: *p < 0.05. Log-rank (Mantel-Cox) test was used to compare survival curves.

3.5.2 CpG-p(PDS-Man) Significantly Outperforms Size Controlled CpG-p(HPMA)

Here we sought to repeat the above efficacy study comparing CpG-p(PDS-Man) to free CpG. Additionally, we wanted to compare CpG-p(PDS-Man) to a CpG-polymer conjugate with a polymer that is controlled for both molecular weight and bioactivity. Furthermore, being that our quantification method for CpG in our CpG-polymer conjugates is via UV/Vis of the fluorophore conjugated to the 3′ end of the CpG construct, here we sought to control for any fluctuations in concentrations by measuring CpG concentration using the same method (UV/Vis at 495 nm) as our CpG-p(PDS-Man). We opted for a weight control polymer to consist exclusively of HPMA, a bioinert comonomer that we copolymerized in our earlier polymeric formulations (p(PDS-Man), p(Man), and p(PDS)). We again selected the 10 μg CpG equivalent dose for this study, with injections occurring 3 times at 3 day intervals.

Significant slowing of tumor growth and enhanced survival was observed in mice treated with the CpG-p(PDS-Man) when compared to CpG-p(HPMA) (Figure 24A,B). Furthermore, when comparing survival of mice treated with CpG-p(HPMA) or free CpG, the survival curves are nearly identical to each other (Figure 24B). By properly controlling for polymer size and CpG concentration we see nearly identical results to free CpG. This strongly lends support to our hypothesis that it is the pyridyl disulfide and mannose side chains that enhance adjuvant retention in the tumor, as well as adjuvant uptake by immune cells in the tumor.

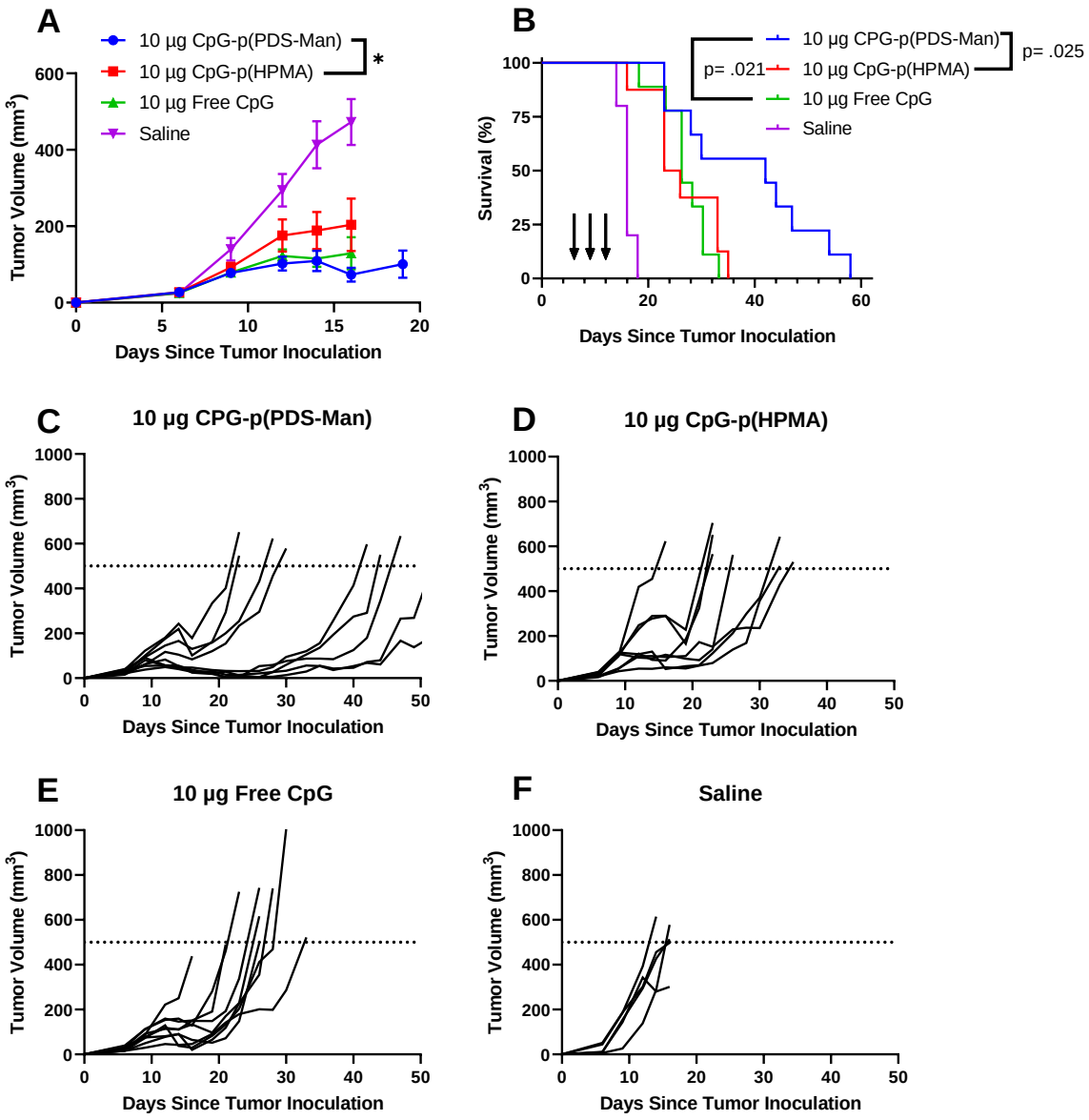

Figure 24: CpG-p(PDS-Man) significantly enhances survival in B16F10 melanoma compared to CpG-p(HPMA)

Mice (*n* = 5-9) were inoculated on day 0 with B16F10 cells as described. Mice were treated on days 6, 9 and 12 with 10 µg of CpG either as CpG-P(PDS-Man), or as CpG-P(HPMA), or as free CpG. (A) Tumor growth curves (volume ± SEM). (B) Survival plots until endpoint. (C-F) Tumor growth curves for all individual mice. Statistical analysis of tumor growth curves was performed using unpaired *t*-tests on day 16: *p < 0.05. Log-rank (Mantel-Cox) test was used to compare survival curves.

3.5.3 CpG-p(PDS-Man) Significantly Slows Tumor Growth Compared to CpG-p(PDS) With a Slight Trend Towards Enhanced Survival

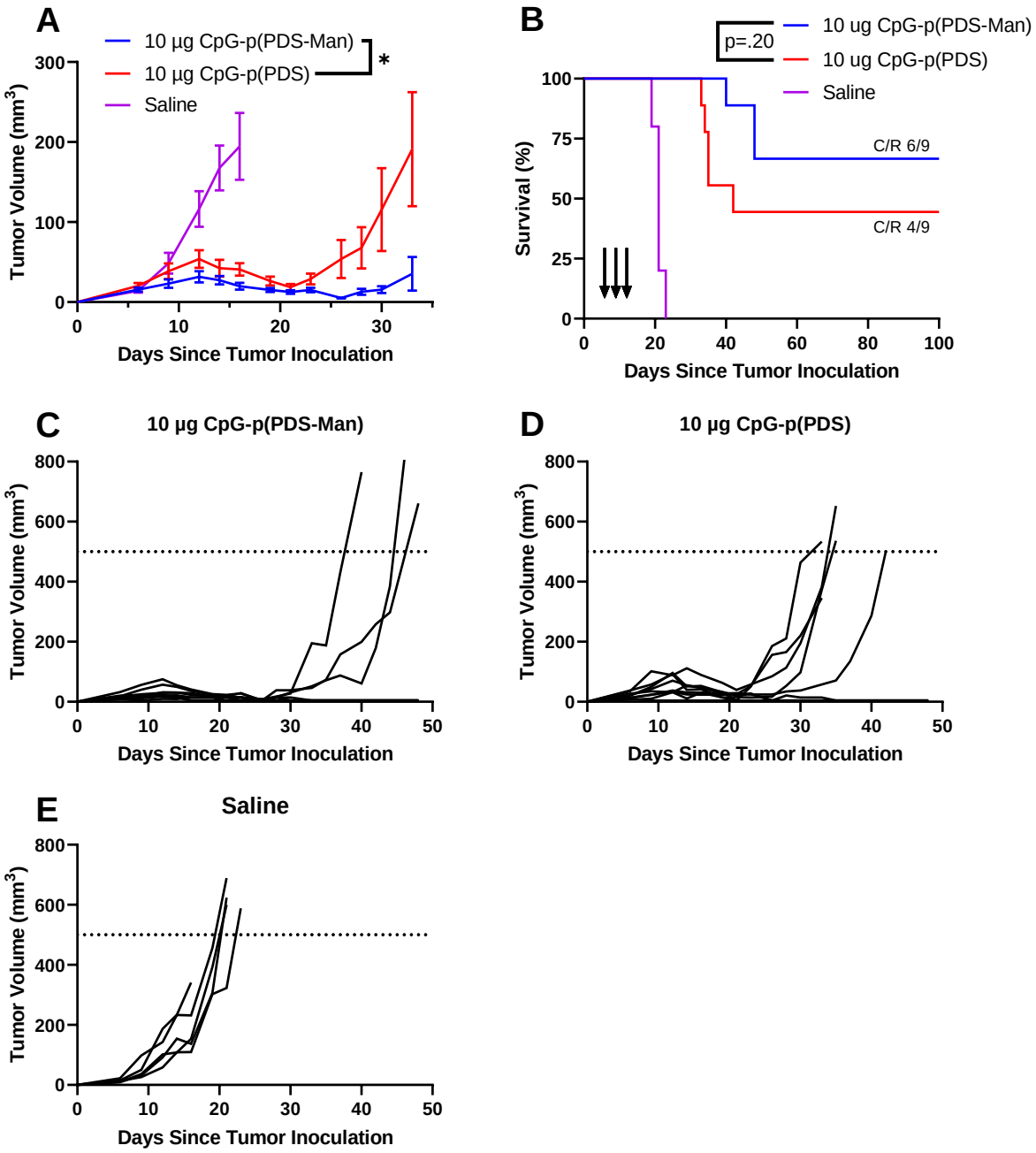

Figure 25: CpG-p(PDS-Man) trends towards enhanced survival in B16F10 melanoma compared to CpG-p(PDS)

Mice (*n* = 5-9) were inoculated on day 0 with B16F10 cells as described. Mice were treated on days 6, 9 and 12 with 10 µg of CpG either as CpG-P(PDS-Man), or as CpG-P(PDS). (A) Tumor growth curves (volume ± SEM). (B) Survival plots until endpoint. (C-E) Tumor growth curves for all individual mice. Statistical analysis of tumor growth curves was performed using unpaired *t*-tests on day 33: *p < 0.05. Log-rank (Mantel-Cox) test was used to compare survival curves.

Upon demonstrating the superiority of the CpG-p(PDS-Man) conjugate over either free CpG, size and concertation controlled CpG-p(HPMA), and pyridyl disulfide controlled CpG-p(Man) we wanted to evaluate the influence of mannose in our CpG-p(Man-PDS) conjugate. Thus, we tested the efficacy of our CpG-p(Man-PDS) conjugate in a head-to-head equimolar experiment against CpG-p(PDS); a polymer consisting of pyridyl disulfide, but not mannose.

In this experiment, we found the tumors to be quite small (25-25 mm^3) on day 6 compared to our earlier studies, however we decided to nonetheless treat the tumor bearing mice on days 6, 9, and 12 after tumor inoculation. As illustrated in Figure 25B, we unfortunately saw only a slight trend towards enhanced survival with mannose, although we do see a significant difference in tumor growth (Figure 25A).

3.6 CpG-p(PDS-Man) Trends Towards Enhanced Efficacy in CT26 Colon Carcinoma

Here we wanted to see if our CpG-p(PDS-Man) construct would enhance the antitumor response in other murine cancer models. For this, we choose the CT26 colon carcinoma model, an extensively used syngeneic mouse tumor model of carcinoma, that is generally viewed as aggressive and has a moderate response rate to ICIs. In this experiment, we evaluated CpG-p(PDS-Man) in a head-to-head comparison to free CpG at 10 µg equivalent CpG. In this experiment we treated on days 7, 10, and 13 after tumor inoculation. Here, we saw a trend towards enhanced survival with our CpG-p(PDS-Man) (Figure 26B), but no difference when evaluating tumor growth curves (Figure 26A).

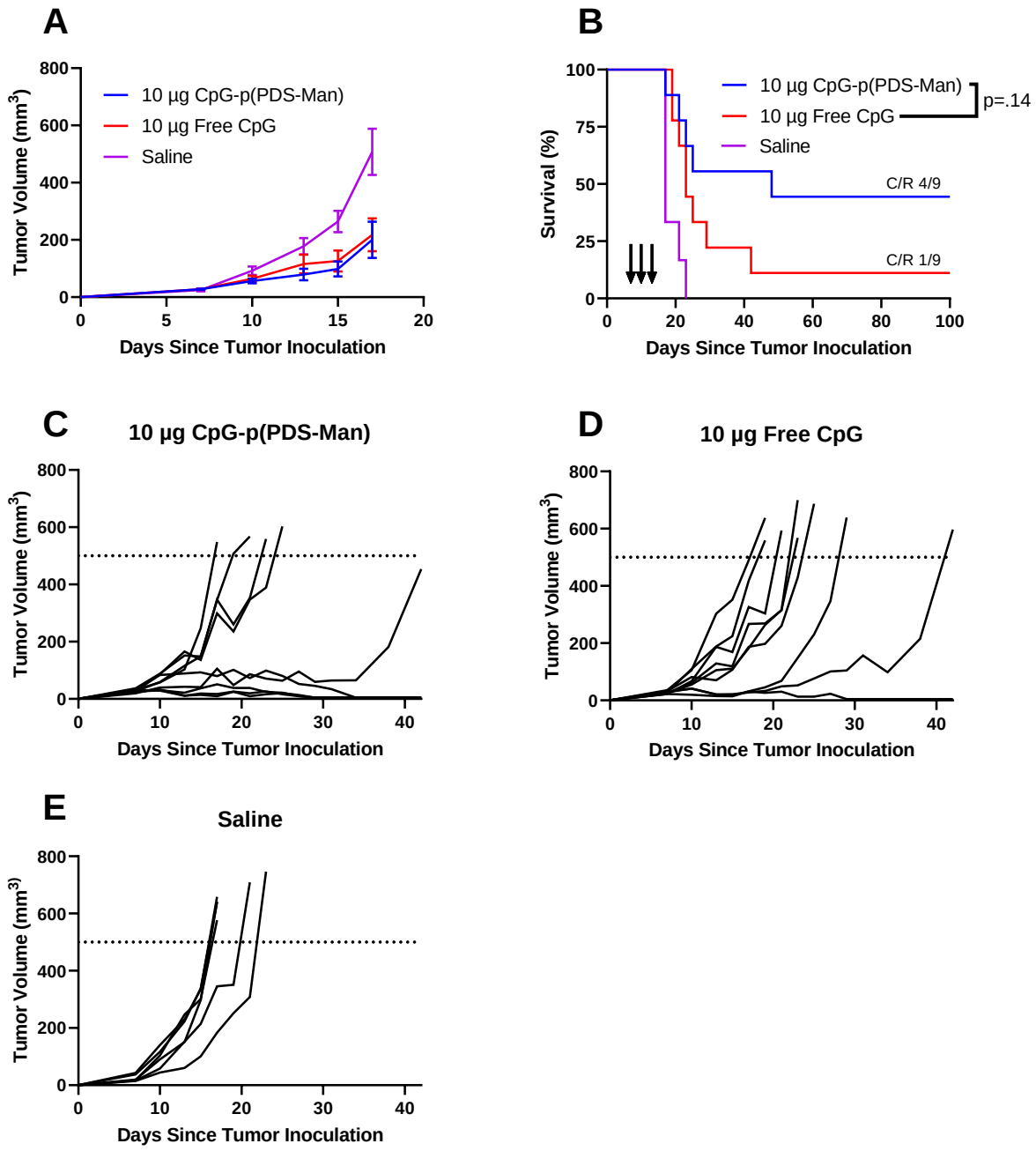

Figure 26: CpG-p(PDS-Man) trends towards enhanced survival in CT26 colon carcinoma compared to free CpG

Mice (*n* = 5-9) were inoculated on day 0 with CT26 cells as described. Mice were treated on days 7, 10, and 13 with 10 µg of CpG either as CpG-P(PDS-Man) or as free CpG. (A) Tumor growth curves (volume ± SEM). (B) Survival plots until endpoint. (C-E) Tumor growth curves for all individual mice. Log-rank (Mantel-Cox) test was used to compare survival curves.

3.7 CpG-p(PDS-Man) Trends Towards Enhanced Efficacy in Combination with anti-PD-1 in B16F10 Melanoma

Checkpoint inhibitors have been used successfully in the clinic since Nivolumab was approved by the FDA in 2014 and represents the largest class of approved immunotherapeutic drugs for cancer. However, their effectiveness varies across tumor types as well as patients. Being that our CpG-p(PDS-Man) demonstrated strong immunotherapeutic efficacy by provoking a strong antitumor immune response, we wanted to evaluate its antitumor efficacy in combination with a more clinically relevant immunotherapeutic, namely checkpoint inhibitor anti-PD-1. Being that immunoadjuvants enhance antigen uptake and processing while immune checkpoint inhibitors inhibit the negative immune regulation in the tumor environment, we wanted to see if our therapy could synergize with anti-PD-1. We again chose the B16F10 melanoma model to evaluate synergy of our CpG-p(PDS-Man) construct in combination with checkpoint therapy. B16F10 melanoma is overall unresponsive with checkpoint inhibitors as a monotherapy, and we already saw significant efficacy with CpG-p(PDS-Man) as a monotherapy.

3.7.1 Evaluation of CpG-p(PDS-Man) in combination with anti-PD-1

Here, we evaluated CpG-p(PDS-Man) in combination with anti-PD-1 to see if we could observe synergy of anti-PD-1 with CpG-p(PDS-Man) as a combination therapy. B16F10 tumors

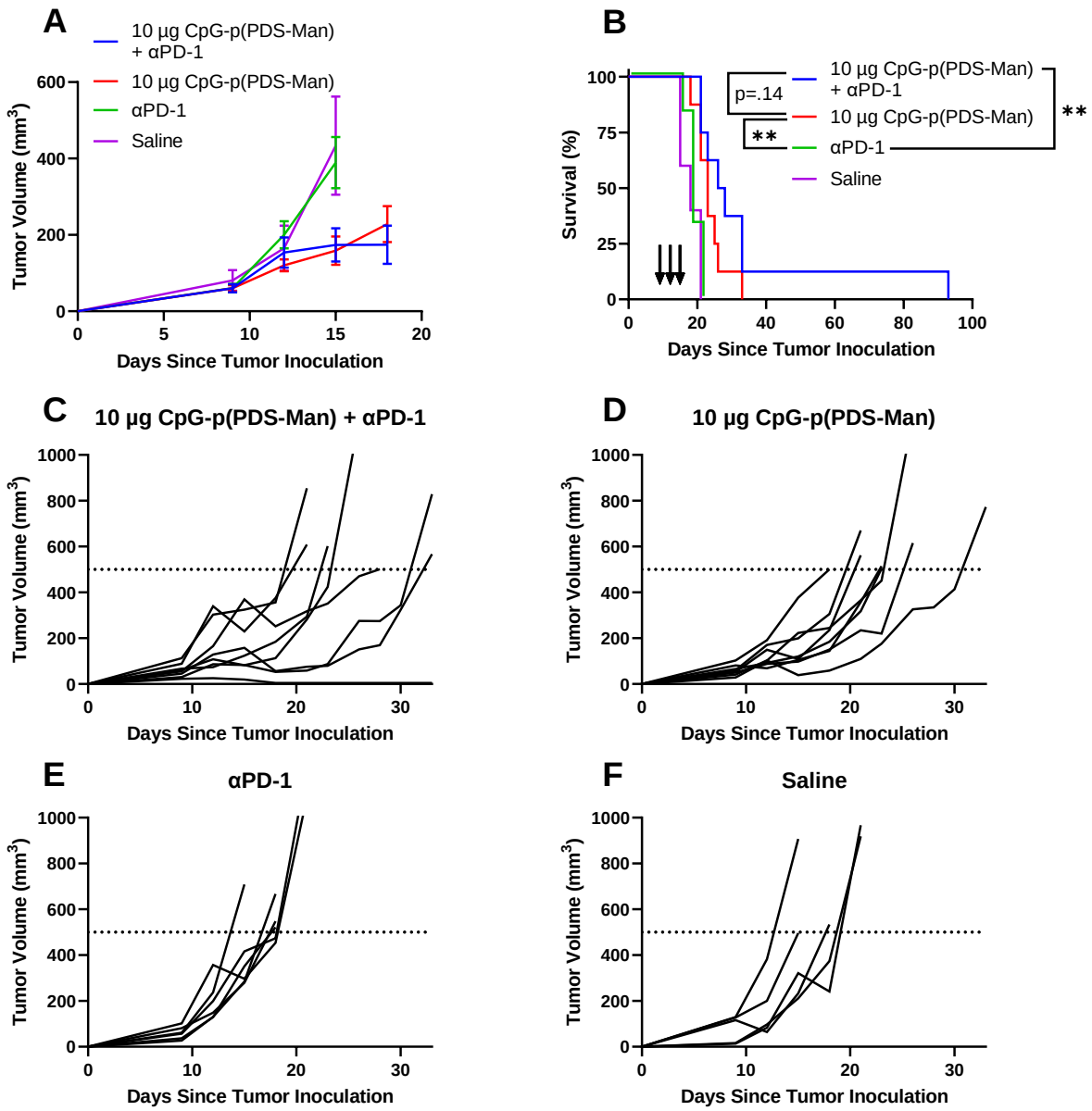

Figure 27: Evaluation of CpG-p(PDS-Man) in combination with anti-PD-1 in B16F10 melanoma

Mice (n = 5-8) were inoculated on day 0 with B16F10 cells as described. Mice were treated on days 9, 12, and 15 with 10 µg of CpG as CpG-P(PDS-Man) in combination with 100 µg anti-PD-1 or as CpG-P(PDS-Man alone, or treated with 100 µg anti-PD-1 alone (A) Tumor growth curves (volume ± SEM). (B) Survival plots until endpoint. (C-F) Tumor growth curves for all individual mice. Log-rank (Mantel-Cox) test was used to compare survival curves: **p < 0.01

grew at a slower than usual rate and treatment began at day 9. Mice were subsequently treated on days 12 and 15 as well for a total of 3 treatments. Mice were dosed with 100 μg anti-PD-1 (interperitoneally) per treatment. In this study, we disappointingly only saw a trend towards enhanced efficacy when comparing our CpG-p(PDS-Man) + anti-PD-1 vs CpG-p(PDS-Man) alone (Figure 27A,B). Although expected, we do however see that our CpG-p(PDS-Man) even as a monotherapy strongly outperforms anti-PD-1 alone (Figure 27A,B).

3.7.2 Further Evaluation of Combination Therapy with Free CpG

Next, we wanted to repeat the above study, but instead of opting for evaluating CpG-p(PDS-Man) + anti-PD-1 vs CpG-p(PDS-Man) alone and looking for a synergistic response, here we wanted to see if our CpG-p(PDS-Man) would still have enhanced efficacy vs free CpG in a

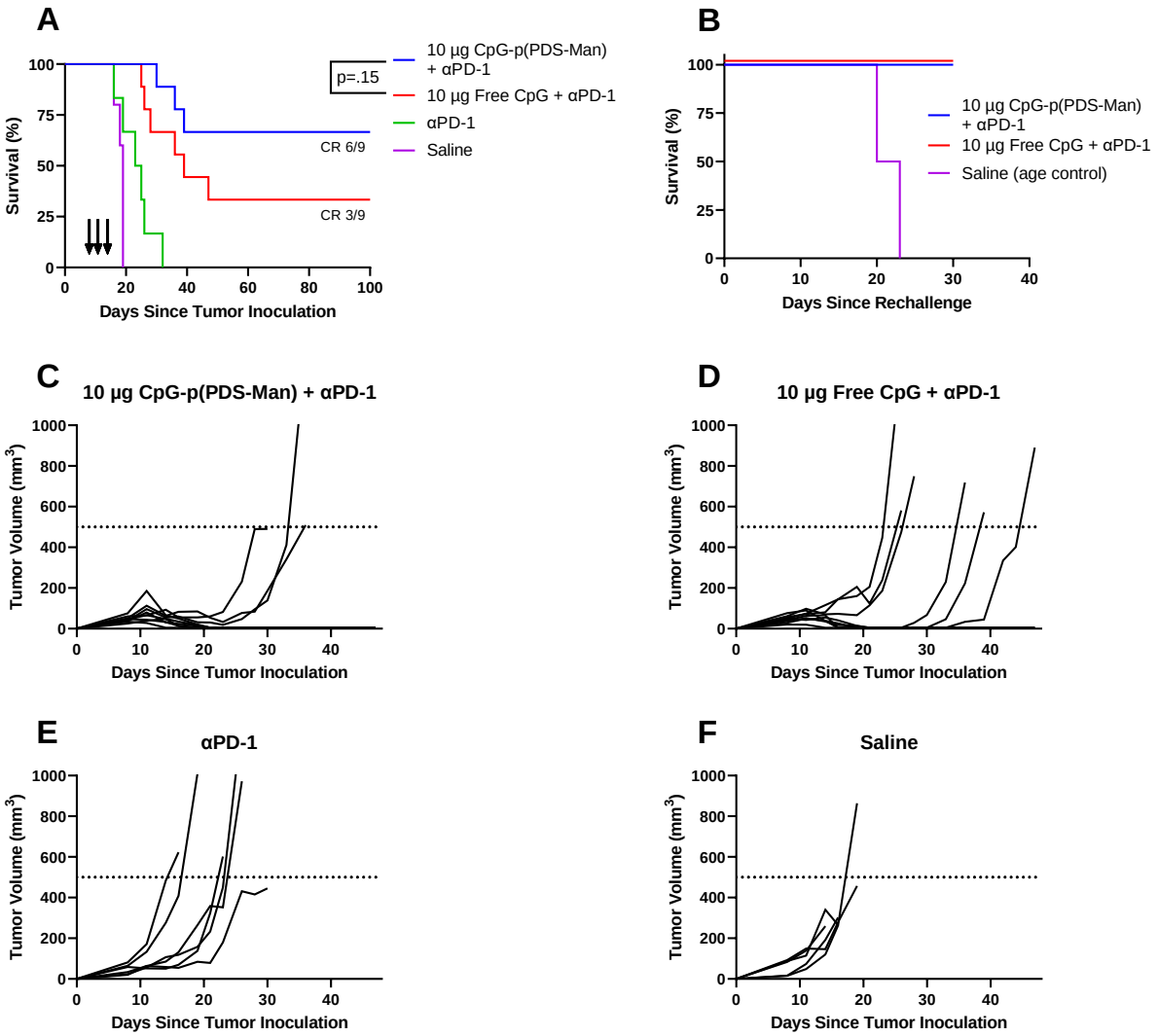

Figure 28: Further evaluation of combination therapy with free CpG in B16F10 melanoma

Mice (*n* = 5-8) were inoculated on day 0 with B16F10 cells as described. Mice were treated on days 8, 11, and 14 with 10 µg of CpG as CpG-P(PDS-Man) in combination with 100 µg anti-PD-1 or as free CpG in combination with 100 µg anti-PD-1,or treated with 100 µg anti-PD-1 alone. (A) Survival plots until endpoint. (B) Mice were subsequently rechallenged with B16F10 tumors after 100 days. (C-F) Tumor growth curves for all individual mice. Log-rank (Mantel-Cox) test was used to compare survival curves

combination experiment with anti-PD-1. Due to tumors growing a little slower than expected we treated on days 8, 11, and 14. Mice were dosed with 100 μg anti-PD-1 per treatment interperitoneally. In this study we observed, 6 out of 9 mice attaining complete tumor remission in the CpG-p(PDS-Man) + anti-PD-1 group, compared to 3 out of 9 mice in the free CpG + anti-PD-1 group (Figure 28A). Furthermore, when rechallenged (after 100 days of initial tumor inoculation) with tumor on the opposite flank, all treated mice cleared the secondary tumor (Figure 28B) indicating that our treatment had induced a robust and durable immune response.

3.8 CpG-p(PDS-Man) Enhances Intratumoral cytokines Compared to Free CpG

Upon observation of the enhanced efficacy of our CpG-p(PDS-Man) in tumor bearing mice, we further probed the therapeutic mechanism behind these immunological responses in the B16F10 melanoma model. To further study the mechanism, we treated B16F10 tumor bearing mice on days 9 and 12 after tumor inoculation with 10 μg of either free CpG or 10 μg equivalent CpG-p(PDS-Man). On day 14, we harvested the tumors and processed them for intratumoral cytokines. Here, we observe a pronounced increase was observed in intratumoral IFN-γ between mice treated with free CpG or CpG-p(PDS-Man) (Figure 29A). A similar trend is observed for many other cytokines/chemokines (Figure 29 C-I).

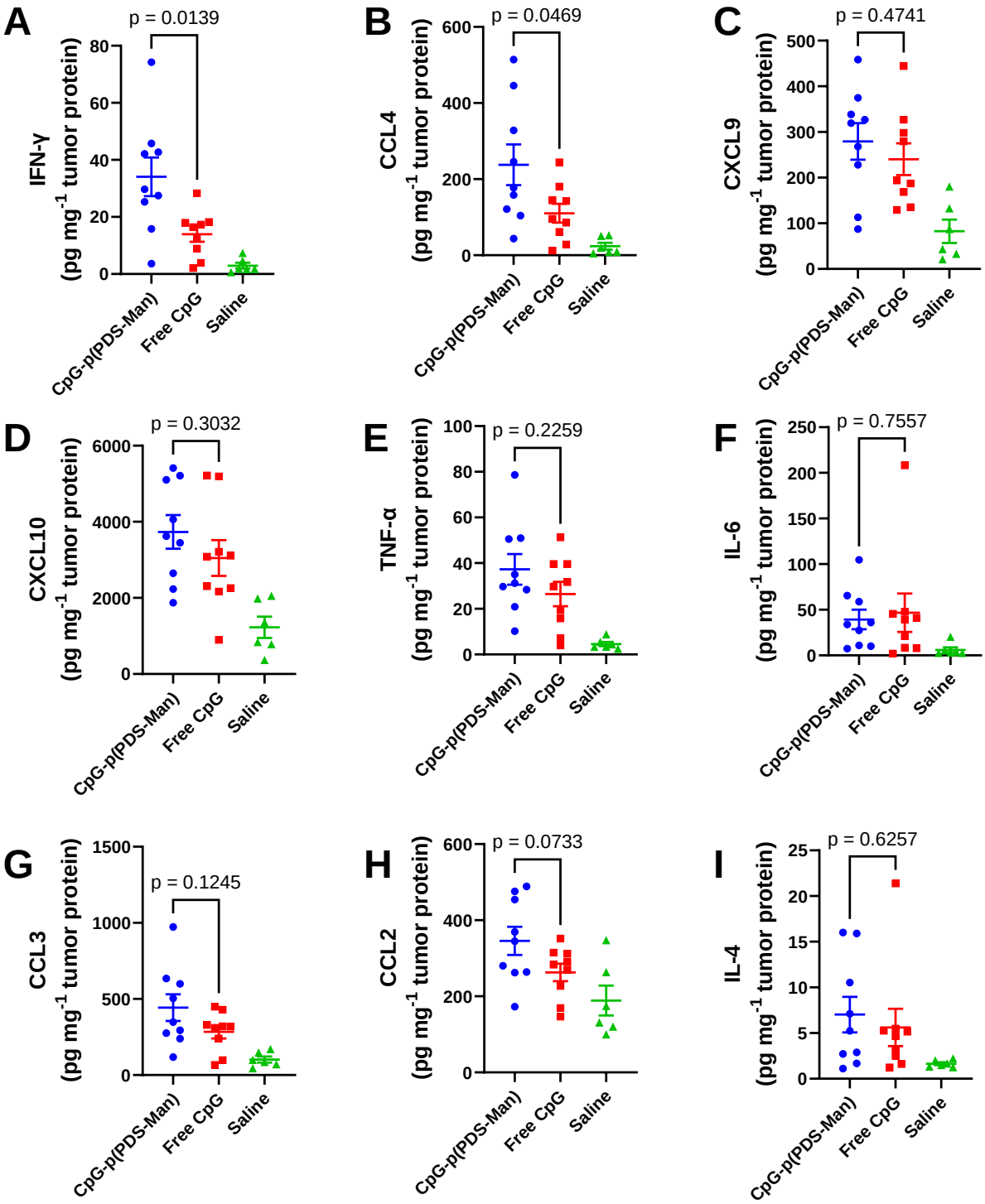

Figure 29: CpG-p(PDS-Man) enhances intratumoral cytokines

Mice (*n* = 5-8) were inoculated on day 0 with B16F10 cells as described. Mice were treated with 10 µg CpG as CpG-p(PDS-Man), or 10 µg free CpG, or with vehicle control (PBS) on days 9 and 12. Tumors were excised on day 14 and homogenized for intratumoral cytokine analysis. (A) IFNγ. (B) CCL4. (C) CXCL9. (D) CXCL10. (E) TNFα. (F) IL-6. (G) CCL3. (H) CCL2. (I) IL-4. Data represents mean ± SEM; Statistical analyses utilized unpaired t-tests.

3.9 CpG-p(PDS-Man) Decreases Systemic Cytokines

Given the hypothesis of increased tumor retention of adjuvant due to the pyridyl disulfide binding to free cysteines in the tumor, we wanted to see if we see if we could observe a decrease in proinflammatory cytokines in the blood. For this, we administered 50 µg of either free CpG or 50 µg equivalent CpG-p(PDS-Man) intratumorally to B16F10 tumor bearing mice on day 9 (tumor size 100-150 mm^3). We then bled the mice at 2, 6, 24 or 48 hours after injection. As illustrated in Figure 30, we found a striking increase in IFN-γ at the 24 hours timepoint in the free CpG group compared to the CpG-p(PDS-Man) group. We further characterized other inflammatory cytokines at the 24-hour timepoint and observed increased CXCL9 and CXCL10, as well as CCL2 in the free CpG group (Figure 30A-F).

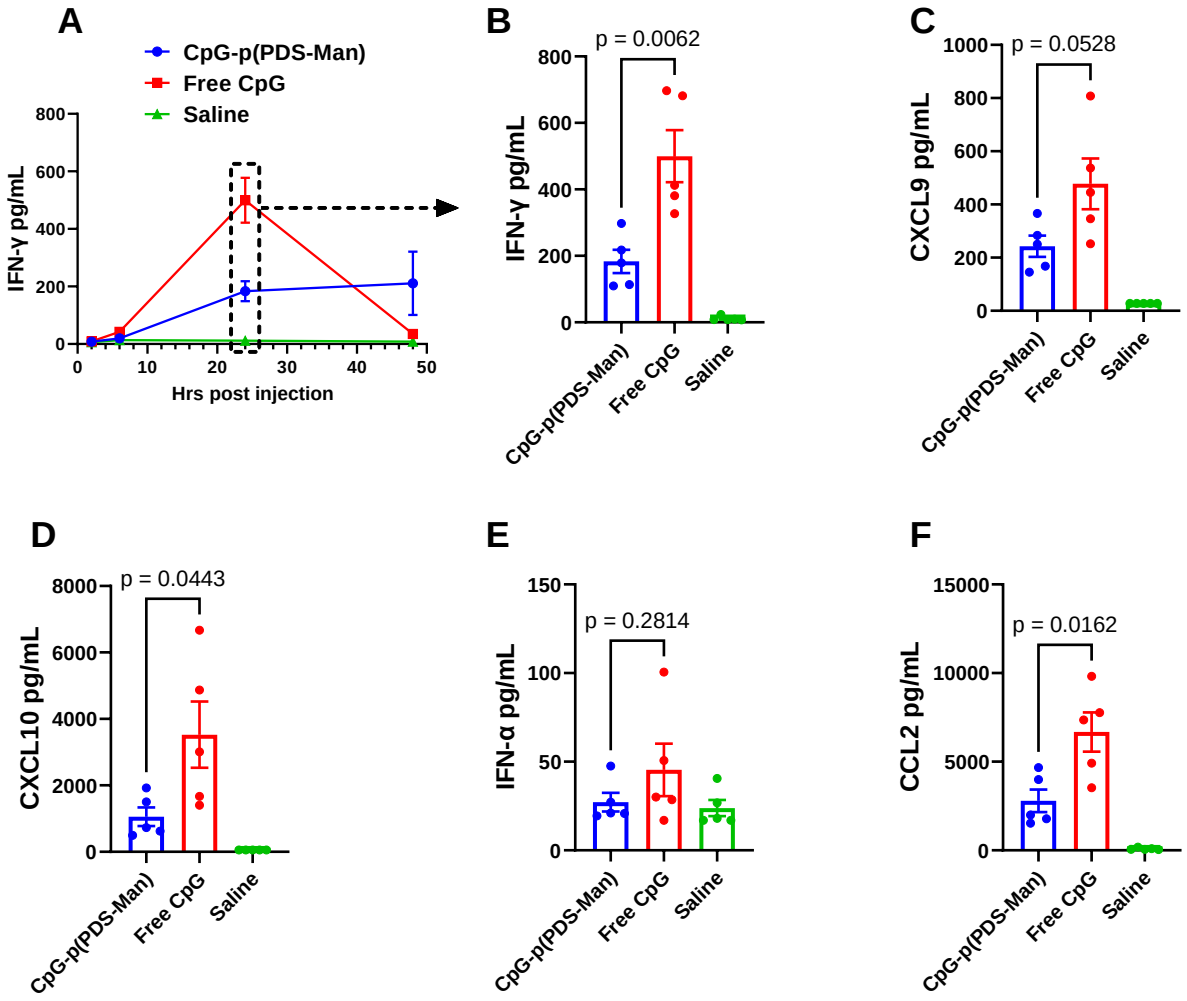

Figure 30: CpG-p(PDS-Man) decreases systemic cytokines in tumor-bearing mice

Mice (n = 5-8) were inoculated on day 0 with B16F10 cells as described. Mice were treated with 50 µg CpG as CpG-p(PDS-Man), or 10 µg free CpG, or with vehicle control (PBS) on day 9. Mice were bled at 2, 6, 24 and 48 hours after injection. (A) kinetics of IFNγ in serum. (B-F) serum cytokine levels at 24 hours for (B) IFNγ. (C) CXC9. (D) CXCL10. (E) IFN-α. (F) CCL2. Columns and error bars indicate mean ± SEM; Statistical analyses utilized unpaired t-tests.

CHAPTER 4:

DISCUSSION

4.1 Summary

In this work, we developed and tested a multifunctional polymer-adjuvant conjugate as an in-situ cancer vaccine. Our multifunctional polymer combined the strength of multiple pyridyl-disulfide side chains for conjugation to unpaired cysteines in tumor debris and on the tumor cell surface with multiple mannose side chains for enhanced APC uptake and endosomal localization of the CpG adjuvant payload. Utilizing intratumoral administration, CpG-p(PDS-Man) provides sustained delivery of adjuvant to the tumor microenvironment, yielding a strong innate immune response, thus leading to tumor antigen presentation, and ultimately generating a robust antitumor immune response. Critically, our CpG-p(PDS-Man) demonstrated superior survival efficacy in B16F10 tumor bearing mice than free substituent CpG. Efficacy is also noted in other tumor models such as MC38 colon carcinoma and CT26 , however the difference is not quite as striking. Furthermore, we observed a significant increase in intratumoral cytokines such as IFN-γ and CCL4 when treating B16F10 tumor bearing mice with our CpG-p(PDS-Man) when compared to free CpG. Additionally, as a combination therapy with αPD-1, we were able to induce complete remission in 6 out of 9 B16F10 melanoma bearing mice. Furthermore, upon subsequent rechallenge of these 6 mice with abscopal B16F10 tumors, all 6 mice successfully cleared their tumors, indicative of robust systemic antitumor memory generated by our platform. Finally, our CpG-p(PDS-Man) demonstrated a noticeable decrease in systemic cytokines after 24 hours, a crucial indicator to enhance the safety profile of immunoadjuvants. Blood chemistry markers of liver, kidney did not show any significant indications of toxicity.

In conclusion, we have developed a robust and modular platform that offers a novel approach to adjuvant-based cancer immunotherapy. It is tumor agnostic and relies exclusively on the patient's endogenous tumor neoantigens. Our formulation offers the potential to improve the efficacy of cancer vaccines, checkpoint inhibitors, and other immunotherapeutics. Our conjugation strategy is straightforward, reproducible, and highly amenable to other biologically relevant payloads. Further studies are needed to explore the full clinical relevance of our polymer-adjuvant strategy for cancer treatment.

4.3 CpG-p(PDS-Man) in Combination with Checkpoint Inhibitor Antibodies

Of particular interest to us was the modest effect of combination therapy utilizing our CpG-p(PDS-Man) in combination with immune checkpoint inhibitor αPD-1. Mechanistically, these two pathways are distinct in their methods to up-regulate T-cell mediated responses against the tumor, and thus should complement each other. CpG primarily enhances the priming phase by inducing an innate immune response, activating APCs and inducing dendritic cells to produce costimulatory molecules, eventually yielding tumor specific CD8+ T cells. On the other hand, immune checkpoint inhibitors remove T-cell inhibition in the effector phase, thus promoting T-cell mediated cytotoxicity of tumor cells. Utilizing a combination of these therapies should result in an enhanced antitumor effect. Indeed, several studies point to that effect[74], both when observing tumor regression, as well preventing resistance[75].

The results from our combination studies in which minimal synergetic effect was observed between CpG-p(PDS-Man) and αPD-1 when compared to CpG-p(PDS-Man) monotherapy can be interpreted in a couple different ways. CpG-p(PDS-Man) is a very effective adjuvant and may induce sufficient innate immune stimulation, whereby tumor immunosuppressive mechanisms are sufficiently weakened, rendering αPD-1 unnecessary. Alternatively, the aggressive murine

B16F10 model, while indeed a very helpful melanoma model, does not sufficiently recapitulate the full breadth and scope of clinically relevant tumors in assessing CpG-p(PDS-Man) and αPD-1 synergy. Assessing synergistic efficacy between CpG-p(PDS-Man) and αPD-1 may be more appropriate in a slower growing murine tumor model that more closely mirrors human patients.

4.3 Future Directions

By leveraging the dysregulated redox state in solid tumors, our CpG-p(PDS-Man) platform can hypothetically be applied to many solid tumor types, entirely in a tumor-agnostic manner. Our primary workhorse in evaluating the antitumor efficacy of CpG-p(PDS-Man) was the B16F10 murine melanoma model, however it was efficacious as well in both the CT26 and MC38 murine carcinoma models. Earlier work utilizing TLR7 monomer side chains demonstrated significantly prolonged survival in the above mentioned models.[62] This work specifically focused on utilizing the polymer chain end for conjugation, in which we were able to reproducibly conjugate a synthetic biomolecule of intermediate size (7.4 kDa) in a straightforward fashion to the azide terminated polymer chain; however, this azide-alkyne click chemistry conjugation strategy is amenable to many other biomolecules or small molecules as well, either as use as a therapeutic or diagnostic. Additionally, the modularity of the RAFT polymer system is flexible to additional functional monomers. Additional monomers may consist of different bioactive small molecules such as sugars or cytotoxic drugs. Alternatively, different cysteine reactive side chains can be envisioned altogether, such as a maleimide based side chains, or other cysteine targeted Michael acceptors[76].

4.4 Clinical Indications

CpG has been noted for its immunostimulatory effects ever since its discovery in 1995[77]. It has been approved as a vaccine adjuvant (CpG-1018) by the FDA in 2018 for a Hepatitis B

vaccine (HEPLISAV-B), in which its use as an adjuvant proved more effective than aluminum salts. A large body of preclinical data indicate its utility as an adjuvant for cancer immunotherapy. However, its successful incorporation into an approved monotherapy for cancer has been stymied. More recently, CpG has been of interest in combination therapy with radiotherapy, chemotherapy, and other immunotherapies. Many clinical trials utilizing CpG in combination with the above therapies are underway in an assortment of solid tumors[78].

Given our CpG-p(PDS-Man) enhances tumor retention and decreases systemic cytokines, we believe our therapy may be of high translational value in enhancing CpG's therapeutic index, a key strategy towards successful clinical implementation. Furthermore, by enhancing CpG retention in the tumor, a stronger depot effect of CpG adjuvant can be achieved, which may itself as a monotherapy be significant in remodeling the tumor immunological landscape and eliciting robust antitumor immunity.

Additionally, by utilizing our cysteine binding chemistry for tumor localization of immune adjuvants, we can avoid other off target effects that has traditionally hindered other tumor targeting agents, namely tumor targeting antibodies. The induction of antidrug antibodies is a limiting factor in many protein-based therapeutics. Being that our delivery strategy utilizes a synthetic polymer-based delivery approach, we envision minimized immunogenicity towards our delivery platform.

4.5 Conclusion

In conclusion, our work has demonstrated that CpG-p(PDS-Man) system represents an important modular drug delivery system to deliver immunotherapeutics or other agents to the tumor microenvironment. In our work, we used CpG as an immunostimulant. We have shown enhanced efficacy of our CpG conjugate, as well as a reduction of systemic cytokines compared

to the free CpG. Given the ease and reproducibility of our click chemistry conjugation to the polymer system, one can readily envision this platform as applicable to a variety of other therapeutic or diagnostic agents. With further development of the polymer system, as well the choice of a suitable therapeutic, we believe that the above-described technology will have further meaningful clinical impact.

REFERENCES

1 Germain, R. N. Vaccines and the Future of Human Immunology. *Immunity* **33**, 441-450 (2010). https://doi.org:10.1016/j.immuni.2010.09.014

2 Chaplin, D. 1. Overview of the human immune response. *Journal of Allergy and Clinical Immunology* **117**, S430-S435 (2006). https://doi.org:10.1016/j.jaci.2005.09.034

3 Marshall, J. S., Warrington, R., Watson, W. & Kim, H. L. An introduction to immunology and immunopathology. *Allergy, Asthma & Clinical Immunology* **14**, 49 (2018). https://doi.org:10.1186/s13223-018-0278-1

4 Turvey, S. E. & Broide, D. H. Innate immunity. *Journal of Allergy and Clinical Immunology* **125**, S24-S32 (2010). https://doi.org:https://doi.org/10.1016/j.jaci.2009.07.016

5 Kagan, J. C. & Barton, G. M. Emerging Principles Governing Signal Transduction by Pattern-Recognition Receptors: Table 1. *Cold Spring Harbor Perspectives in Biology* **7**, a016253 (2015). https://doi.org:10.1101/cshperspect.a016253

6 Bonilla, F. A. & Oettgen, H. C. Adaptive immunity. *Journal of Allergy and Clinical Immunology* **125**, S33-S40 (2010). https://doi.org:https://doi.org/10.1016/j.jaci.2009.09.017

7 Kawai, T. & Akira, S. TLR signaling. *Cell Death & Differentiation* **13**, 816-825 (2006). https://doi.org:10.1038/sj.cdd.4401850

8 Duan, T., Du, Y., Xing, C., Wang, H. Y. & Wang, R.-F. Toll-Like Receptor Signaling and Its Role in Cell-Mediated Immunity. *Front Immunol* **13** (2022). https://doi.org:10.3389/fimmu.2022.812774

9 Fitzgerald, K. A. & Kagan, J. C. Toll-like Receptors and the Control of Immunity. *Cell* **180**, 1044-1066 (2020). https://doi.org:10.1016/j.cell.2020.02.041

10 Napolitani, G., Rinaldi, A., Bertoni, F., Sallusto, F. & Lanzavecchia, A. Selected Toll-like receptor agonist combinations synergistically trigger a T helper type 1–polarizing program in dendritic cells. *Nature Immunology* **6**, 769-776 (2005). https://doi.org:10.1038/ni1223

11 Barquet, N. & Domingo, P. Smallpox: the triumph over the most terrible of the ministers of death. *Ann Intern Med* **127**, 635-642 (1997). https://doi.org:10.7326/0003-4819-127-8_part_1-199710150-00010

12 KAHN, C. History of Smallpox and Its Prevention. *American Journal of Diseases of Children* **106**, 597-609 (1963). https://doi.org:10.1001/archpedi.1963.02080050599011

13 Riedel, S. Edward Jenner and the history of smallpox and vaccination. *Proc (Bayl Univ Med Cent)* **18**, 21-25 (2005). https://doi.org:10.1080/08998280.2005.11928028

14 Stark, R. B. Immunization saves Washington's army. *Surg Gynecol Obstet* **144**, 425-431 (1977).

15 Plotkin, S. History of vaccination. *Proceedings of the National Academy of Sciences* **111**, 12283-12287 (2014). https://doi.org:doi:10.1073/pnas.1400472111

16 Guest, S., Pilipenko, E., Sharma, K., Chumakov, K. & Roos, R. P. Molecular mechanisms of attenuation of the Sabin strain of poliovirus type 3. *J Virol* **78**, 11097-11107 (2004). https://doi.org:10.1128/JVI.78.20.11097-11107.2004

17 Orsini, D. & Martini, M. Albert Bruce Sabin: The Man Who Made the Oral Polio Vaccine. *Emerg Infect Dis* **28**, 743-746 (2022). https://doi.org:10.3201/eid2803.204699

18 Klein, N. P. Licensed pertussis vaccines in the United States. *Human Vaccines & Immunotherapeutics* **10**, 2684-2690 (2014). https://doi.org:10.4161/hv.29576

19 Delrue, I., Verzele, D., Madder, A. & Nauwynck, H. J. Inactivated virus vaccines from chemistry to prophylaxis: merits, risks and challenges. *Expert Review of Vaccines* **11**, 695-719 (2012). https://doi.org:10.1586/erv.12.38

20 Kew, O. M., Sutter, R. W., Gourville, E. M. d., Dowdle, W. R. & Pallansch, M. A. VACCINE-DERIVED POLIOVIRUSES AND THE ENDGAME STRATEGY FOR GLOBAL POLIO ERADICATION. *Annual Review of Microbiology* **59**, 587-635 (2005). https://doi.org:10.1146/annurev.micro.58.030603.123625

21 Croce, E. *et al.* Safety of live vaccinations on immunosuppressive therapy in patients with immune-mediated inflammatory diseases, solid organ transplantation or after bone-marrow transplantation – A systematic review of randomized trials, observational studies and case reports. *Vaccine* **35**, 1216-1226 (2017). https://doi.org:https://doi.org/10.1016/j.vaccine.2017.01.048

22 Nanishi, E., Dowling, D. J. & Levy, O. Toward precision adjuvants: optimizing science and safety. *Current Opinion in Pediatrics* **32** (2020).

23 Schijns, V. E. J. C. Immunological concepts of vaccine adjuvant activity: Commentary. *Current Opinion in Immunology* **12**, 456-463 (2000). https://doi.org:https://doi.org/10.1016/S0952-7915(00)00120-5

24 Mbow, M. L., De Gregorio, E. & Ulmer, J. B. Alum's adjuvant action: grease is the word. *Nature Medicine* **17**, 415-416 (2011). https://doi.org:10.1038/nm0411-415

25 Marrack, P., McKee, A. S. & Munks, M. W. Towards an understanding of the adjuvant action of aluminium. *Nat Rev Immunol* **9**, 287-293 (2009). https://doi.org:10.1038/nri2510

26 Pulendran, B., S. Arunachalam, P. & O'Hagan, D. T. Emerging concepts in the science of vaccine adjuvants. *Nature Reviews Drug Discovery* **20**, 454-475 (2021). https://doi.org:10.1038/s41573-021-00163-y

27 Mbow, M. L., De Gregorio, E., Valiante, N. M. & Rappuoli, R. New adjuvants for human vaccines. *Curr Opin Immunol* **22**, 411-416 (2010). https://doi.org:10.1016/j.coi.2010.04.004

28 Daniel & Mellman, I. Oncology Meets Immunology: The Cancer-Immunity Cycle. *Immunity* **39**, 1-10 (2013). https://doi.org:10.1016/j.immuni.2013.07.012

29 Schietinger, A., Philip, M. & Schreiber, H. Specificity in cancer immunotherapy. *Seminars in Immunology* **20**, 276-285 (2008). https://doi.org:https://doi.org/10.1016/j.smim.2008.07.001

30 Cloosen, S. *et al.* Expression of tumor-associated differentiation antigens, MUC1 glycoforms and CEA, in human thymic epithelial cells: implications for self-tolerance and tumor therapy. *Cancer research* **67**, 3919-3926 (2007).

31 Gilboa, E. The risk of autoimmunity associated with tumor immunotherapy. *Nature immunology* **2**, 789-792 (2001).

32 Chheda, Z. S. *et al.* Novel and shared neoantigen derived from histone 3 variant H3.3K27M mutation for glioma T cell therapy. *Journal of Experimental Medicine* **215**, 141-157 (2017). https://doi.org:10.1084/jem.20171046

33 Zitvogel, L. *et al.* The anticancer immune response: indispensable for therapeutic success? *J Clin Invest* **118**, 1991-2001 (2008). https://doi.org:10.1172/jci35180

34 Finn, O. J. Immuno-oncology: understanding the function and dysfunction of the immune system in cancer. *Ann Oncol* **23 Suppl 8**, viii6-9 (2012). https://doi.org:10.1093/annonc/mds256

35 Upadhaya, S., Neftelinov, S. T., Hodge, J. & Campbell, J. Challenges and opportunities in the PD1/PDL1 inhibitor clinical trial landscape. *Nat Rev Drug Discov* **21**, 482-483 (2022). https://doi.org:10.1038/d41573-022-00030-4

36 Bai, L. *et al.* Promising targets based on pattern recognition receptors for cancer immunotherapy. *Pharmacological Research* **159**, 105017 (2020). https://doi.org:https://doi.org/10.1016/j.phrs.2020.105017

37 Berraondo, P. *et al.* Cytokines in clinical cancer immunotherapy. *British Journal of Cancer* **120**, 6-15 (2019). https://doi.org:10.1038/s41416-018-0328-y

38 June, C. H., O'Connor, R. S., Kawalekar, O. U., Ghassemi, S. & Milone, M. C. CAR T cell immunotherapy for human cancer. *Science* **359**, 1361-1365 (2018). https://doi.org:doi:10.1126/science.aar6711

39 Jin, S. *et al.* Emerging new therapeutic antibody derivatives for cancer treatment. *Signal Transduction and Targeted Therapy* **7**, 39 (2022). https://doi.org:10.1038/s41392-021-00868-x

40 Fukuhara, H., Ino, Y. & Todo, T. Oncolytic virus therapy: A new era of cancer treatment at dawn. *Cancer Sci* **107**, 1373-1379 (2016). https://doi.org:10.1111/cas.13027

41 Farkona, S., Diamandis, E. P. & Blasutig, I. M. Cancer immunotherapy: the beginning of the end of cancer? *BMC Medicine* **14**, 73 (2016). https://doi.org:10.1186/s12916-016-0623-5

42 Fellner, C. Ipilimumab (yervoy) prolongs survival in advanced melanoma: serious side effects and a hefty price tag may limit its use. *P T* **37**, 503-530 (2012).

43 Hodi, F. S. *et al.* Improved Survival with Ipilimumab in Patients with Metastatic Melanoma. *New England Journal of Medicine* **363**, 711-723 (2010). https://doi.org:10.1056/NEJMoa1003466

44 Fares, C. M., Allen, E. M. V., Drake, C. G., Allison, J. P. & Hu-Lieskovan, S. Mechanisms of Resistance to Immune Checkpoint Blockade: Why Does Checkpoint Inhibitor Immunotherapy Not Work for All Patients? *American Society of Clinical Oncology Educational Book*, 147-164 (2019). https://doi.org:10.1200/edbk_240837

45 Schumacher, T. N. & Schreiber, R. D. Neoantigens in cancer immunotherapy. *Science* **348**, 69-74 (2015). https://doi.org:10.1126/science.aaa4971

46 Fridman, W. H., Pagès, F., Sautès-Fridman, C. & Galon, J. The immune contexture in human tumours: impact on clinical outcome. *Nat Rev Cancer* **12**, 298-306 (2012). https://doi.org:10.1038/nrc3245

47 Sharma, P. & Allison, J. P. Immune checkpoint targeting in cancer therapy: toward combination strategies with curative potential. *Cell* **161**, 205-214 (2015). https://doi.org:10.1016/j.cell.2015.03.030

48 Cheng, L., Wang, Y. & Du, J. Human Papillomavirus Vaccines: An Updated Review. *Vaccines (Basel)* **8** (2020). https://doi.org:10.3390/vaccines8030391

49 Zhao, H., Zhou, X. & Zhou, Y.-H. Hepatitis B vaccine development and implementation. *Human Vaccines & Immunotherapeutics* **16**, 1533-1544 (2020). https://doi.org:10.1080/21645515.2020.1732166

50 Schiller, J. & Lowy, D. Explanations for the high potency of HPV prophylactic vaccines. *Vaccine* **36**, 4768-4773 (2018). https://doi.org:10.1016/j.vaccine.2017.12.079

51 Tota, J. E. *et al.* Efficacy of AS04-Adjuvanted Vaccine Against Human Papillomavirus (HPV) Types 16 and 18 in Clearing Incident HPV Infections: Pooled Analysis of Data From the Costa Rica Vaccine Trial and the PATRICIA Study. *The Journal of Infectious Diseases* **223**, 1576-1581 (2020). https://doi.org:10.1093/infdis/jiaa561

52 Campbell, J. D. Development of the CpG Adjuvant 1018: A Case Study. *Methods Mol Biol* **1494**, 15-27 (2017). https://doi.org:10.1007/978-1-4939-6445-1_2

53 Stephens, A. J., Burgess-Brown, N. A. & Jiang, S. Beyond Just Peptide Antigens: The Complex World of Peptide-Based Cancer Vaccines. *Front Immunol* **12** (2021). https://doi.org:10.3389/fimmu.2021.696791

54 Abd-Aziz, N. & Poh, C. L. Development of Peptide-Based Vaccines for Cancer. *J Oncol* **2022**, 9749363-9749363 (2022). https://doi.org:10.1155/2022/9749363

55 Vansteenkiste, J. F. *et al.* Efficacy of the MAGE-A3 cancer immunotherapeutic as adjuvant therapy in patients with resected MAGE-A3-positive non-small-cell lung cancer (MAGRIT): a randomised, double-blind, placebo-controlled, phase 3 trial. *The Lancet Oncology* **17**, 822-835 (2016). https://doi.org:https://doi.org/10.1016/S1470-2045(16)00099-1

56 Schwartzentruber, D. J. *et al.* gp100 peptide vaccine and interleukin-2 in patients with advanced melanoma. *N Engl J Med* **364**, 2119-2127 (2011). https://doi.org:10.1056/NEJMoa1012863

57 Khong, H. & Overwijk, W. W. Adjuvants for peptide-based cancer vaccines. *J Immunother Cancer* **4**, 56 (2016). https://doi.org:10.1186/s40425-016-0160-y

58 Bezu, L. *et al.* Trial watch: Peptide-based vaccines in anticancer therapy. *Oncoimmunology* **7**, e1511506-e1511506 (2018). https://doi.org:10.1080/2162402X.2018.1511506

59 Marincola, F. M., Jaffee, E. M., Hicklin, D. J. & Ferrone, S. Escape of human solid tumors from T-cell recognition: molecular mechanisms and functional significance. *Adv Immunol* **74**, 181-273 (2000). https://doi.org:10.1016/s0065-2776(08)60911-6

60 Okada, M., Shimizu, K. & Fujii, S.-I. Identification of Neoantigens in Cancer Cells as Targets for Immunotherapy. *Int J Mol Sci* **23**, 2594 (2022). https://doi.org:10.3390/ijms23052594

61 Vacchelli, E. *et al.* Trial watch: FDA-approved Toll-like receptor agonists for cancer therapy. *Oncoimmunology* **1**, 894-907 (2012). https://doi.org:10.4161/onci.20931

62 Slezak, A. J. *et al.* Tumor Cell-Surface Binding of Immune Stimulating Polymeric Glyco-Adjuvant via Cysteine-Reactive Pyridyl Disulfide Promotes Antitumor Immunity. *ACS Cent Sci* **8**, 1435-1446 (2022). https://doi.org:10.1021/acscentsci.2c00704

63 Menchise, V. *et al.* In Vivo Labeling of B16 Melanoma Tumor Xenograft with a Thiol-Reactive Gadolinium Based MRI Contrast Agent. *Molecular Pharmaceutics* **8**, 1750-1756 (2011). https://doi.org:10.1021/mp2001044

64 Gray, L. T. *et al.* Generation of potent cellular and humoral immunity against SARS-CoV-2 antigens via conjugation to a polymeric glyco-adjuvant. *Biomaterials* **278**, 121159 (2021). https://doi.org:https://doi.org/10.1016/j.biomaterials.2021.121159

65 Wilson, D. S. *et al.* Antigens reversibly conjugated to a polymeric glyco-adjuvant induce protective humoral and cellular immunity. *Nature Materials* **18**, 175-185 (2019). https://doi.org:10.1038/s41563-018-0256-5

66 Bode, C., Zhao, G., Steinhagen, F., Kinjo, T. & Klinman, D. M. CpG DNA as a vaccine adjuvant. *Expert review of vaccines* **10**, 499-511 (2011). https://doi.org:10.1586/erv.10.174

67 Zhuang, X. *et al.* Dose-effect relationship of CpG oligodeoxyribonucleotide 1826 in murine Lewis lung cancer treated with irradiation. *Onco Targets Ther* **6**, 549-554 (2013). https://doi.org:10.2147/OTT.S42485

68 Jie, J. *et al.* CpG ODN1826 as a Promising Mucin1-Maltose-Binding Protein Vaccine Adjuvant Induced DC Maturation and Enhanced Antitumor Immunity. *Int J Mol Sci* **19**, 920 (2018). https://doi.org:10.3390/ijms19030920

69 Fairbanks, B. D., Gunatillake, P. A. & Meagher, L. Biomedical applications of polymers derived by reversible addition – fragmentation chain-transfer (RAFT). *Advanced Drug Delivery Reviews* **91**, 141-152 (2015). https://doi.org:https://doi.org/10.1016/j.addr.2015.05.016

70 Delplace, V. & Nicolas, J. Degradable vinyl polymers for biomedical applications. *Nature Chemistry* **7**, 771-784 (2015). https://doi.org:10.1038/nchem.2343

71 Hirosue, S., Kourtis, I. C., van der Vlies, A. J., Hubbell, J. A. & Swartz, M. A. Antigen delivery to dendritic cells by poly(propylene sulfide) nanoparticles with disulfide conjugated peptides: Cross-presentation and T cell activation. *Vaccine* **28**, 7897-7906 (2010). https://doi.org:https://doi.org/10.1016/j.vaccine.2010.09.077

72 Efremova, M. *et al.* Targeting immune checkpoints potentiates immunoediting and changes the dynamics of tumor evolution. *Nat Commun* **9**, 32-32 (2018). https://doi.org:10.1038/s41467-017-02424-0

73 Cillo, C., Dick, J. E., Ling, V. & Hill, R. P. Generation of Drug-resistant Variants in Metastatic B16 Mouse Melanoma Cell Lines1. *Cancer Research* **47**, 2604-2608 (1987).

74 Warming "Cold" Melanoma with TLR9 Agonists. *Cancer Discovery* **8**, 670-670 (2018). https://doi.org:10.1158/2159-8290.Cd-nd2018-004

75 Chuang, Y.-C. *et al.* Adjuvant Effect of Toll-Like Receptor 9 Activation on Cancer Immunotherapy Using Checkpoint Blockade. *Front Immunol* **11** (2020). https://doi.org:10.3389/fimmu.2020.01075

76 Krishnan, S. *et al.* Design of Reversible, Cysteine-Targeted Michael Acceptors Guided by Kinetic and Computational Analysis. *Journal of the American Chemical Society* **136**, 12624-12630 (2014). https://doi.org:10.1021/ja505194w

77 Krieg, A. M. *et al.* CpG motifs in bacterial DNA trigger direct B-cell activation. *Nature* **374**, 546-549 (1995). https://doi.org:10.1038/374546a0

78 Dongye, Z., Li, J. & Wu, Y. Toll-like receptor 9 agonists and combination therapies: strategies to modulate the tumour immune microenvironment for systemic anti-tumour immunity. *British Journal of Cancer* **127**, 1584-1594 (2022). https://doi.org:10.1038/s41416-022-01876-6